Scholars' Mine

Masters Theses   Student Theses and Dissertations

Spring 2011

Impact of combustion phasing on energy and availability distributions of an internal combustion engine

Shawn Nicholas Wildhaber

IMPACT OF COMBUSTION PHASING ON ENERGY AND AVAILABILITY

DISTRIBUTIONS OF AN INTERNAL COMBUSTION ENGINE

by

SHAWN NICHOLAS WILDHABER

A THESIS

Presented to the Faculty of the Graduate School of the

MISSOURI UNIVERSITY OF SCIENCE AND TECHNOLOGY

In Partial Fulfillment of the Requirements for the Degree

MASTER OF SCIENCE IN MECHANICAL ENGINEERING

2011

Approved by

James A. Drallmeier, Advisor
Bassem F. Armaly
Ralph W. Wilkerson
David W. Riggins

ABSTRACT

High fuel efficiency has become an extremely desirable trait for internal combustion engines. This motivation has driven extensive research on methods to improve fuel efficiency on engines of various sizes. Many of these methods involve changes to the properties of the combustion process. One way to induce these property changes is through varying the phasing of combustion. Combustion phasing can be defined as the time in the engine cycle, specifically the compression and expansion strokes, where combustion occurs. A change in combustion phasing causes a change in combustion duration. The duration of combustion impacts how the energy and work potential of the energy (availability) from the fuel are utilized. Analysis techniques based on the first and second law of thermodynamics have been developed to determine the energy and availability distributions. These distributions are utilized to visualize and quantify any improvements made to engine efficiency as combustion phasing is altered. The test engine utilized is a spark ignition (SI) engine meaning that the combustion phasing variations are completed by varying the ignition timing. In light of the test platform being a two-cylinder, industrial-use engine, this thesis focuses on determining the impact of combustion phasing on energy and availability distributions in an air-cooled, rich running utility engine subject to tight manufacturing cost constraints.

ACKNOWLEDGMENTS

First and foremost, I would like to express my sincere gratitude to my advisor, Dr. James Drallmeier, whose support, guidance, and sound advice enabled this thesis to become a reality. The knowledge he imparted and the opportunities he presented to me will continue to open doors for the rest of my career. I would also like to thank Dr. Bassem Armaly, Dr. Ralph Wilkerson, and Dr. David Riggins, for their advice and time commitment as members of my graduate committee. I am also indebted to Kawasaki Motors Manufacturing for their financial and technical support which allowed this research to proceed.

I would also like to express my appreciation to the many friends and mentors I have had during my collegiate career: Jeff Massey, whose immense knowledge and undying willingness to help will not be forgotten; Cory Huck, Josh Bettis, Avinash Singh, and Aaron Attebery for their amity and assistance with coursework and research; and my close friends outside the classroom, who have always been there for me.

Last and most important, I would like to thank my family, particularly my parents, Jim and Lisa Wildhaber. The love, support, and solid foundation they have provided my entire life have made my accomplishments possible.

v

TABLE OF CONTENTS

Page

LIST OF ILLUSTRATIONS

LIST OF TABLES

NOMENCLATURE

Symbol	Description
Φ	Equivalence Ratio
CA50	Crank angle at which MFB equals 50%
A	Availability
a	Specific Availability
N	Engine Speed
T	Temperature

ABBREVIATIONS

A/F	Air-to-Fuel Ratio
ATDC	After Top Dead Center
BDC	Bottom Dead Center
BMEP	Brake Mean Effective Pressure
BTDC	Before Top Dead Center
CAD	Crank Angle Degree
CI	Compression Ignition
EVC	Exhaust Valve Closed
EVO	Exhaust Valve Open
IVC	Intake Valve Closed
IVO	Intake Valve Open
LHV	Lower Heating Value
MBT	Maximum Brake Torque
MFB	Mass Fraction Burned
MON	Motored Octane Number
RON	Research Octane Number
RPM	Revolutions Per Minute
SI	Spark Ignition
SOC	Start of Combustion
TDC	Top Dead Center
UTG96	Unleaded Test Gasoline with 96 RON

1. INTRODUCTION

1.1. SCOPE OF THE INVESTIGATION

With the gradual but continuous rise in the price of crude oil comes an increased focus on improving the fuel efficiency of internal combustion engines. The automotive industry has received much of this attention for several years but the scope has not been expanded to encompass all small engines utilized in generators, powered equipment, and implements. Therefore, this thesis focuses on small air-cooled engines that are limited by low manufacturing cost constraints.

In order to improve the efficiency of an engine, the energy supplied by the fuel must be utilized more effectively. This means that the amount of fuel energy used for work output should be maximized while the amount going toward losses in the system (combustion inefficiency, sensible exhaust energy, heat transfer, and friction) should be minimized. This energy flow is shown in Figure 1.1. Combustion inefficiency is relatively high in a typical small spark ignition engine due to the fuel rich mixtures inducted into the engine. Since most of these engines are carbureted, rich mixtures are used to improve the engines' ability to handle sudden changes in load or engine speed, called transients. Although transient operation is improved by using rich mixtures, not all of the fuel is consumed in the combustion reaction which reduces the fuel efficiency of the engine.
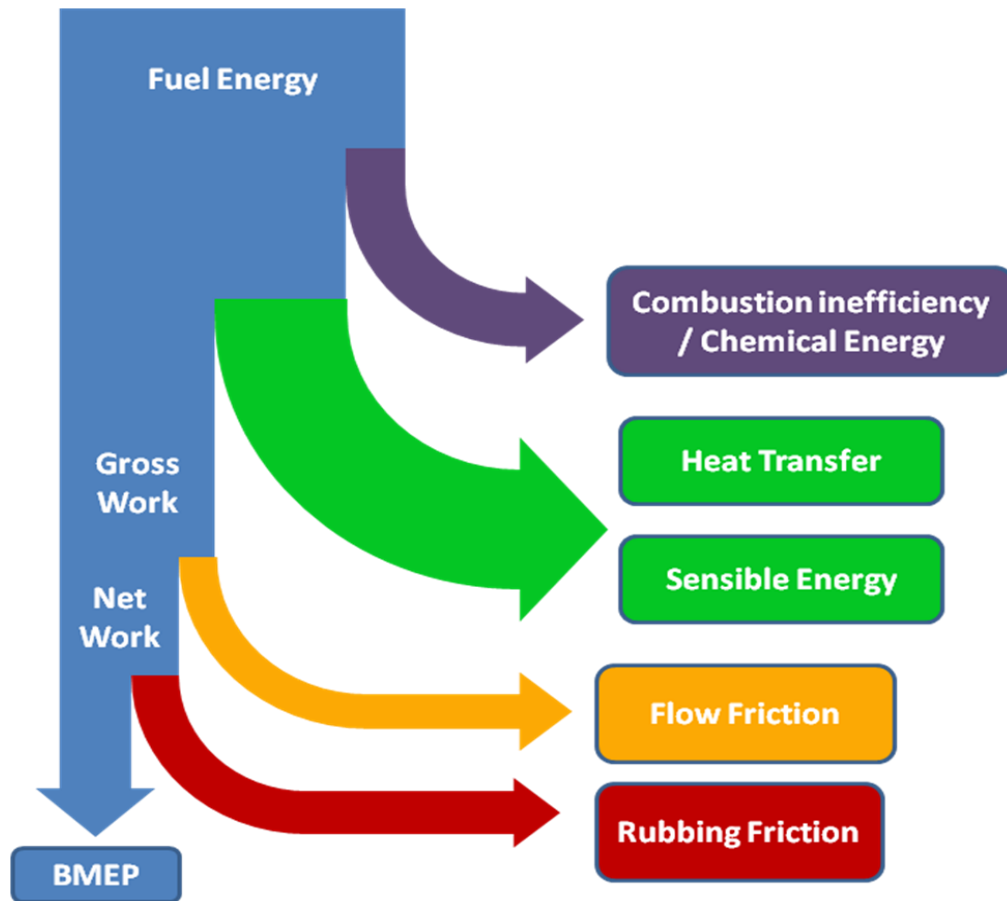
Figure 1.1: Energy flow for an internal combustion engine

One way to utilize the fuel energy more effectively is to change the behavior of the combustion process, specifically the duration and time at which it occurs during the engine cycle. The timing is also referred to as combustion phasing. If the combustion phasing is shifted toward the optimal setting for a particular engine, more fuel energy will be utilized for brake power production and engine efficiency will improve. Furthermore, the effectiveness at which the fuel energy is utilized can be quantified by determining where and in what relative amounts the energy is expelled during engine operation. An energy distribution analysis makes up a portion of this investigation.

The first law of thermodynamics can be used to develop an energy balance analysis which quantifies the energy supplied to an engine in the form of fuel as well as all the output energy forms. These output forms include brake power, energy expelled through heat transfer, and energy lost in the exhaust gas. When these energy forms are quantified, all the output forms sum to the value of the energy supplied in the fuel. This energy distribution is beneficial because it helps in identifying areas to focus on in order to improve the energy distribution and, therefore, engine efficiency. It also aids in the quantification of improvements when engine configuration or operating parameters are varied.

The second law of thermodynamics is used in conjunction with the first law approach to obtain a more complete picture of the combustion process. The second law uses quality of energy concepts to determine the amount of energy, in each form, that can actually be utilized for useful work. This is also referred to as the availability of energy and is used to obtain more realistic quantifications when improvements in efficiency are desired. This particular analysis is also capable of identifying the amount of irreversibility inherent in the energy conversion process completed in the combustion chamber of an engine.

Since combustion phasing directly impacts the duration of the combustion process, a quantification of duration parameters is desirable. This is achieved through a model that calculates heat release rate (HRR) or energy release rate. This model was developed specifically for this investigation and uses the measured cylinder pressure to complete the calculations. From the HRR model, calculations can be completed that determine the mass fraction of fuel that is burned at any crank angle in the engine cycle.

This is referred to as mass fraction burned (MFB). Both heat release rate and mass fraction burned help to quantify the duration of combustion.

Once the analysis techniques have been developed, the combustion phasing is varied with the ignition timing in an attempt to utilize more of the fuel energy and improve engine efficiency. The varying combustion phasing causes the combustion duration to change in ways that can be deciphered with the heat release rate and mass fraction burned models. A shift in combustion duration results in redistribution of the energy and availability output from the engine. From this the amount of improvement in engine efficiency can be determined.

1.2. BACKGROUND FROM LITERATURE REVIEW

Analyzing the combustion process in an internal combustion engine is a very complex problem with many significant phenomena. The combustion process starts before the end of the compression stroke and ends in the early part of the expansion stroke, after the peak pressure location [1]. In a spark ignition engine, the exact location in the engine cycle at which combustion starts is controlled by the timing of the spark event. The spark event is when the electrode of the spark plug ignites the fuel and air mixture in the combustion chamber which initiates spherical flame propagation through the volatile mixture. This event normally occurs during the compression stroke shortly before the piston reaches top dead center, shown in Figure 1.2. The timing of the spark event is also referred to as combustion phasing. Due to the tight cost constraints present in small engine manufacturing, a simple and reliable system is used which keeps the spark timing fixed at a certain value regardless of engine speed or load. The fixed spark

timing system installed on the test engine initiates a secondary spark event near top dead center of the exhaust stroke. This is referred to as a "wasted" spark because it does not result in combustion or power output from the engine.
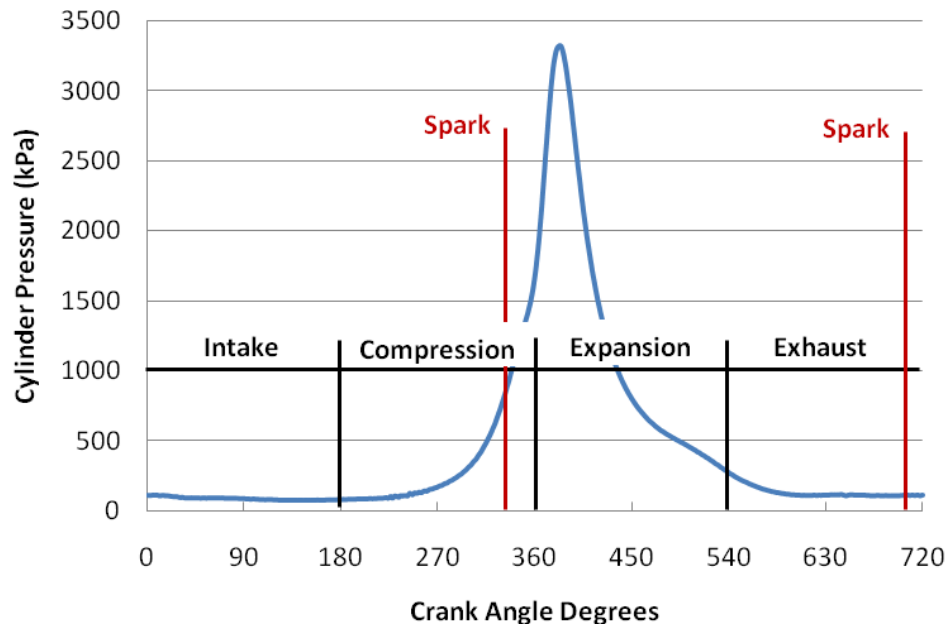
Figure 1.2: Spark events in a spark ignition engine

The majority of the combustion related phenomena are affected by the timing of the spark event. Spark timing can be modified to occur later in the engine cycle, called retarding, or earlier in the engine cycle, advancing. Retarding the spark causes peak pressure location to occur later in the engine cycle. It also causes a reduction in the magnitude of this peak pressure. These two effects decrease the expansion stroke work transfer which is the work transfer from the cylinder gases to the piston [1]. On the other hand, spark timing advancement causes an increase in the compression stroke work transfer, the work transfer from the piston to the cylinder gases, but also increases the expansion stroke work transfer [1]. This is due to an increase in peak cylinder pressure

magnitude and the occurrence of peak pressure earlier in the engine cycle. One can see

how gains in engine work output can be realized by advancing the spark timing. This is

evidenced in Figure 1.3 which is modeled after a figure in [1] but generated from data

collected during engine testing for this thesis. Here work output, shown as brake power,

increases as spark timing is advanced to a certain point then decreases.
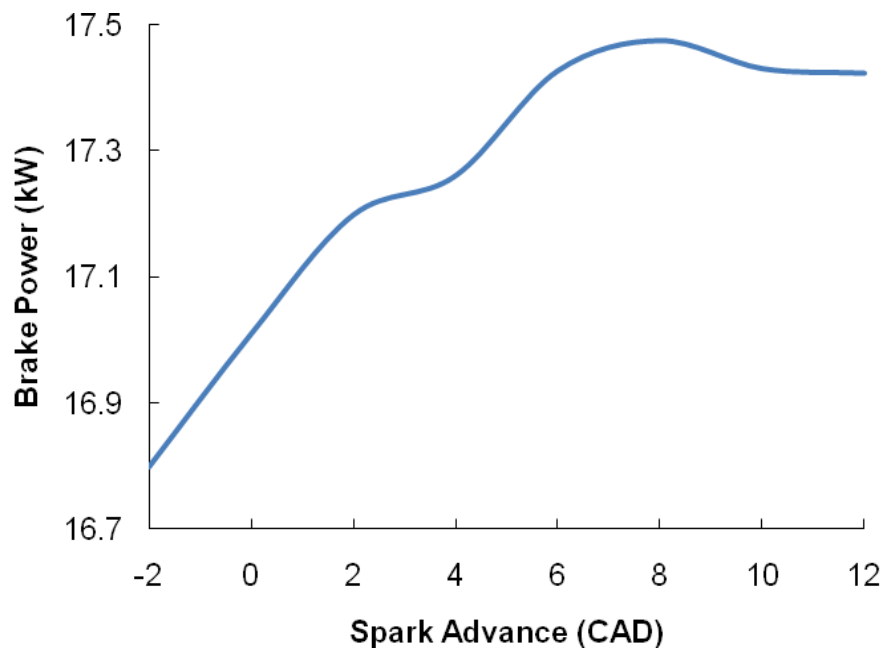
Figure 1.3: Variations in power output with advanced spark timing

Changes in combustion phasing also affects the duration of the combustion

process through burn rate, the rate that the reactants are consumed in the chemical

reaction. Combustion duration decreases with an increase in burn rate. Burn rate is

increased with an increase in flame front area, laminar flame speed, turbulence within the

intake charge, and density of the unburned portion of the mixture. This relation is shown

in Figure 1.4 where: A_f = flame front area, S_L = laminar flame speed, and ρ_u = unburned mixture density.
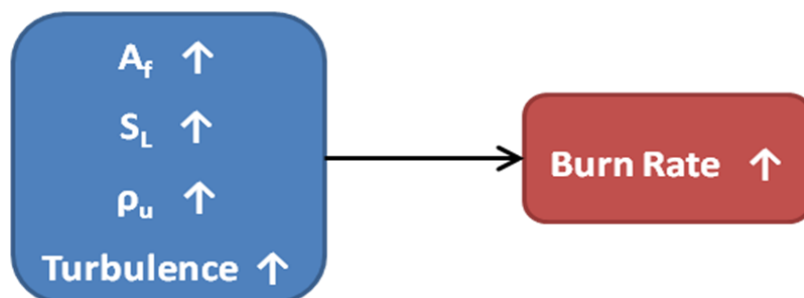
Figure 1.4: Burn rate relation

It is also known that turbulence increases with engine speed meaning that, in regard to turbulence, burn rates increase with engine speed. Density is directly correlated to pressure. From this and the previous paragraph, it can be inferred that the density of the unburned mixture will increase as peak cylinder pressure increases with spark timing advancement. It is known from internal combustion engine dynamics that minimal combustion chamber volume, clearance volume, is seen when the piston is at top dead center. This volume increases as one focuses earlier or later in the cycle. As spark timing is advanced further from top dead center, it is set to occur at larger combustion chamber volumes. This larger volume allows the spherical flame to grow larger than it would if combustion was phased closer to top dead center. This increase in flame front area causes only a minor increase in burn rate due to the large changes in flame front area seen during combustion. Laminar flame speed is more complicated in nature and is dependent on flame temperature, equivalence ratio, residuals, and fuel type. At a given engine set point, the only variable of these four parameters is flame temperature. As

spark timing is advanced, the temperature of the gases within the combustion chamber increases. These are also called bulk gases. An increase in the bulk gas temperature causes an increase in flame temperature which results in greater laminar flame speed. An increase in laminar flame speed means an increase in burn rate. From all these effects, one clear observation can be made. As spark timing is advanced, burn rate is increased which causes a reduction in combustion duration.

This advancement is limited by the onset of abnormal combustion. This is a combustion occurrence whose initiation, procession, or both is different than what is desired or expected. Every fuel used in internal combustion engines has a specific ignition condition that must be reached in order for the oxidation reaction to start. During normal combustion, this ignition condition is very quickly reached at the spark plug electrode during the spark event due to the extremely high temperature. Steady flame propagation continues from there. As spark timing is advanced, the bulk gas temperature increases meaning that the unburned fuel and air mixture in the combustion chamber is closer to its ignition condition. The higher pressures and heat transfer from the engine also help to increase the temperature of the bulk gas. Since larger combustion chamber volumes are also associated with spark timing advancement, it takes a longer time for the flame front to reach the combustion chamber walls. If spark timing is advanced beyond a certain point, this allows enough time for the gas near the chamber walls, end gas, to reach its ignition condition which results in combustion. This is also known as autoignition. Due to the homogeneous mixture of fuel and air, there is not steady flame propagation through the end gas. Rather, instantaneous combustion occurs causing a rapid release of energy and extremely high peak pressures. This autoignition of the end

gas can be very harmful to engine components and also creates much engine noise, called "knock". For this reason, there are boundary conditions placed on variations in spark timing.

1.2.1. First Law Effects. Shortened combustion duration due to an increase in burn rate has many effects on the energy distribution determined through the first law analysis. As combustion duration is reduced, there is less time available for energy to be lost from the combustion process in the form of heat transfer to the environment. This heat transfer energy is redistributed to brake power. There is a countering effect in regard to heat transfer due to the higher gas temperatures, seen with advanced spark timing, creating larger heat transfer from the cylinder walls to the environment. The occurrence of these two countering effects will minimize improvements in energy lost to heat transfer. Also as combustion duration is reduced, the energy release occurs at a much faster rate causing an increase in expansion stroke work transfer, i.e. brake power. Advancing the phasing of combustion means that it is occurring further from the opening of the exhaust valve and the exhaust stroke. This means that the combustion process is allowed more time to oxidize the reactants, reducing the chemical exhaust energy, and utilize the components of the exhaust containing energy in the form of heat. This last phenomenon reduces the sensible exhaust energy term. The energy gained from a reduction in both forms of exhaust energy is redistributed to brake power. This effect will have a negligible impact unless the ignition event is advanced from an extremely late timing. All of these phenomena dictate that the first law efficiency will also be increased due to reduced combustion duration.

1.2.2. Second Law Effects. Variations in spark timing also have an influence on the availability distributions determined with the second law analysis. The chemical exhaust, heat transfer, and exhaust flow availabilities will all be reduced and redistributed to brake power availability just like the chemical exhaust, heat transfer, and sensible exhaust energies are in the first law analysis. Availability destroyed is also affected by variations in spark timing. Studies have been conducted which show that an increase in combustion duration decreases the availability destroyed due to combustion but increases the availability destroyed via heat transfer by a much greater amount [8]. In total, an increase in availability destroyed is observed due to reduced combustion temperatures and pressures. Therefore shortened combustion duration due to advanced spark timing results in reduction of availability destroyed [8].

These literature review observations are primarily taken from studies conducted on large automotive-type engine platforms. No second law analyses have been conducted on small, air-cooled, rich-running engines. This provides motivation for the research.

2. EXPERIMENTAL FACILITY AND PROCEDURE

2.1. EXPERIMENTAL FACILITY

The experimental data is collected in the Internal Combustion Engine Laboratory on the Missouri S&T campus where engine performance, emission, and combustion analysis can be completed. The following describes the experimental test bed utilized for this investigation.

2.1.1. Engine. A four-stroke V-twin is the engine considered in this study. It is characterized as a naturally aspirated, forced air-cooled, spark-ignition engine which is desirable for this investigation. The normal engine speed range is 1550 RPM to 3600 RPM with the majority of testing occurring at 3060 RPM. The remaining properties and dimensions of interest can be seen in the following table. This engine can also be seen in Table 2.1.

Table 2.1: Test engine specifications

Cylinders	2
Cylinder Layout	90° V-Twin
Displacement (cm^3)	852.0
Bore (mm)	84.5
Stroke (mm)	76.0
Connecting Rod Length (mm)	122.0
Compression Ratio	8.2

2.1.2. Engine Performance Measurements. The output shaft from the vertical shaft engine is connected to a Warner 5218-261 electric clutch to allow effortless engagement to a Land and Sea water-brake dynamometer. The dynamometer provides a

loading mechanism as well as measurement of engine performance parameters through the dynamometer's associated software (Dynomax). This software is installed on a laptop in the engine control section of the lab which allows complete engine control and monitoring from a single station. Due to the weight of the dynamometer, a platform was fabricated to support it from the bottom side so the thrust bearing in the engine will not be over-stressed. Freedom of rotation is still allowed for the dynamometer through the use of two large thrust bearings mounted on the platform and connected to the dynamometer. Along with engine speed, brake power, and torque, several temperature measurements are also collected with type K thermocouples. These include intake temperature (measured at the air filter), intake port temperature for each cylinder (measured at the intake valve), oil temperature, combustion chamber wall temperature, and exhaust gas temperature for both cylinders. The previously mentioned instrumentation can be seen in the picture included in Figure 2.1. A close-up of the dynamometer is included in Figure 2.2.

Missouri S&T also has the ability to quantify fuel flow rate with a Max Machinery fuel control system. This system consists of a fuel metering unit (Model: 710) and an indicator (Model: 121). Additionally, oil pressure is measured along with ambient pressure, temperature, and humidity which are used for correcting the brake power measurement so that direct comparison of tests completed on different days can occur.
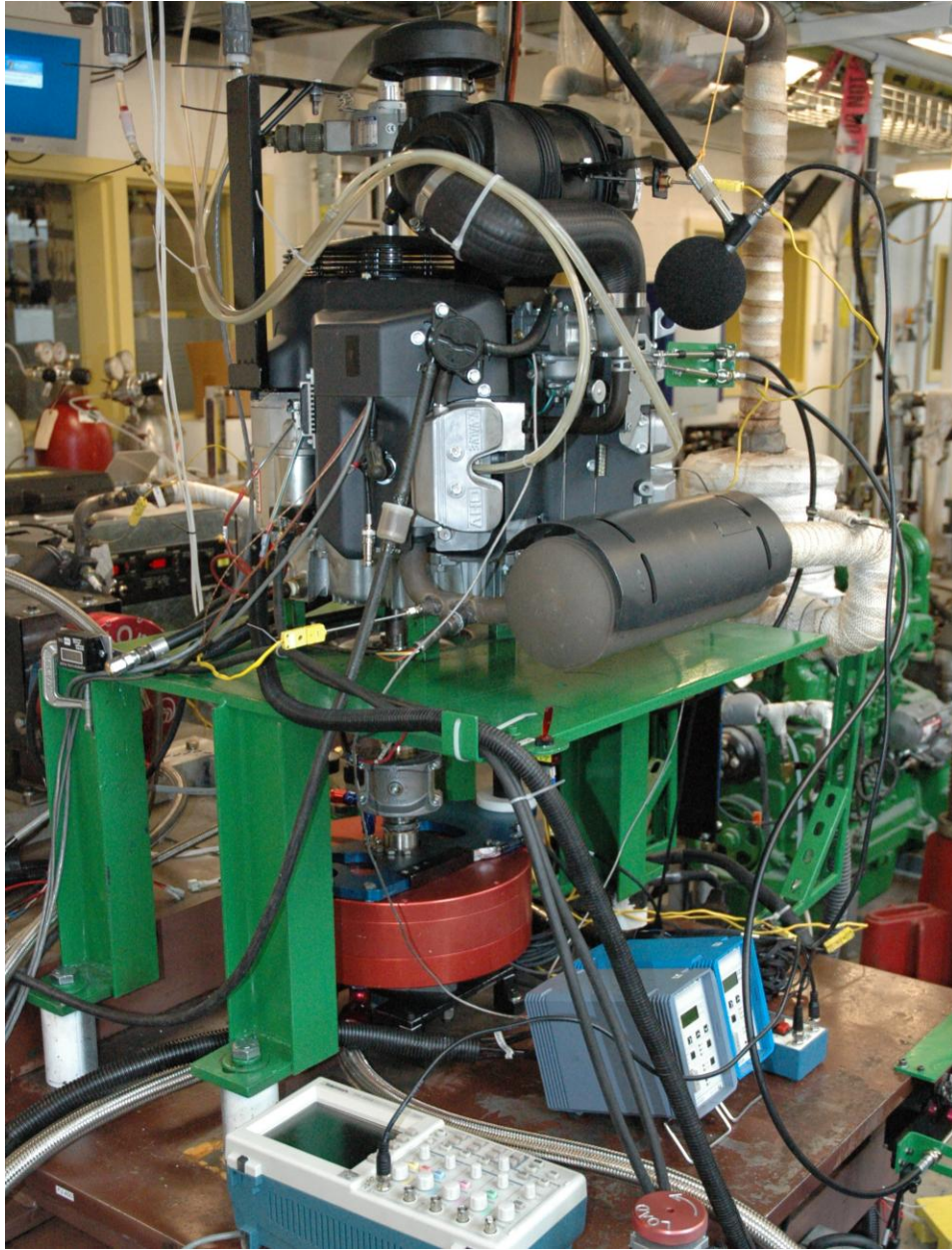
Figure 2.1: Test engine stand with associated instrumentation
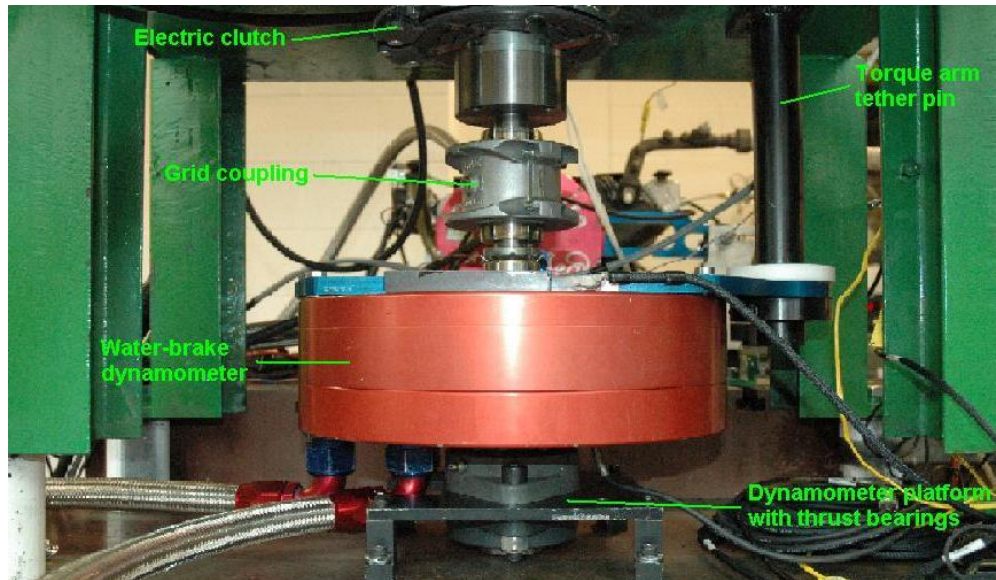
Figure 2.2: Close-up of dynamometer hardware and instrumentation

2.1.3. Emissions Measurements. In order to complete the desired analysis, a number of different exhaust species must be measured. Three separate California Analytical emissions analyzers are used to determine the concentration of each species contained in the exhaust gases. A model 300 dry gas analyzer is used to determine CO, CO_2, and O_2 percentages by condensing the H_2O out of the measured exhaust stream before analyzing it. Wet gas analyzers are utilized to obtain the remaining species concentrations. A model 300M-HFID determines unburned hydrocarbons (uHC) in parts per million C while a model 400-HCLD determines the NO_x concentration. Cylinder specific air-to-fuel ratio (A/F) comes from two NGK Spark Plug brand UEGO sensors mounted in the exhaust manifold. The voltage output from each TC-6000 series controller is collected in a data acquisition system then converted to (A/F) using a Matlab code.

2.1.4. Combustion Analysis. The timing and speed of the combustion process, among other parameters, is determined by using cylinder pressure data collected from a Kistler 6061B dynamic pressure transducer mounted in the combustion chamber of each cylinder. These transducers are water-cooled piezoelectric transducers that provide accurate dynamic pressure measurements but must be referenced to known pressure values in order to obtain the actual pressure value at a given point in the engine cycle. This referencing is done to intake manifold pressure for each cylinder using two Motorola MPX4115AP static pressure transducers. The output from each pressure transducer is recorded by data acquisition hardware at ½ crank angle increments determined by a BEI Optical Shaft Encoder (model: XHS35F-100-R2-SS-720-ABZC-28V/V-SM18). This shaft encoder, driven by a shaft extension of the crankshaft on the top of the engine, allows for cyclic (0 – 720 CAD) viewing of collected data. The shaft encoder along with its tethering bracket can be seen in Figure 2.3.
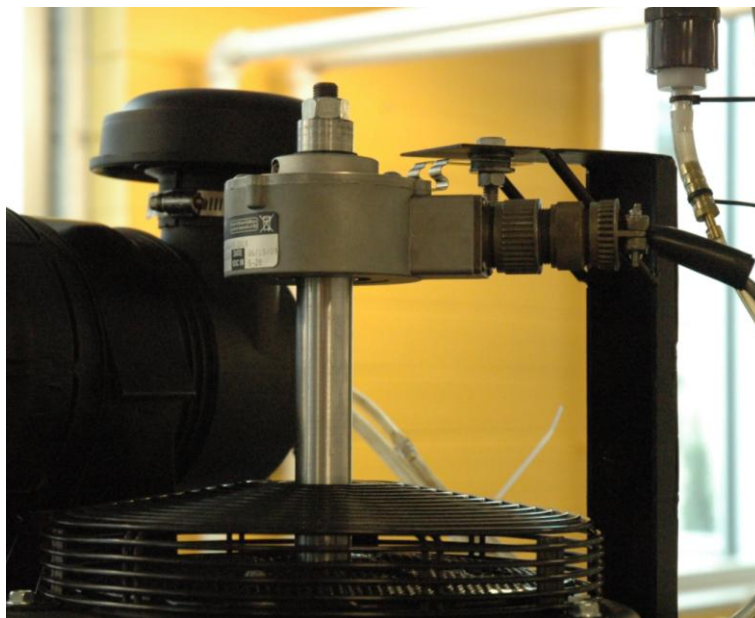
Figure 2.3: Shaft encoder mounted above the flywheel

2.2. EXPERIMENTAL PROCEDURE

The experimental test procedure used for engine performance data collection in this investigation is the Cycle B Six-Mode engine test procedure described in SAE J1088 and Appendix B to Subpart E of Part 89 of the Code of Federal Regulations. This test requires several engine parameters to be recorded at six different set points. The first five set points use an engine speed of 100% (3060 RPM for the test engine) and differing load values ranging from 100% down to 10%. The last set point uses the idle engine speed (1550 RPM) and no load. This information is given in Table 2.2 along with weighting factors for each mode.

Table 2.2: Six-mode cycle B test procedure

Mode	1	2	3	4	5	6
Rated Speed (RPM)	3060	3060	3060	3060	3060	1550
Speed Setting (% Rated)	100	100	100	100	100	Idle
Load Setting (% Rated)	100	75	50	25	10	0
Weighting Factors (%)	9	20	29	30	7	5

This test procedure was chosen due to its wide acceptance for accurately analyzing engine performance and emissions parameters. It also enables a direct comparison to the data set collected by the engine manufacturer with the same engine.

3. ENERGY BALANCE – FIRST LAW

The energy balance is a beneficial engineering tool used in analyzing engine performance data. This first law of thermodynamics approach is extremely useful in determining where and in what relative amounts the input chemical energy is distributed during engine operation. The flow rate of fuel being inducted into the engine is used to determine the rate at which energy is being supplied to the system. From there, this input energy is divided among several different output avenues including brake power output, sensible exhaust energy, chemical exhaust energy, and convective heat transfer to the environment. Due to the conservative property of energy, the quantification of these output energy forms add to the same value as the input energy. A detailed explanation of the input energy and each of the output energy forms is given in this section. Also included is a description of the numerical code developed and all associated calculations required to quantify results.

3.1. CODE DESCRIPTION

Microsoft Excel was chosen as the software platform to construct this energy balance due to its calculation capability, graphing/plotting utilities, and overall ease of use.

3.1.1. Input Parameters and Preliminary Calculations. Several engine parameters must be collected in order to complete this energy balance analysis. Engine speed (RPM) and corrected brake power (kW) are inputs into the energy balance and are used to calculate torque (N-m) using the following equation.

$$T = \dot{W}_B \Big/ 2\pi N \tag{1}$$

where: $\dot{W}_B$ = brake power and N = engine speed

Mass fuel flow (gm/hr) is collected along with emission gas concentrations of CO_2 (%),

CO (%), O_2 (%), uHC (ppm C), and NO_X (ppm). The CO_2, CO, and O_2 data is taken

from a dry gas analyzer while the remaining species are each collected from wet gas

analyzers.

Intake, oil, and exhaust gas temperature (˚C) are also measured and input into the

balance. The exhaust gas temperature from each cylinder is averaged and used for

further calculations. The remaining pieces of measured data are engine displacement,

ambient conditions (pressure, temperature, and humidity), and information on the fuel

used which includes H/C ratio, lower heating value, and molecular weight. M_F is

calculated using the following formula from [1]:

$$M_F = 12.01 + 1.008 \left(H \Big/ C \right) \tag{2}$$

The H_2O concentration (%) is not collected during engine tests and thus must be

calculated. This is completed using some of the other collected emissions data and the

following equation [1]:

$$(H_2O) = 0.5 \left(\frac{H}{C} \right) \left(\frac{(CO_2) + (CO)}{(CO) \big/ \left[K(CO_2) \right] + 1} \right) \tag{3}$$

where: ( ) = molar concentration in percent

In the above equation, K is defined as the water-gas reaction equilibrium constant. A

generally accepted empirical determination of K is the constant 3.8. This water-gas

reaction is used in conjunction with the atom balances of the global reaction to derive the

(H₂O) equation. This global reaction is supplied below and explained in a succeeding section of this report.

$$C_xH_y + a(O_2 + 3.76N_2) \rightarrow bCO_2 + cH_2O + dCO + eH_2 + fO_2 + gN_2 \qquad (4)$$
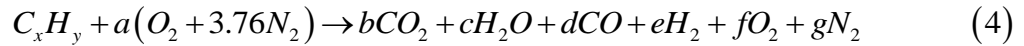
3.1.2. Air-to-Fuel Ratio Determination. Air-to-fuel ratio is determined by three different methods. The simplest uses the data collected from UEGO (Universal Exhaust Gas Oxygen) sensors mounted in the exhaust stream of each cylinder. UEGO sensors output a voltage corresponding to a specific concentration of oxygen in the exhaust gas. Using each sensor's calibration, this voltage is then converted to an air-to-fuel ratio. An average is taken of these readings which can then be used for subsequent calculations.

The remaining two methods both use a Spindt exhaust gas analysis. It is known that the make-up of combustion products, or exhaust gases, is linked to the air-to-fuel ratio. Therefore, air-to-fuel ratio can be calculated by configuring the concentration of each exhaust gas species in one of a few equations developed by R. S. Spindt [1, 2]. Previous investigations [5] have concluded that Spindt analyses return values within 0.1 air-to-fuel ratio of the true value if the engine is run on gasoline and the sampling location is before an exhaust catalyst. Since these two conditions are met in this experimental setup, the Spindt analyses are deemed appropriate.

The first Spindt method calculates the equivalence ratio based on a wet uHC and dry inorganic gas analysis. This is the most accurate for the experimental engine stand due to the inorganic gas concentrations (CO_2, CO, and O_2) being determined from a dry gas analyzer while the uHC concentration is given in a wet gas analysis. The following formulas were used for this computation [1].

$$\phi = \frac{2n_{O_2}}{n_P x_{H_2O} + n_P\left(1 - x_{H_2O}\right)\left(x^*_{CO} + 2x^*_{CO_2} + 2x^*_{O_2} + x^*_{NO} + 2x^*_{NO_2}\right)} \tag{5}$$

where:

$$n_{O_2} = x + y/4 \quad \text{(O}_2\text{ molecules required for complete combustion of fuel C}_x\text{H}_y\text{)} \tag{6}$$

$$x^*_i = \text{dry mole fraction of component } i$$

$$x_i = \text{wet mole fraction of component } i$$

$$x_i = \left(1 - x_{H_2O}\right)x^*_i \tag{7}$$

$$n_P = \frac{x}{x_{uHC} + (1 - x_{H_2O})(x^*_{CO} + x^*_{CO_2})} \quad \text{(total moles of exhaust products)} \tag{8}$$

$$x_{H_2O} = \frac{y}{2x}\frac{x^*_{CO} + x^*_{CO_2}}{\left[1 + x^*_{CO}/\left(K x^*_{CO_2}\right) + (y/2x)\left(x^*_{CO} + x^*_{CO_2}\right)\right]} \tag{9}$$

The air-to-fuel ratio can then be calculated with the knowledge that:

$$\left(A/F\right) = \frac{1}{\phi\left(F/A\right)_S} \tag{10}$$

where: $\left(F/A\right)_S = 0.0685$ (stoichiometric fuel-to-air ratio for gasoline)

The remaining Spindt calculation uses a dry uHC component and is determined with the following equation [1].

$$\left(A/F\right) = 4.773\left(\frac{M_A}{M_F}\right)\frac{(CO_2) + (CO)/2 + (H_2O)/2 + (NO)/2 + (NO_2) + (O_2)}{(HC) + (CO) + (CO_2)} \tag{11}$$

This Spindt method is not used for subsequent calculations but is included as a check of the other methods used in obtaining air-to-fuel ratio. It compares to the wet uHC Spindt calculation with a percent error of approximately 0.6%. A slightly larger

percent error of 5 – 8% is found when the wet uHC Spindt method is compared to an average of the UEGO readings. The uncertainty here is a result of the relatively high unburned hydrocarbon concentrations seen for the rich-running test engine. The Spindt calculations take this measurement into consideration while the UEGO sensors do not resulting in different values for air-to-fuel ratio.

3.1.3. Energy Forms. As previously mentioned, the energy supplied to the system via the fuel is divided among the four different output avenues of brake power output, sensible exhaust energy, chemical exhaust energy, and heat transfer to the environment. Only part of the input chemical energy is actually released during combustion. The unreleased part is not utilized and is expelled in the exhaust products. The released portion goes toward brake power output, convective heat transfer, and sensible exhaust energy. The unreleased input energy is exported as chemical exhaust energy leaving via the exhaust flow. The diagram in Figure 3.1 illustrates this concept.
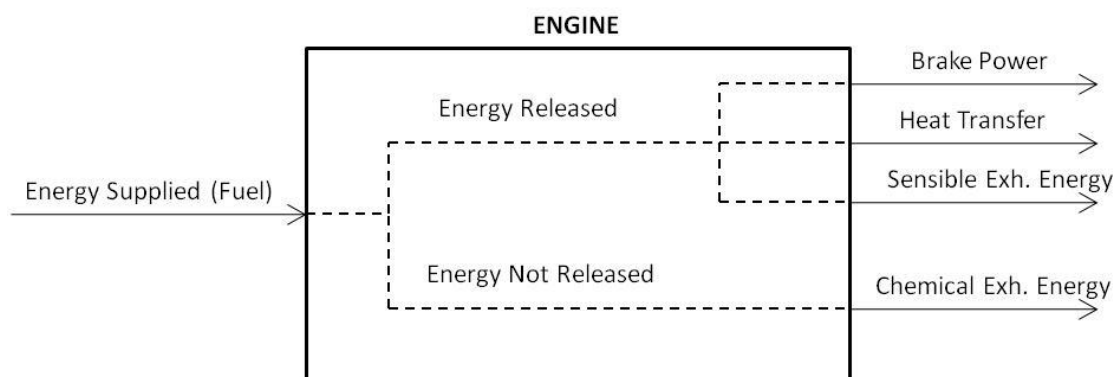
Figure 3.1: Energy distribution for air-cooled engines

Chemical exhaust energy is the energy expelled in the exhaust gas due to incomplete combustion and is directly correlated to the air to fuel ratio. As one would expect, this chemical energy lost will be significantly higher for rich running engines and would tend to zero for a stoichiometrically operating engine. Sensible exhaust energy is equivalent to the heat energy in the exhaust gas and is found by calculating the difference in combustion product enthalpies if the exhaust gas is taken at ambient temperature. Essentially, the sensible exhaust energy is the energy in the exhaust gas related to the high temperature of the exhaust flow and, like convective heat transfer, is not utilized in power production. The energy balance equation utilized in this investigation is given in time rate of change notation as:

$$\dot{E}_{FUEL} = \dot{W}_B + \dot{Q}_{HT} + \dot{E}_{SE} + \dot{E}_{CE} \tag{12}$$

where:

$\dot{W}_B =$ brake power $\dot{Q}_{HT} =$ heat transfer energy

$\dot{E}_{SE} =$ sensible exhaust energy $\dot{E}_{CE} =$ chemical exhaust energy

$\dot{E}_{FUEL} =$ chemical energy supplied by fuel

The calculation procedure for each of these energy forms is discussed at length in the next section of this report.

3.1.3.1 Input chemical energy. The calculation of the input chemical energy, or chemical energy supplied, from the fuel is completed using the mass flow rate (kg/s) and lower heating value of fuel (kJ/kg) in the following equation:

$$\dot{E}_{FUEL} = (LHV)\dot{m}_F \tag{13}$$

The fuel used in the data collection is Indolene (UTG-96) which has specific gravity of 0.742 kg/L, H/C ratio of 1.796, and a LHV of 43210 kJ/kg. The energy rate unit attained from this equation is kW which is the same unit used to quantify the output energy forms. These output energies are also presented as percentage of chemical energy supplied in order to provide a visualization of efficiencies and energy distributions.

3.1.3.2 Brake power. Brake power is the most desirable avenue for output energy and is collected at each engine set point. Therefore, no extensive calculation is done to compute or analyze this performance parameter.

3.1.3.3 Convective heat transfer. A primary avenue for energy output from an engine is through convection to the environment. Determination of this convective energy flow is made possible with the knowledge that it and brake power are the only energy forms supplied by the chemical energy that is released during combustion. This chemical energy released quantification is completed with a detailed thermochemistry calculation that follows. The exhaust gas concentrations, air-to-fuel ratio, and fuel properties are used to establish the specifics of the oxidation reaction occurring during combustion. This reaction as well as the equations to calculate the coefficients are included below.

$$C_xH_y + a(O_2 + 3.76N_2) \rightarrow bCO_2 + cH_2O + dCO + eH_2 + fO_2 + gN_2 \qquad (14)$$
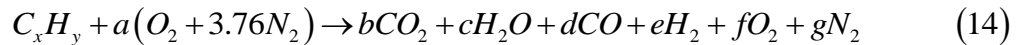
where:

$$n_T = \frac{x}{x_{CO} + x_{CO_2}} \qquad\qquad a = \frac{\left(A/F\right)\left(MW_F\right)}{(4.76)(29)}$$

$$b = n_T\left(x_{CO_2}\right) \qquad\qquad d = n_T\left(x_{CO}\right)$$

$$f = n_T\left(x_{O_2}\right) \qquad\qquad c = 2a - 2b - 2f - d$$

$$e = \frac{1}{2}y - c \qquad\qquad g = 3.76a$$

Once the reaction coefficients are known, the chemical energy released can be found using exhaust gas temperature measurements along with known and calculated enthalpy values. This is done by subtracting the energy found in the reactants (fuel and air) from the energy found in the products with the equation listed below. The energy units obtained from the equation are kJ/kmol fuel. A conversion to kW is completed with the mass flow rate and molecular weight of fuel.

$$\Delta H = H_P - H_R = \sum_P n_i \left(\overline{h_f^o} + \Delta \overline{h} \right)_i - \sum_R n_i \left(\overline{h_f^o} + \Delta \overline{h} \right)_i \qquad (15)$$

$$\Delta H = b \left(\overline{h_{f_{CO_2}}^o} + \Delta \overline{h_{CO_2}} \right) + c \left(\overline{h_{f_{H_2O}}^o} + \Delta \overline{h_{H_2O}} \right) + d \left(\overline{h_{f_{CO}}^o} + \Delta \overline{h_{CO}} \right) + e \Delta \overline{h_{H_2}}$$
$$+ f \Delta \overline{h_{O_2}} + g \Delta \overline{h_{N_2}} - \left(\overline{h_{f_{C_xH_y}}^o} + \Delta \overline{h_{C_xH_y}} \right) - a \Delta \overline{h_{O_2}} - 3.76a \Delta \overline{h_{N_2}} \qquad (16)$$

Within this equation, some additional determinations must be made. The enthalpy of formation values are universally known and tabulated constants. The $\Delta \overline{h_i}$ values are computed with an empirical method found in [1]. The following equation and coefficients are valid only for CO_2, H_2O, CO, H_2, O_2, and N_2 at a pressure equal to P_o which is the pressure of the standard atmosphere (1.01325 bar) [6].

$$\Delta \overline{h_i} = \tilde{R} T_i \left(a_{i1} + \frac{a_{i2}}{2} T_i + \frac{a_{i3}}{3} T_i^2 + \frac{a_{i4}}{4} T_i^3 + \frac{a_{i5}}{5} T_i^4 + \frac{a_{i6}}{T_i} \right) - \overline{h_i^o(T_{ref})} \qquad (17)$$

where:

T_i = temperature of species i

$\tilde{R}$ = universal gas constant = 8.314 kJ/kmol*K

$\overline{h_i^o(T_{ref})}$ = enthalpy of species i at a reference temperature of 298 K

The coefficients for each species i (a_i) for either a reactant or a product can be seen in the Table 3.1. These coefficients are also used in an entropy calculation discussed later in this thesis.

Table 3.1: Coefficients for enthalpy and entropy calculations [1]

Species	R/P	$a_{i\,1}$	$a_{i\,2}$	$a_{i\,3}$	$a_{i\,4}$	$a_{i\,5}$	$a_{i\,6}$	$a_{i\,7}$
CO_2	Product	4.46E+00	3.10E-03	-1.24E-06	2.27E-10	-1.55E-14	-4.90E+04	-9.86E-01
H_2O	Product	2.72E+00	2.95E-03	-8.02E-07	1.02E-10	-4.85E-15	-2.99E+04	6.63E+00
CO	Product	2.98E+00	1.49E-03	-5.79E-07	1.04E-10	-6.94E-15	-1.42E+04	6.35E+00
H_2	Product	3.10E+00	5.11E-04	5.26E-08	-3.49E-11	3.69E-15	-8.77E+02	-1.96E+00
O_2	Product	3.62E+00	7.36E-04	-1.97E-07	3.62E-11	-2.89E-15	-1.20E+03	3.62E+00
	Reactant	3.63E+00	-1.88E-03	7.06E-06	-6.76E-09	2.16E-12	-1.05E+03	4.31E+00
N_2	Product	2.90E+00	1.52E-03	-5.72E-07	9.98E-11	-6.52E-15	-9.06E+02	6.16E+00
	Reactant	3.67E+00	-1.21E-03	2.32E-06	-6.32E-10	-2.26E-13	-1.06E+03	2.36E+00

Since the previously discussed method is not valid for calculating $\overline{\Delta h_{C_xH_y}}$, the following equation was utilized.

$$\overline{\Delta h_{C_xH_y}} = c_p \left(MW_F \right)\left(T_{C_xH_y} - T_{ref} \right) \tag{18}$$

Due to the fact that chemical energy released only goes toward the output energy forms of power and heat transfer, a simple calculation of the following form is completed to determine the energy expelled via heat transfer.

$$\dot{Q}_{HT} - \dot{W}_B = \Delta H \quad \rightarrow \quad \dot{Q}_{HT} = \dot{W}_B + \Delta H \tag{19}$$

3.1.3.4 Sensible exhaust energy. Sensible exhaust energy, defined as the heat energy contained in the exhaust gas, is calculated using the exhaust gas concentrations and the enthalpy change that would occur if the exhaust gas temperature was reduced to

ambient. The previously determined enthalpy values are used in the following equation

to determine the energy difference between the current state and the ambient state.

$$\dot{E}_{SE} = \frac{\dot{m}_F}{MW_F}\left(H_P\left(T_{amb}\right) - H_P\left(T_{exh}\right)\right) = \frac{\dot{m}_F}{MW_F}\left(\sum_P n_i\left(\overline{h_f^o} + \overline{\Delta h\left(T_{amb}\right)}\right)_i - \sum_P n_i\left(\overline{h_f^o} + \overline{\Delta h\left(T_{exh}\right)}\right)_i\right)$$

$$(20)$$

where:

T_{amb} = ambient temperature T_{exh} = exhaust temperature

Since $\overline{\Delta h\left(T_{amb}\right)} = 0$, the previous equation simplifies to:

$$\dot{E}_{SE} = -\frac{\dot{m}_F}{MW_F}\left(\sum_P n_i\left(\overline{\Delta h\left(T_{exh}\right)}\right)\right) \tag{21}$$

$$\dot{E}_{SE} = -\frac{\dot{m}_F}{MW_F}\left(b\overline{\Delta h_{CO_2}} + c\overline{\Delta h_{H_2O}} + d\overline{\Delta h_{CO}} + e\overline{\Delta h_{H_2}} + f\overline{\Delta h_{O_2}} + g\overline{\Delta h_{N_2}}\right) \tag{22}$$

3.1.3.5 Chemical exhaust energy. Many of the energy balance analyses

discussed in the literature make the assumption of complete combustion. The extremely

rich mixtures (air-to-fuel ratios of $11 - 14$) inducted into the test engine make the

complete combustion assumption unacceptable for this investigation. Therefore, the final

output energy form to be calculated is chemical exhaust energy and is the energy expelled

in the exhaust due to incomplete combustion. Combustion efficiency is crucial to this

computation and is determined with the following equation:

$$\eta_C = \frac{\left[\sum_R n_i\overline{h_f^o} - \sum_P n_i\overline{h_f^o}\right]_{Actual}}{\left[\left(LHV\right)\left(MW\right)\right]_F} = \frac{\overline{h_{f_{C_xH_y}}^o} - b\overline{h_{f_{CO_2}}^o} - c\overline{h_{f_{H_2O}}^o} - d\overline{h_{f_{CO}}^o}}{\left[\left(LHV\right)\left(MW\right)\right]_F} \tag{23}$$

Once combustion efficiency is quantified, the amount of unburned fuel exhausted from

the engine is known which enables the chemical energy expelled to be calculated using

the following:

$$\dot{E}_{CE} = (1 - \eta_C)(\dot{m}_F)(LHV) \tag{24}$$

3.1.4. Energy Balance. The energy balance is then checked with the

following energy balance equation which was described previously.

$$\dot{E}_{FUEL} = \dot{W}_B - \dot{Q}_{HT} + \dot{E}_{SE} + \dot{E}_{CE} \tag{25}$$

The last computation to be completed is a quantification of first law efficiency. This

indicates how effectively chemical energy is converted to useful work and is computed

for each mode with a simple equation given below [5].

$$\eta_I = \frac{\dot{W}_B}{\dot{E}_{FUEL}} \tag{26}$$

Total efficiency for the engine is found by multiplying the weighting factors for

each mode, as shown in Table 2.2, by the respective efficiency then summing all modes.

This gives a single quantification that can be compared among different engine

configurations.

3.2. TYPICAL RESULTS AND CONCLUSIONS

The previously discussed energy balance analysis is compatible with small air-

cooled engines and has been applied to several sets of engine test data collected using the

test engine platform. This engine provides results typical of small industrial engines.

This discussion of results is initiated by showing energy distributions for the standard six-

mode cycle B test procedure (SAE J1088) used for small engine testing in Table 3.2.

Table 3.2: Typical energy balance values at each set point of the six-mode test

Typical Energy Balance Values						
Energy (kW)	Mode 1	Mode 2	Mode 3	Mode 4	Mode 5	Mode 6
Brake Power	16.12	11.81	7.83	4.35	2.87	0.16
Convective Heat Transfer	19.82	15.32	13.29	11.74	11.82	5.79
Sensible Exhaust Energy	19.28	14.73	11.46	8.99	8.46	2.08
Chemical Exhaust Energy	23.44	18.20	12.94	7.26	5.83	1.06
Total	**78.65**	**60.06**	**45.51**	**32.35**	**28.98**	**9.09**
Chemical Energy Supplied	78.55	60.01	45.51	32.36	28.99	9.10
First Law Efficiency (%)	20.53	19.68	17.21	13.44	9.88	1.80

One can see in Table 3.2 that, when all the output energy forms are added together, a value very close to the chemical energy supplied is attained. The difference is due to rounding errors in the calculation of each energy form. It can also be seen that the first law efficiency at each mode is quite low especially at the lower load and engine speed set points. Because of this, the weighted efficiency of the engine, 15.59%, is also very low. These metrics will be used to help quantify overall improvement in engine efficiency. Several beneficial observations can be drawn when all the output energy forms are taken as percentages of the chemical energy supplied. This is displayed in Figure 3.2 again in each mode of the six-mode test procedure.

Many of these output energy amounts are typical of small internal combustion engines, including the large amount lost to convective heat transfer at low engine speeds. Heat transfer increases at low speeds due to there being a much longer time interval between engine cycles which results in larger convective heat losses. One will also notice that, at high engine speed and load, roughly 30% of the chemical energy supplied is contained in the exhaust gases as chemical exhaust energy. This is due to the rich

mixture being inducted into the engine (low air-to-fuel ratios) resulting in incomplete combustion products being exhausted at these modes. This can be seen in Figure 3.3.

From these two charts, it is evident that air-to-fuel ratio has a direct correlation to the chemical exhaust energy. An increase in air-to-fuel ratio significantly reduces the chemical energy lost through the exhaust.
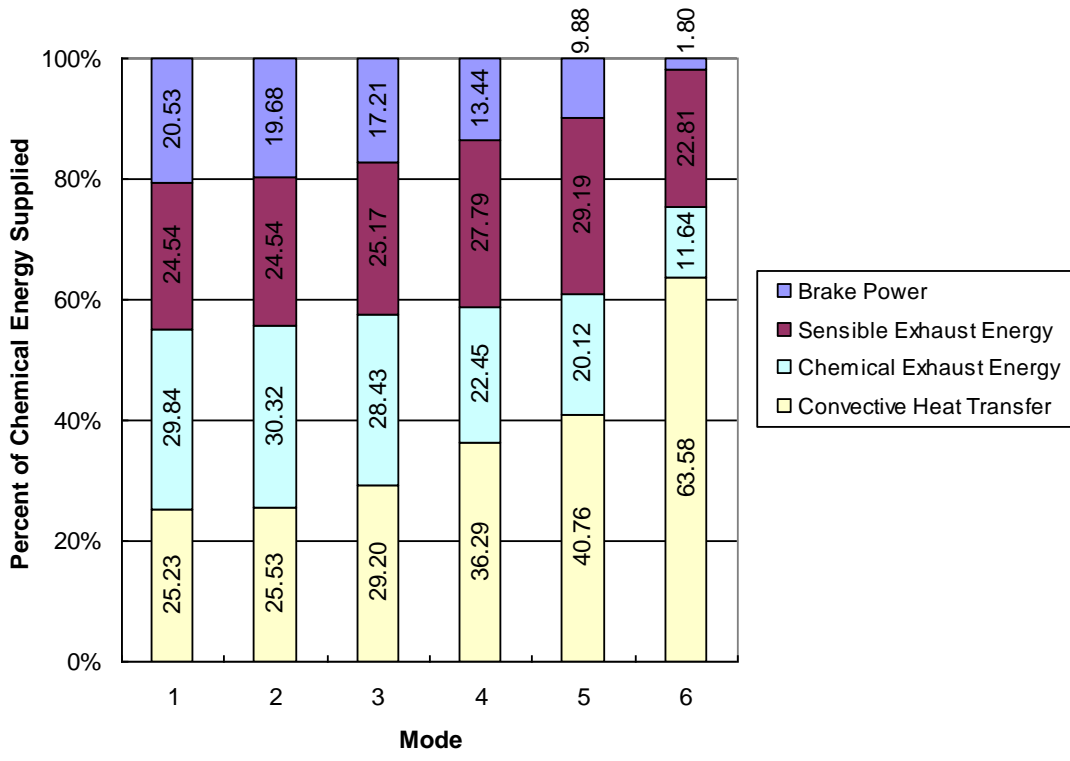
Figure 3.2: Energy balance results per mode
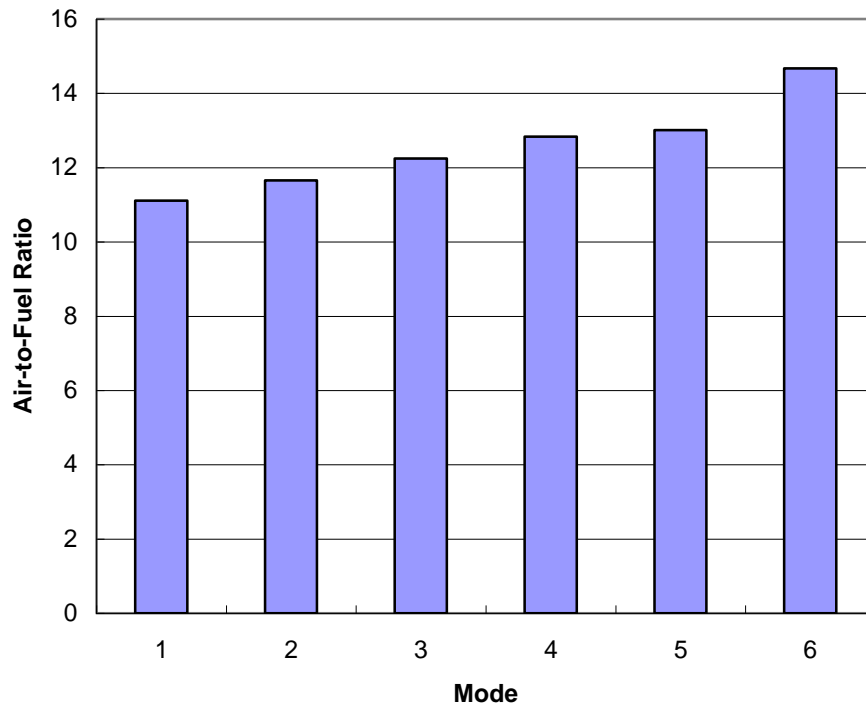
Figure 3.3: Air-to-fuel ratio per mode

These energy distributions are also plotted with respect to brake mean effective

pressure, BMEP, in Figure 3.4 which provides a slightly different picture. Brake mean

effective pressure is a normalized brake torque value that is independent of engine size.

This plot shows how the output energy forms are exchanged as BMEP or load is

increased. Several important observations can be made. Chemical exhaust energy varies

inversely with air-to-fuel ratio. As A/F moves towards a richer mixture, lower A/F, the

chemical exhaust energy increases. This is very obvious at high BMEP where the

majority of the output energy is composed of this chemical exhaust energy, the

incomplete combustion products discussed previously. Significant improvement in fuel

efficiency can be attained in this area by utilizing a leaner mixture. Additional

improvements in fuel efficiency may be realized at low BMEP where roughly 75% of the

fuel energy leaves the system through heat transfer and sensible exhaust energy. These

energy flows can be affected by combustion duration and phasing which can be

controlled by spark timing.

Figure 3.4: Output energy distributions plotted against BMEP

4. AVAILABILITY BALANCE – SECOND LAW

Upon completion of the previously discussed first law analysis, the second law of thermodynamics can be used to obtain different but also enormously valuable observations relating 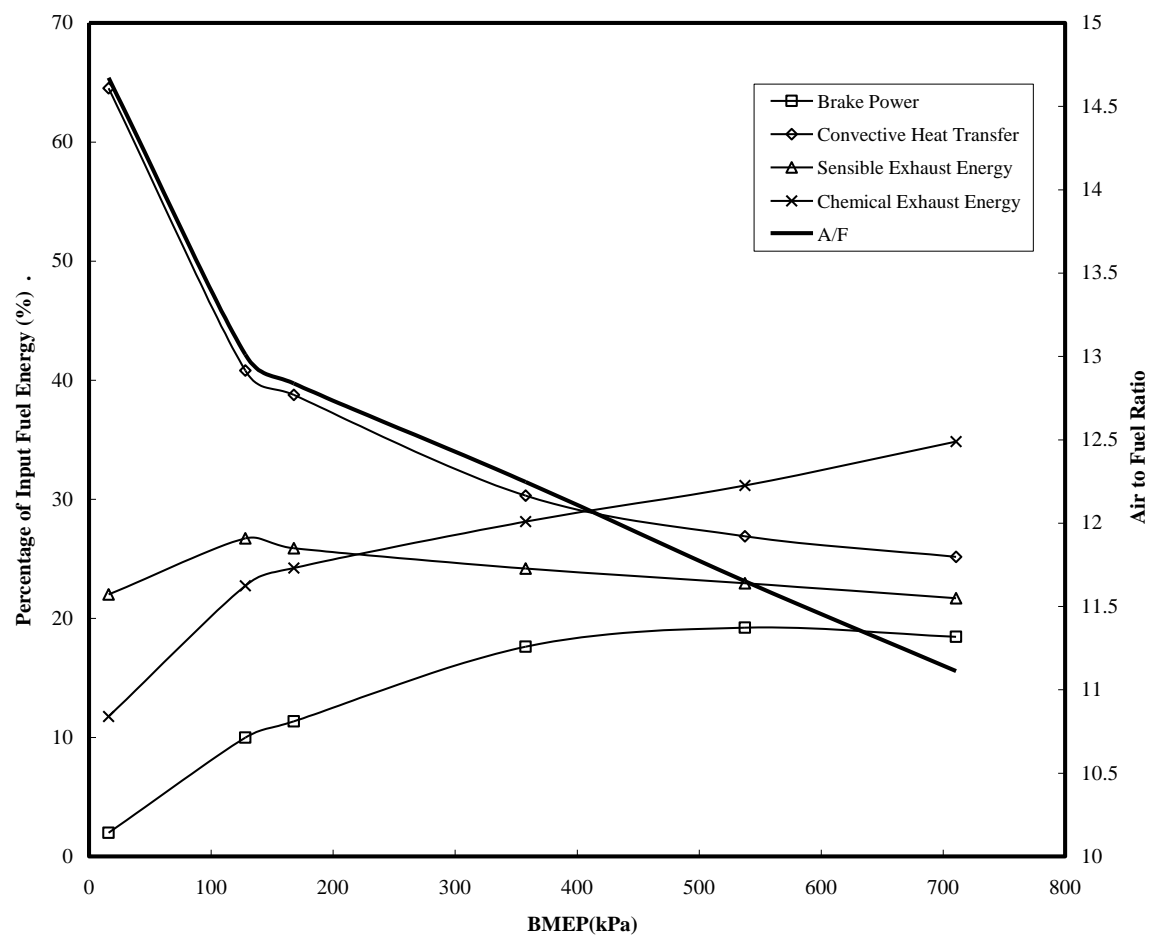to the combustion process occurring in an internal combustion engine. Several thermodynamic properties determined with the first law analysis, and required to complete the second law analysis, dictate that the analyses must be completed in this respective order. The major differences in the two methods lie in the fact that the first law merely reports the energy distributions but does not differentiate between the heat and work energy forms. Each output energy form is treated equivalently on an energy basis and no information is provided giving the usefulness of each energy form [7]. The second law analysis incorporates the quality of energy aspect by determining the capability of each output energy form to produce useful work [7], also known as energy availability. This provides a more accurate quantification when determining where, and in what relative amounts, efficiency gains can be attained. Unlike the first law, the second law also identifies the irreversibilities inherent in the system, most important of which are due to combustion and heat transfer [8].

4.1. CONCEPT DESCRIPTION

Just like energy is the primary metric in the first law analysis, availability is the parameter of interest for the second law analysis. Availability is defined as the maximum useful work that can be produced as the system is brought reversibly to thermal, mechanical, and chemical equilibrium with its environment [8]. Availability, also known as exergy, is dependent upon the state of the system as well as the properties of the

environment. Several availability outputs, designated A_x, are determined in this investigation and use specific availability for their calculation. Specific availability, a, is simply the mass specific availability and carries the units kJ/kg.

4.2. CODE DESCRIPTION

The second law approach utilized for this investigation uses an availability balance, similar to the energy balance previously discussed, which accounts for all different input and output availability forms. By using the availability balance, the distributions of availability as well as the quantification of each form can easily be compared to energy balance results and availability results taken from different engine configurations. The balance can be found in [5] and is given below in rate (kW) notation.

$$\dot{A}_{INT} + \dot{A}_{FUEL} = \dot{A}_B + \dot{A}_{HT} + \dot{A}_{EX} + \dot{A}_{CE} + \dot{A}_{LOSS} \tag{27}$$

One will notice that many of the availability inputs and outputs occur in the same forms as in the energy balance. These terms are:

$\dot{A}_{FUEL}$ = fuel chemical availability supplied $\qquad$ $\dot{A}_B$ = brake power availability

$\dot{A}_{HT}$ = heat transfer availability $\qquad$ $\dot{A}_{CE}$ = chemical exhaust availability

The remaining terms that are somewhat different than in the previous analysis include:

$\dot{A}_{INT}$ = intake flow availability $\qquad$ $\dot{A}_{EX}$ = exhaust flow availability

$\dot{A}_{LOSS}$ = availability destroyed

The meaning and means of computation behind all these availability balance terms is provided in the following paragraphs.

4.2.1. Fuel Chemical Availability. Fuel chemical availability is defined as the work potential of the fuel being inducted into the engine. This is not the charge mixture, as air will be accounted for later. The following equation was formulated from [9] and [10] and used to calculate fuel chemical availability.

$$\dot{A}_{FUEL,CH} = \dot{m}_F \left(a_{FUEL,CH} \right) \tag{28}$$

Since fuel chemical specific availability, $a_{FUEL,CH}$, is not a typically known value, it must be calculated with the following equation [6] for fuel C_xH_y:

$$a_{FUEL,CH} = LHV \left(1.04224 + 0.011925 \left(\frac{y}{x} \right) - \frac{0.042}{x} \right) \tag{29}$$

This equation has been deemed accurate only for liquid fuels that are sulfur free.

4.2.2. Flow Availability. The availability balance equation incorporates two separate types of flow availability; one for the intake and one for the exhaust. Flow availability can be defined as the availability associated with mass flows across a boundary [11] and is comprised of two parts. One part accounts for the available energy of a component due to a temperature difference between the component and the environment (ambient). The enthalpy computation utilized to complete the energy balance is also used to determine this part of flow availability. The remaining portion of flow availability comes from the actual mass flow, or movement, of a component. Entropy is the parameter used to quantify this portion. For flows out of the system, the flowing matter is the cylinder contents. For flows into the system, the flowing matter is the fuel and air taken at the measured intake temperature [12].

Specific availability of flows is the primary calculation that must be completed in order to determine flow availability. The following generic equation, developed from [5], was used to find the specific availability of flow across any boundary of the system.

$$a_i = x_i \left[\left(H_i - H_{io} \right) - T_o \left(\overline{s}_i - \overline{s}_{io} \right) \right] \tag{30}$$

where:

$$x_i = \text{mole fraction of species } i$$

$$T_o = \text{temperature of the dead state} = 298.15 \text{ K } [6]$$

$$H_{io} = \text{enthalpy of species } i \text{ at the dead state}$$

$$\overline{s}_{io} = \text{entropy of species } i \text{ at the dead state}$$

Equation 30 can be simplified with the following expression.

$$H_i = \left(\overline{h}_f^o + \Delta \overline{h} \right)_i \tag{31}$$

$$H_i - H_{io} = \left(\overline{h}_f^o + \Delta \overline{h} - \overline{h}_{fo}^o - \Delta \overline{h}_o \right)_i = \left(\Delta \overline{h} - \Delta \overline{h}_o \right)_i \tag{32}$$

Since the enthalpy reference temperature is equal to 298.15 K which is also equal to the temperature of the dead state, $\Delta \overline{h}_o = 0$. Taking all this into account, the simplified form of Equation 30 can then be seen as:

$$a_i = x_i \left[\Delta \overline{h}_i - T_o \left(\overline{s}_i - \overline{s}_{io} \right) \right] \tag{33}$$

Specific availability calculated with Equation 33 is in units of kJ/kmol fuel. To obtain the desired units of kJ/kg, the molecular weight of fuel, MW_F, is used in the following manner.

$$a_i = \frac{x_i}{MW_F} \left[\Delta \overline{h}_i - T_o \left(\overline{s}_i - \overline{s}_{io} \right) \right] \tag{34}$$

The methods for making the enthalpy determinations for each species i have been described in the first law discussion that precedes this one. An empirical formula, found in [1], similar to the enthalpy formula (Equation 17) was used to calculate the entropy values required by Equation 34. A simplification of the entropy terms as well as the equation used to calculate the change in entropy can be seen below.

$$\overline{s_i} - \overline{s_{io}} = \Delta \overline{s_i} \tag{35}$$

$$\Delta \overline{s_i} = \tilde{R} \left(a_{i1} \ln(T_i) + a_{i2}T_i + \frac{a_{i3}}{2}T_i^2 + \frac{a_{i4}}{3}T_i^3 + \frac{a_{i5}}{4}T_i^4 + a_{i7} \right) - \overline{s_{io}} \tag{36}$$

where:

T_i = temperature of species i

$\tilde{R}$ = universal gas constant = 8.314 kJ/kmol*K

The coefficients for each species i (a_i) for either a reactant or a product are found in Table 3.1 which was given previously. As mentioned before, in order to use these coefficients in this empirical formula one must make the assumption that the pressure of each species, P_i, is equal to P_o, the pressure of the standard atmosphere (1.01325 bar) [6].

Since the empirical method for entropy calculation is only valid for CO_2, H_2O, CO, H_2, O_2, and N_2, a separate computation must be completed to determine the entropy change of the fuel, C_xH_y. A commonly used thermodynamic equation was utilized to quantify $\Delta \overline{s_{C_xH_y}}$.

$$\Delta \overline{s_{C_xH_y}} = MW_F \left(c_p \ln\left(\frac{T_i}{T_o}\right) - R \ln\left(\frac{P_i}{P_o}\right) \right) \tag{37}$$

Continuing with the assumption that $P_i = P_o$, Equation 37 simplifies to the following.

$$\Delta \overline{s_{C_xH_y}} = MW_F \left(c_p \ln\left(\frac{T_i}{T_o}\right) \right) \tag{38}$$

Equations 37 and 38 are formulated from the ideal gas law. In order to use such a relation for the flow availability computation, it is assumed that the fuel is in a gaseous phase. Much of the literature supports this assumption. In the analyses by Heywood [1] and Caton [9, 10, 12, 13], it is stated that the fuel is completely vaporized. Other sources simply state that the working fluid is an ideal gas [6, 7, 14, 15]. This assumption can also be validated by the fact that the vast majority of the fuel is atomized as it is pulled into the airstream at the carburetor. It then travels along the intake manifold where conduction from the warm engine will vaporize fuel which still remains in liquid phase. Due to this reasoning, a phase change of fuel is irrelevant for the flow availability computation.

4.2.2.1 Intake flow availability. Once the general form of the specific availability of flows equation is known, it can be applied to the intake stream to compute the specific availability of the intake flow. Since there are multiple species contained in the intake charge, the specific availability of each component must be calculated separately. Fuel flow specific availability is found with Equation 39 below,

$$a_F = a_{C_xH_y} = \frac{x_{C_xH_y}}{MW_F}\left[\Delta\overline{h_{C_xH_y}} - T_o\left(\overline{s_{C_xH_y}} - \overline{s_{C_xH_y,o}}\right)\right] \tag{39}$$

while air (two separate species) is computed with the following equation.

$$a_A = a_{O_2} + a_{N_2} = \frac{x_{O_2}}{MW_F}\left[\Delta\overline{h_{O_2}} - T_o\left(\overline{s_{O_2}} - \overline{s_{O_2,o}}\right)\right] + \frac{x_{N_2}}{MW_F}\left[\Delta\overline{h_{N_2}} - T_o\left(\overline{s_{N_2}} - \overline{s_{N_2,o}}\right)\right]$$

$$\tag{40}$$

Flow availability is then determined by combining the components in the following manner.

$$\dot{A}_{INT} = \dot{m}_F \left(a_F \right) + \dot{m}_A \left(a_A \right)$$ (41)

4.2.2.2 Exhaust flow availability. As previously mentioned, exhaust flow availability is defined as the available energy due to mass flow of the exhaust gas across the system boundary. Equation 34 was used as a template to generate a formula capable of quantifying the exhaust specific availability of flows. This is supplied below as the summation of the specific availability of each species contained in the exhaust stream.

$$
\begin{aligned}
a_{EX} &= a_{CO_2} + a_{H_2O} + a_{CO} + a_{H_2} + a_{O_2} + a_{N_2} \\
&= \frac{1}{MW_F}
\begin{bmatrix}
x_{CO_2} \left(\Delta \overline{h_{CO_2}} - T_o \left(\overline{s_{CO_2}} - \overline{s_{CO_2,o}} \right) \right) + x_{H_2O} \left(\Delta \overline{h_{H_2O}} - T_o \left(\overline{s_{H_2O}} - \overline{s_{H_2O,o}} \right) \right) + \\
x_{CO} \left(\Delta \overline{h_{CO}} - T_o \left(\overline{s_{CO}} - \overline{s_{CO,o}} \right) \right) + x_{H_2} \left(\Delta \overline{h_{H_2}} - T_o \left(\overline{s_{H_2}} - \overline{s_{H_2,o}} \right) \right) + \\
x_{O_2} \left(\Delta \overline{h_{O_2}} - T_o \left(\overline{s_{O_2}} - \overline{s_{O_2,o}} \right) \right) + x_{N_2} \left(\Delta \overline{h_{N_2}} - T_o \left(\overline{s_{N_2}} - \overline{s_{N_2,o}} \right) \right)
\end{bmatrix}
\end{aligned}
$$

(42)

Exhaust flow availability is then determined by using Equation 42 and the mass flow of the exhaust gases. This mass flow is not known but can be approximated as the sum of the mass flow of air and the mass flow of fuel with the knowledge that mass is conserved.

$$\dot{A}_{EX} = \left(\dot{m}_F + \dot{m}_A \right) a_{EX}$$ (43)

The intake and exhaust flow availability equations can be found in [5].

4.2.3. Brake Power Availability. The simplest of the output availability forms to be computed is brake power availability. Since availability has been defined as the capability of an energy form to produce useful work, it can be accurately assumed that all of the energy contained in the brake power measurement is available for useful work.

Therefore, from [5], brake power is determined to be equal to the brake power availability.

4.2.4. Heat Transfer Availability. The availability contained in heat transfer from the engine can be computed by using heat transfer energy $\left(\dot{Q}_{HT} \right)$ from the first law analysis in the equation below taken from [5].

$$\dot{A}_{HT} = \dot{Q}_{HT} \left(1 - \frac{T_o}{T_{oil}} \right) \quad (44)$$

where:

$T_{oil} = $ engine oil temperature

$T_o = $ temperature of the dead state $= 298.15$ K [6]

Since this is a convective heat transfer problem, the temperature measure of interest is one that quantifies the average temperature of the engine from which heat transfer occurs. Oil temperature is a logical parameter to use for this due to the fact that it will reach a near equilibrium state with the average temperatures of the hot engine surfaces. The use of oil temperature for this calculation is validated by installing a type K thermocouple on the engine surface near the combustion chamber of cylinder 1. Typical engine oil and surface temperatures can be seen in Table 4.1.

Table 4.1: Typical engine oil and surface temperature measurements

Mode	1	2	3	4	5	6
Oil (°F)	214	253	241	235	226	224
Surface (°F)	230	228	215	208	203	207

There exists a fairly constant difference between the two temperature measurements that decreases slightly at mode 6. This is due to the cooling fan moving at a much slower speed resulting in less cooling air moving over the thermocouple which allows it to read a more accurate surface temperature. Heat transfer availability calculations are completed with both of these temperature parameters. The maximum difference in results from the two methods is approximately 1.5% when the results are viewed as percentages of supplied availability. Due to this negligible difference in results and the engine speed dependence of the surface temperature, oil temperature is used for the computation of heat transfer availability.

4.2.5. Chemical Exhaust Availability. The chemical availability found in incomplete combustion products can be determined two different ways. The first method uses several previously calculated values in a relatively simple computation. Similar to the calculation of $\dot{E}_{CE}$, the amount of unburned fuel exhausted from the engine is determined with combustion efficiency (from Equation 23) and mass fuel flow. Availability is then computed with the fuel chemical specific availability value attained from Equation 29.

$$\dot{A}_{CE} = \dot{m}_F \left(1 - \eta_C\right) a_{FUEL,CH} \qquad (45)$$

The second method uses information about the energy-containing components of the exhaust that are measured in the engine tests. These components are CO and unburned hydrocarbons (uHC) where uHC is calibrated to propane, C_3H_8. First, the chemical specific availability of the exhaust is found with the following equation.

$$a_{EX,CH} = x_{uHC} a_{uHC,CH} + x_{CO} a_{CO,CH} \qquad (46)$$

where:

$$x_i = \text{mole fraction of species } i$$

$$a_{uHC,CH} = \text{chemical specific availability of uHC} = a_{C_3H_8} = 47{,}100 \text{ kJ/kg [13]}$$

$$a_{CO,CH} = \text{chemical specific availability of CO} = 9{,}180 \text{ kJ/kg [13]}$$

Specific availability is then used in the equation given next in order to calculate the chemical exhaust availability.

$$\dot{A}_{CE} = \left(\dot{m}_A + \dot{m}_F \right) a_{EX,CH} \tag{47}$$

The second method described is a more accurate approach than the alternative due to the fact that it is based on the energy available in measured exhaust species. It also does not assume that all the chemical exhaust availability is in the form of the fuel being inducted into the engine. For these reasons, the second method is used in the availability balance but the first method is included in the code as a check.

4.2.6. Availability Destroyed. Due to the fact that availability is not a conserved property, irreversibilities in a system can be quantified with a second law analysis. The vast majority of these irreversibilities are caused by heat transfer and combustion processes [8]. In order to complete this availability balance approach, these irreversibilities are quantified by the availability destroyed term, $\dot{A}_{LOSS}$. The equations used for the calculation of this term can be found in [5].

A new parameter, $\dot{W}_{B,MAX}$, is used in this computation and is defined as the maximum brake power that can be extracted from the system [5]. It accounts for all the available energy entering and leaving the system as seen below.

$$\dot{W}_{B,MAX} = \dot{A}_{FUEL} + \dot{A}_{HT} + \dot{A}_{INT} - \dot{A}_{EX} - \dot{A}_{CE} \tag{48}$$

Maximum brake power is then used with measured brake power to determine the availability destroyed.

$$\dot{A}_{LOSS} = \dot{W}_{B,MAX} - \dot{W}_B \qquad (49)$$

4.2.7. Availability Balance. The second law analysis code is concluded with the completion of the availability balance using Equation 27 described above. Additionally, the second law efficiency is determined. This is useful for indicating the relative loss of useful work due to irreversibilities in the system [5].

$$\eta_{II} = \frac{\dot{W}_B}{\dot{W}_{B,MAX}} \qquad (50)$$

Total second law efficiency for the engine is found by multiplying the weighting factors for each mode by the respective efficiency then summing all modes.

4.3. TYPICAL RESULTS AND CONCLUSIONS

This availability balance has been applied to the same test data sets as the energy balance analysis. Typical results are included in this discussion, Table 4.2, and are displayed in the same manner that the energy balance results are to provide ease of comparison.

In Table 4.2, raw availability values (kW) can be seen for each of the six modes of the test procedure. The intake flow availability and fuel chemical availability are summed so they can be displayed as a single term, availability supplied. The results can then be verified with the application of Equation 27 which shows that the summation of all the output availability forms returns a number approximately equal to the availability supplied. Any slight deviation is due to several assumptions that were made and

rounding errors in the code itself. One will also notice the trend of decreasing availability with decreasing engine speed and load which is due to less availability being inducted, converted, and expelled from the engine. The results obtained for availability destroyed agree very well with those reported by Alkidas in [5]. The remaining availability forms are somewhat different due to the fact that Alkidas assumes complete combustion in his analysis. This investigation does not make the same assumption. Furthermore, the test engine utilized for this thesis operates with an extremely rich air-to-fuel ratio, resulting in significant chemical exhaust availabilities. The presence of this additional availability form, not included by other investigations, is the cause of the differences in availability distributions.

Table 4.2: Typical availability balance values at each set point of the six-mode test

Typical Availability Balance Values						
Availability (kW)	Mode 1	Mode 2	Mode 3	Mode 4	Mode 5	Mode 6
Convective Heat Transfer	4.08	3.67	3.04	2.51	2.45	1.20
Exhaust Flow	2.65	2.03	1.58	1.27	1.21	0.26
Brake Power	16.12	11.81	7.83	4.35	2.87	0.16
Chemical Exhaust	24.81	19.26	13.69	7.69	6.17	1.12
Availability Destroyed	41.52	31.51	25.30	20.03	19.17	7.00
Total	**89.19**	**68.28**	**51.44**	**35.85**	**31.87**	**9.75**
Availability Supplied	83.14	63.51	48.17	34.25	30.69	9.63
Second Law Efficiency (%)	27.97	27.27	23.64	17.84	13.00	2.29

The second law efficiencies for each mode can also be seen in Table 4.2. These, when averaged using the six-mode weights, result in a total second law efficiency of 21.2%. These efficiencies, although larger than the first law counterparts, are very low which indicates that a large portion of the supplied availability is lost due to

irreversibilities. This is evidenced by the large availability destroyed values in Table 4.2 and the availability destroyed percent distributions found in Figure 4.1 below. The fact that the second law efficiencies are slightly larger than the first law efficiencies show that, although much efficiency can be gained by more completely converting and using the input energy, these gains will be smaller than predicted by the first law. The reason for this is that only a portion of this "unused" energy is actually available for useful work. The portion of each energy form that is unavailable for work production is accounted for as availability destroyed in the second law analysis but is grouped into each respective energy form in the first law analysis. Second law efficiency values will be used to quantify overall improvements when the engine configuration is changed.

A somewhat different view of the availability values can be seen below where each availability output is displayed as a percent of availability supplied. This is shown in Figure 4.1. When this figure is used in conjunction with Table 4.2, a complete picture of the availability distributions can be obtained. The same trends found in Figure 3.2 from the energy balance are evident in Figure 4.1. These include increasing heat transfer availability and decreasing chemical exhaust availability with decreasing load and engine speed. The quantities of heat transfer and chemical exhaust availability are much lower than their corresponding first law (energy) values. This tells us that a large portion of the energy in these forms is lost and less useful work can be gained by minimizing these terms than expected from the energy balance analysis. Exhaust flow availability contributes a negligible amount to total availability. The largest portion of supplied availability is lost due to irreversibilities, seen in the availability destroyed term. Most of these irreversibilities are a result of combustion, specifically the mixing and heat transfer

that occurs between the burned and unburned components in the chemical reactions. This will be a major focus for extracting more useful work at all set points of engine operation since the availability gained through the reduction of irreversibilites will be redistributed to other availability forms.
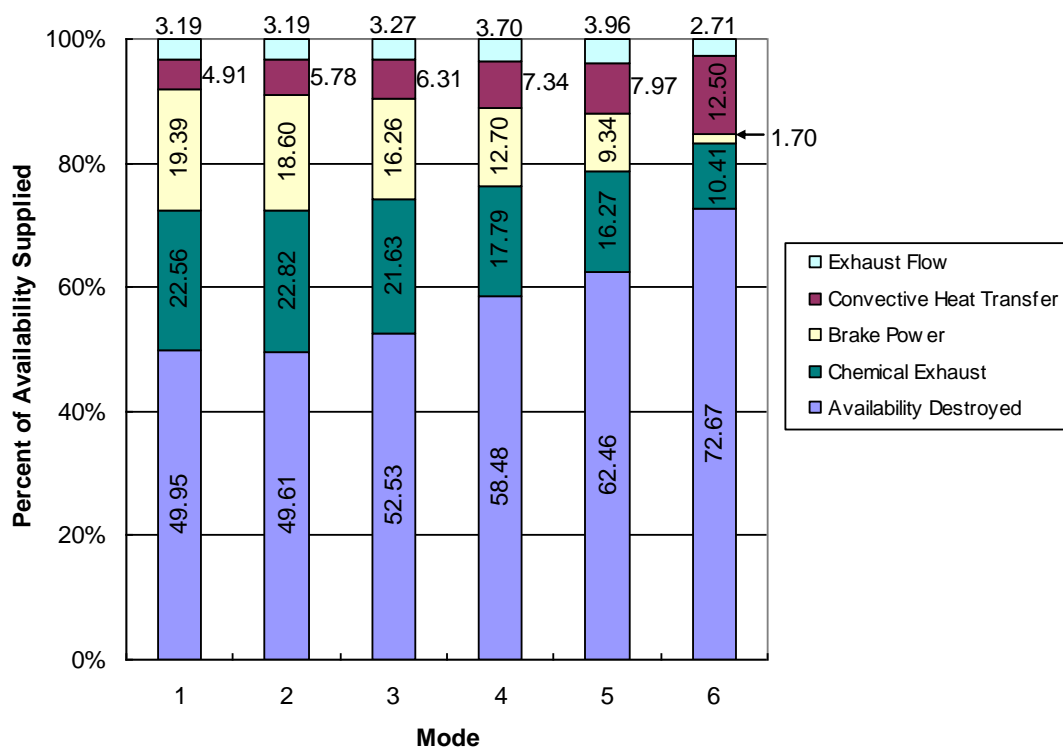
Figure 4.1: Availability balance results per mode

The variations in availability distributions with changing engine load are also shown in Figure 4.2. This chart displays the output availability forms in relation to BMEP. The most notable observation to be made is the large increase in availability destroyed as load is decreased. This is a result of slightly lower combustion temperatures and pressures as load is decreased. Decreasing combustion pressure with decreasing load can very easily be seen in cylinder pressure data collected on many engine test setups.

The increase in availability destroyed is also caused by inappropriate combustion phasing and duration seen at low loads and must be combated with variations in spark timing.
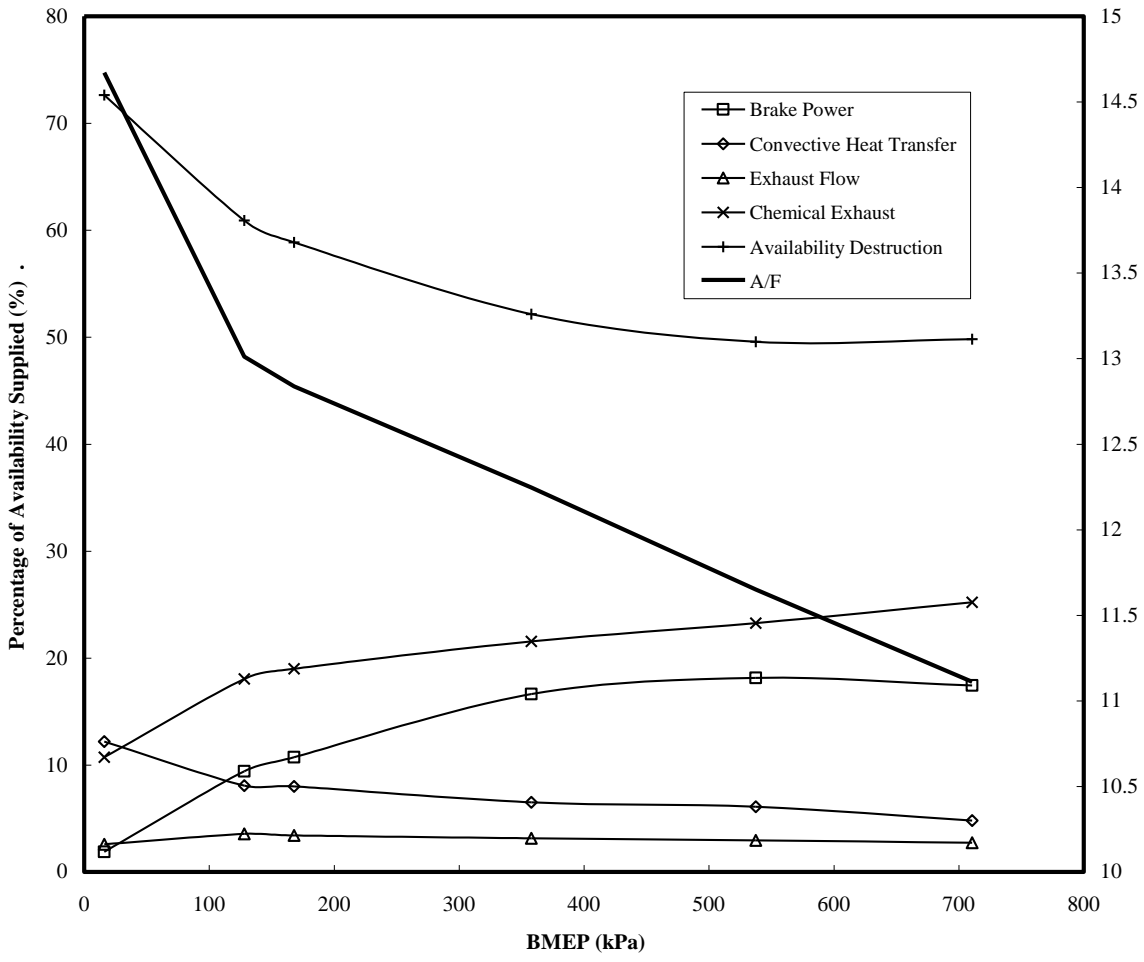
Figure 4.2: Output availability distributions plotted against BMEP

5. ENGINE BASE SPARK TIMING

5.1. NOMINAL VALUES

Before varying the spark timing on the test engine, the starting point, or stock configuration must be determined. The stock configuration, also called base spark timing in this discussion, is reported for the six engine operating set points defined in the Six-Mode test procedure. This was achieved with the use of a timing light whose sensor is placed on the spark plug wire of the cylinder being investigated. The strobe of the timing light is then pointed at an optical sensor whose signal is routed into the data acquisition system. This allows for crank angle resolved spark signal data as well as the normal crank angle resolved cylinder and intake manifold pressure data. This method provides reasonably accurate crank angle values for the initiation of ignition and shows any trends that may be present as engine speed and load are increased. The timing in degrees before top dead center (BTDC) acquired from this test is given in Table 5.1.

Table 5.1: Base spark timing for the test engine at each set point of the six-mode test

Mode	1	2	3	4	5	6
Cylinder 1 (°BTDC)	19	19	19	19	19	20
Cylinder 2 (°BTDC)	19	19	19.5	19.5	19.5	20

This engine uses a solid state ignition system and permanent magnets mounted on the flywheel which maintains nearly constant ignition timing regardless of engine speed or load. This nominal value is approximately 19° BTDC. Because of the different rate of motion of the magnets past the coils at different engine speeds, the discharge and hence spark timing changes slightly at different engine speeds. This can be seen in Table 5.1 as

the spark timing values, in degrees BTDC, appear to slightly retard with increasing engine speed. In order to attain optimum fuel efficiency and engine performance, peak cylinder pressure and mass fraction burned values need to occur at the appropriate times in the engine cycle. This is achieved by advancing the ignition timing as engine speed is increased which can be done with a variable spark timing system.

5.2. DISPERSION ANALYSIS

The dispersion of spark timing values is also investigated. Again, spark timing values are gathered with a timing light and optical sensor. All the spark timing values acquired during an engine performance test and the frequency of those values can be seen in Figures 5.2 – 5.5 which follow this discussion. Each separate chart displays the spark timing dispersions for different modes. It is made evident in these figures that there exists a reasonably tight dispersion of spark timing values at certain modes (0.5 CAD) and much wider dispersions at others (1.5 CAD). The wider dispersions are much more evident for cylinder 2 than for cylinder 1. This can also be seen in the following figures.

Due to the nature of the stock spark timing system utilized on this engine, there are two spark plug discharges for every engine cycle. This means that one spark occurs during the compression stroke and results in combustion. The other occurs during the exhaust stroke and is essentially a wasted spark. This is displayed in Figure 5.1 below in relation to cylinder pressure. Since only the "fired" sparks are applicable to engine performance comparisons, the dispersion of these "fired" values is also examined. These results are included, in Figures 5.6 – 5.9, below in the same manner as the previously reported spark timing results. One will notice that the dispersions are very similar to the

results taken with all the spark occurrences verifying that including the wasted spark timings in a dispersion analysis does not negatively affect the accuracy.
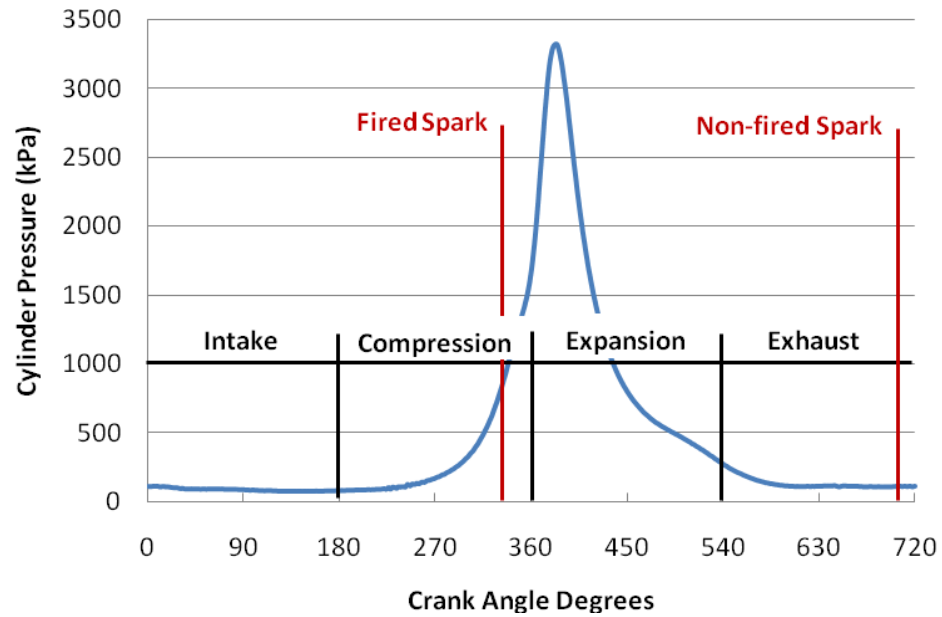
Figure 5.1: Spark event and cylinder process diagram
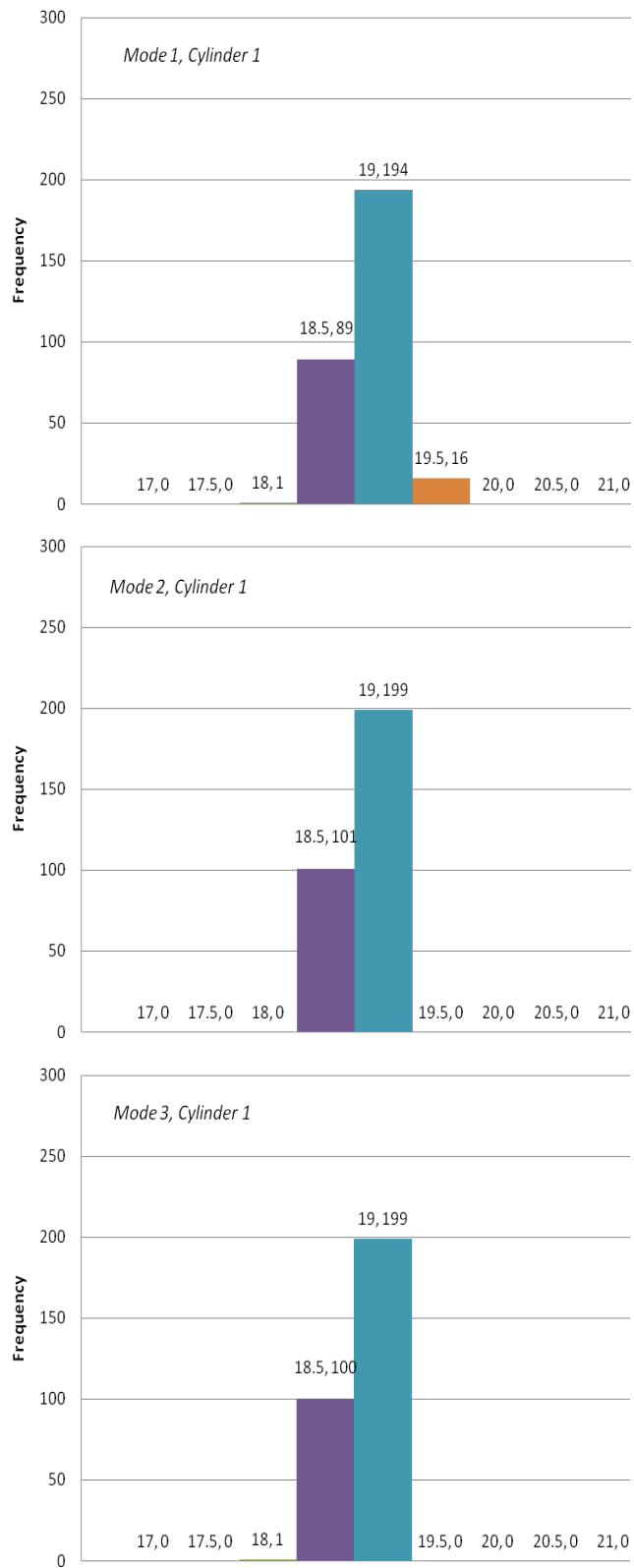
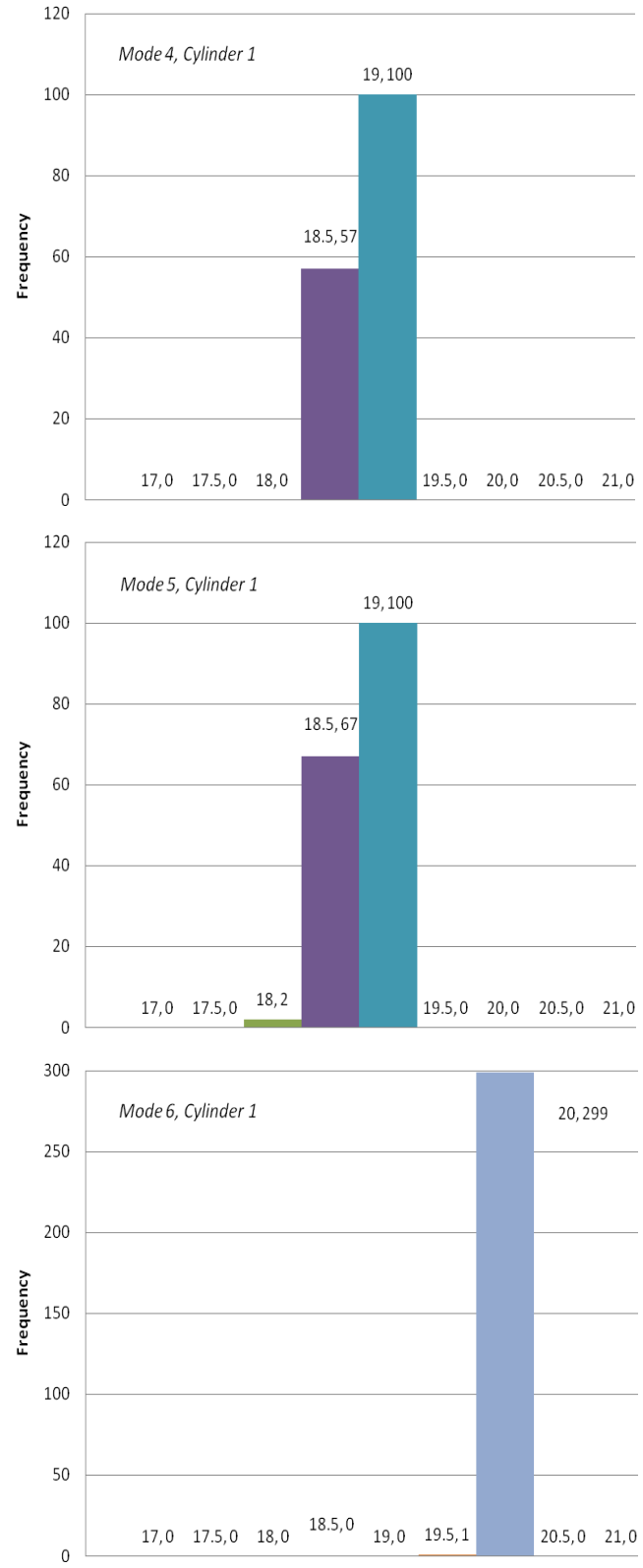**Figure 5.2:** Cylinder 1 spark timing dispersions for modes 1 through 3
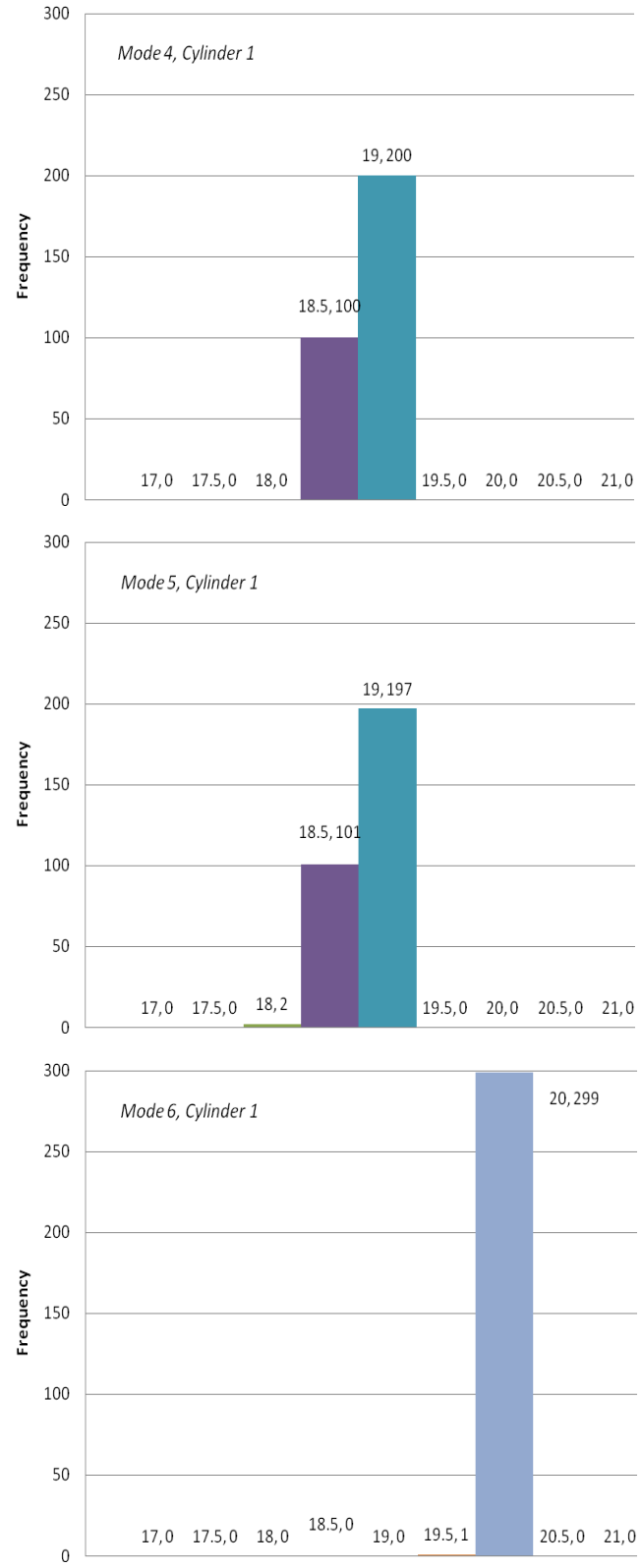
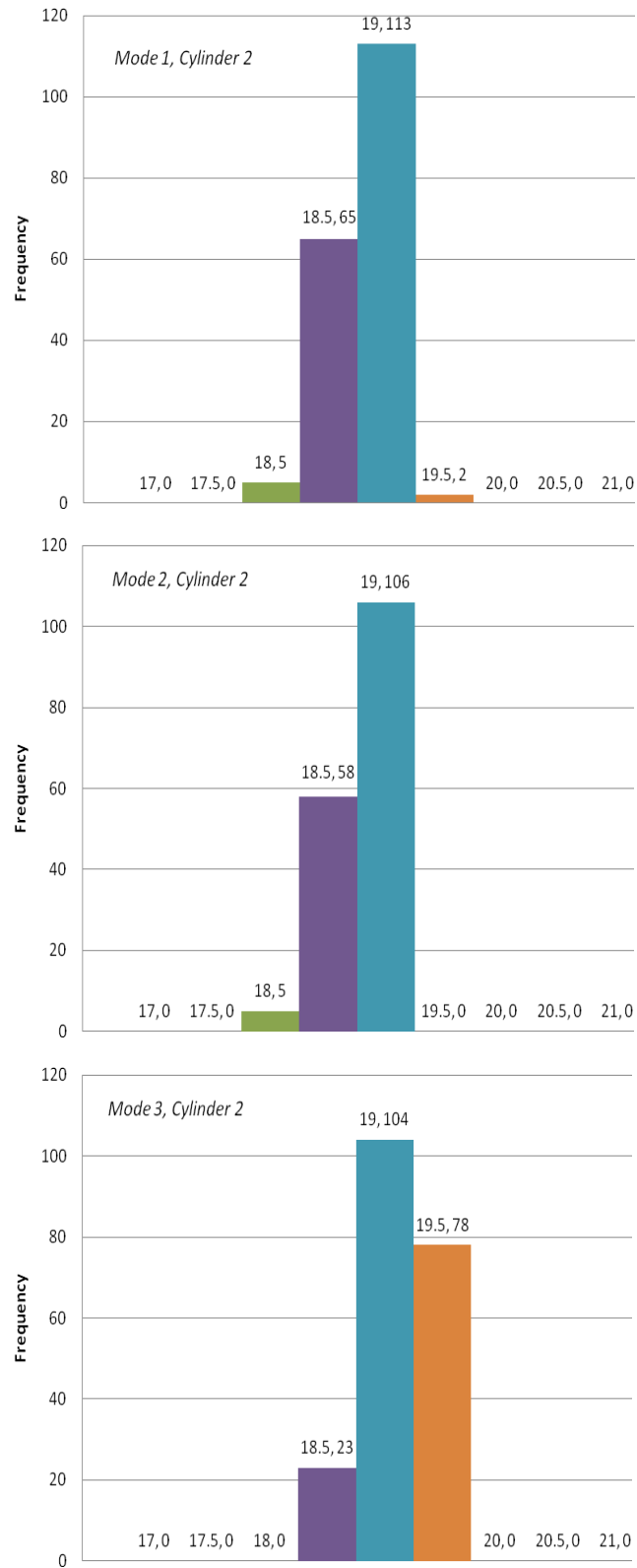**Figure 5.3:** Cylinder 1 spark timing dispersions for modes 4 through 6
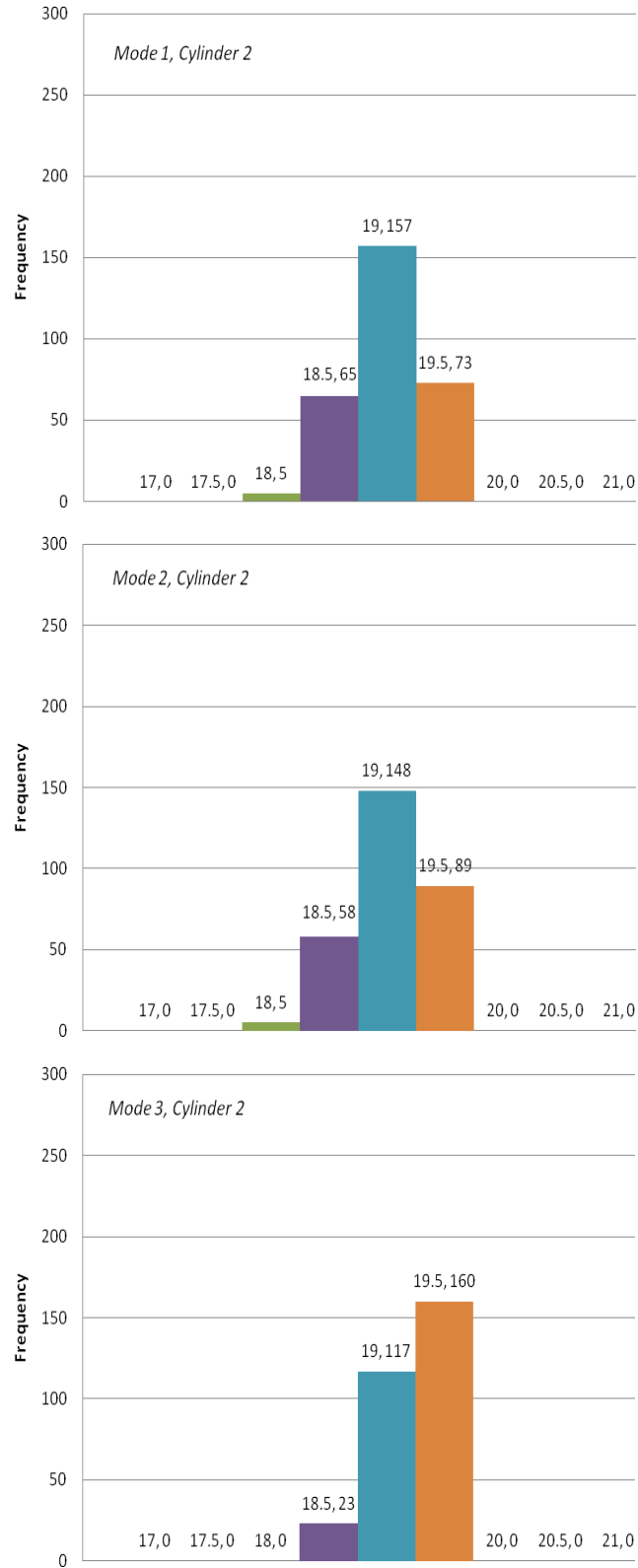
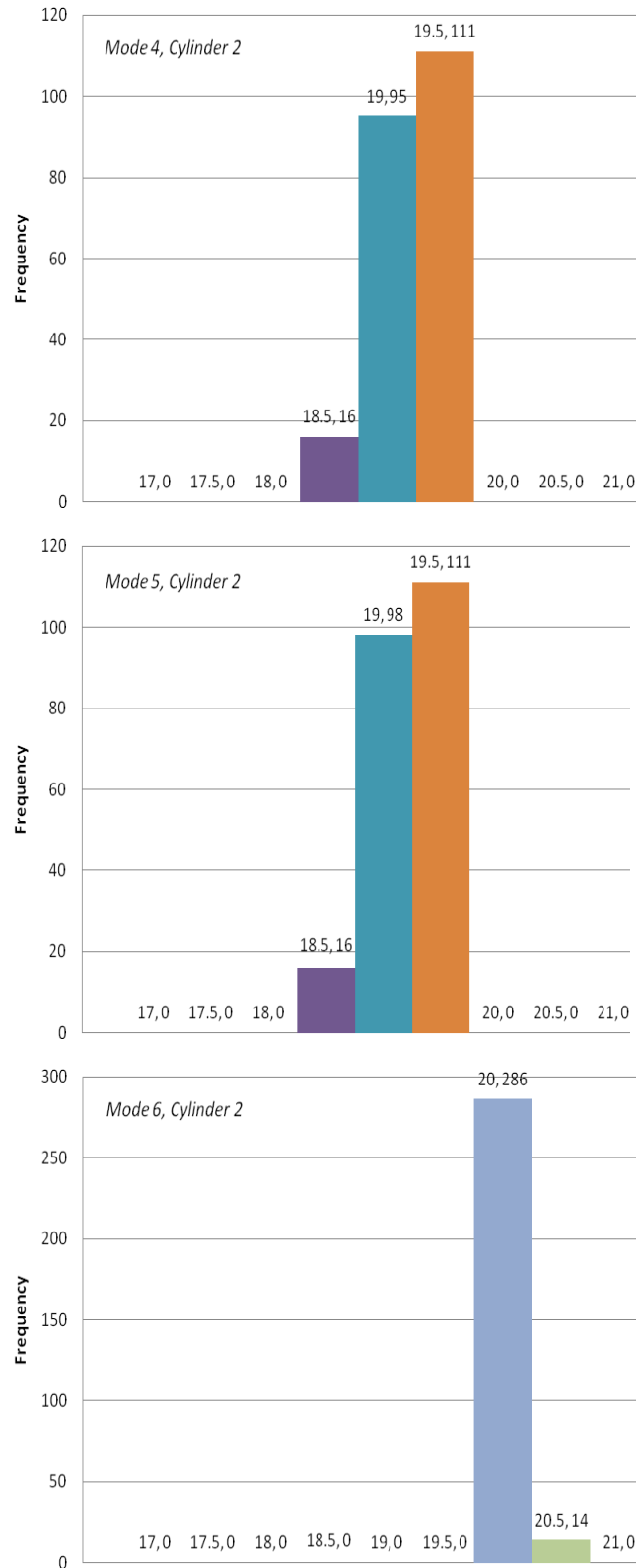**Figure 5.4:** Cylinder 2 spark timing dispersions for modes 1 through 3
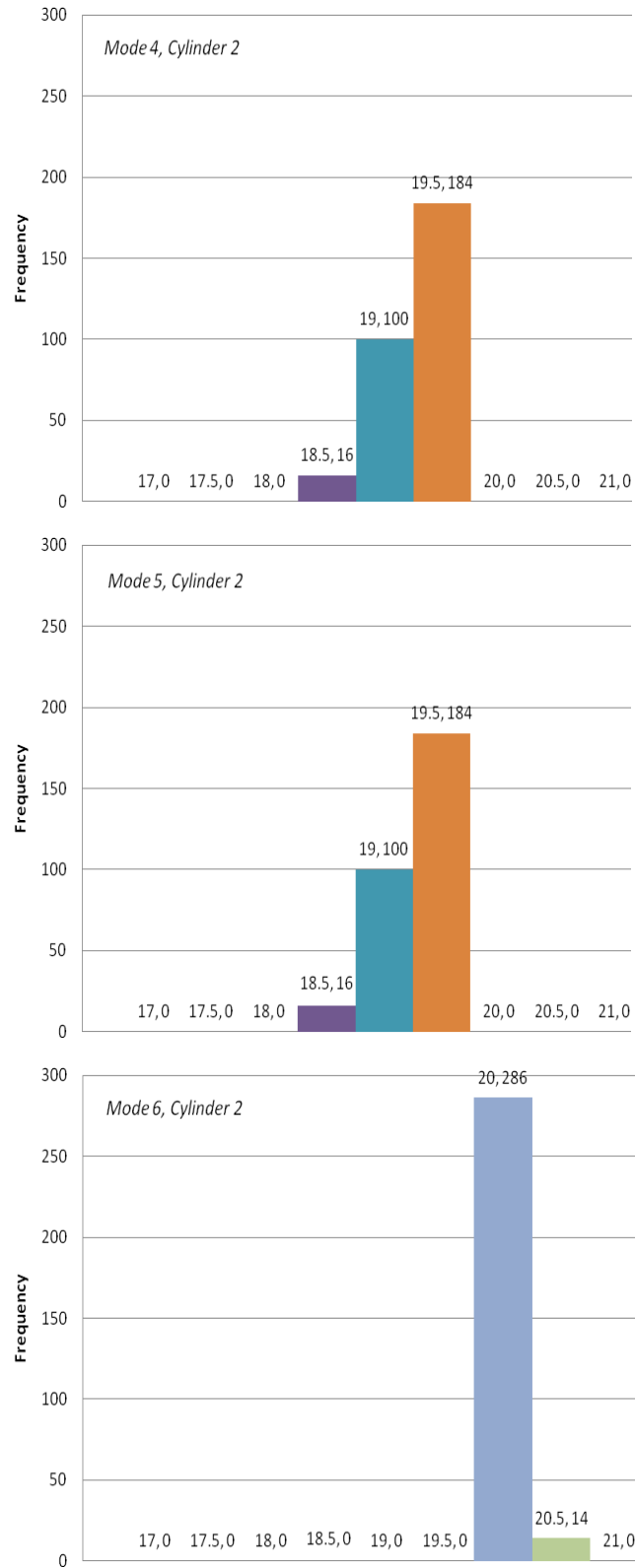
Figure 5.5: Cylinder 2 spark timing dispersions for modes 4 through 6
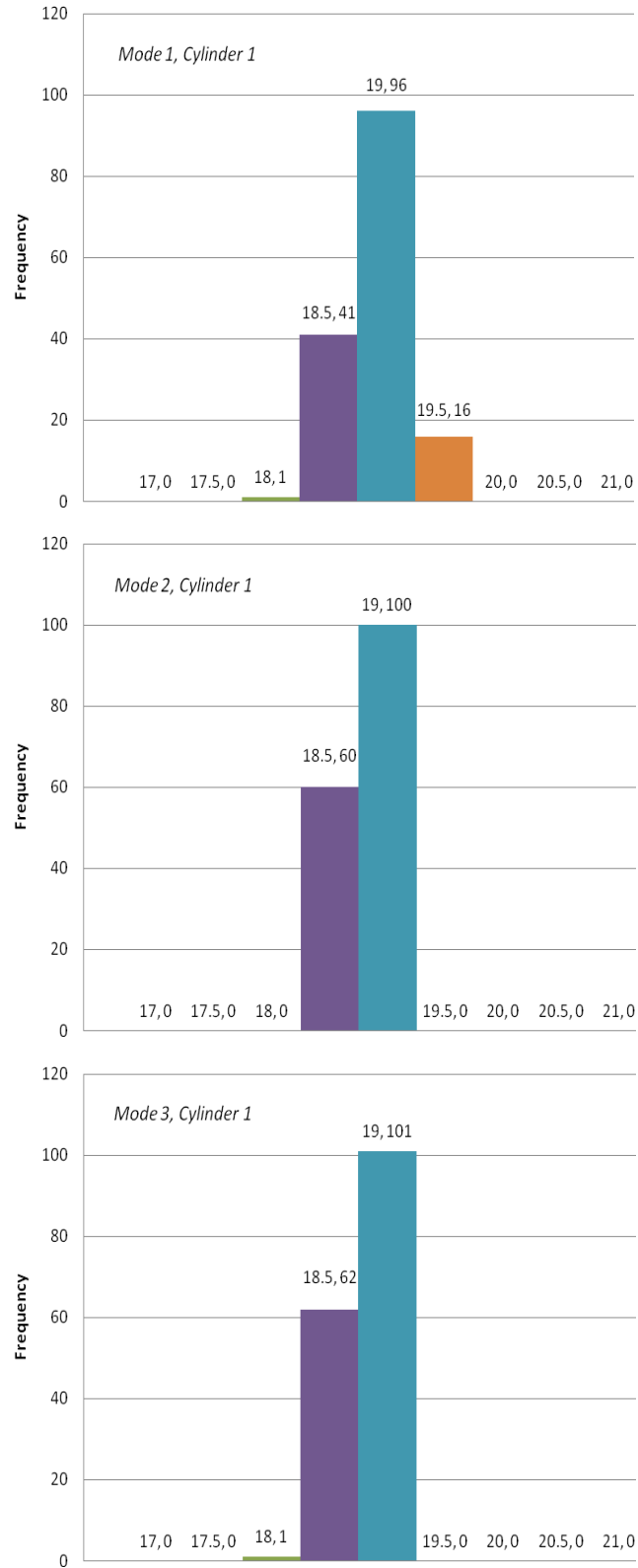
Figure 5.6: Cylinder 1 fired spark timing dispersions for modes 1 through 3

Figure 5.7: Cylinder 1 fired spark timing dispersions for modes 4 through 6

Figure 5.8: Cylinder 2 fired spark timing dispersions for modes 1 through 3

Figure 5.9: Cylinder 2 fired spark timing dispersions for modes 4 through 6

6. IN-CYLINDER PRESSURE ANALYSIS

6.1. PRESSURE MEASUREMENTS

In-cylinder pressure was recorded for both cylinders at a half crank angle resolution with Kistler 6061B piezoelectric pressure transducers. Piezoelectric pressure transducers measure dynamic pressure as opposed to absolute pressure which is needed for many engine performance calculations. To achieve this, a pressure referencing technique was developed on a cycle-to-cycle basis which scales the cylinder pressure to the intake manifold pressure, obtained with a Motorola MPX4115A pressure transducer, near bottom dead center (BDC) of the intake stroke. BDC was chosen as the referencing point due to the piston's relatively slow speed several crank angles before and after this point. After this referencing/scaling technique is applied, exact values for cylinder pressure are determined which improves the accuracy and reliability of engine performance calculations. Pressure traces, Figures 6.1 and 6.2, can then be generated.

6.2. PRESSURE OBSERVATIONS

Several beneficial observations can be drawn from in-cylinder pressure measurements. One can see in the figures that follow that peak pressure decreases as engine load decreases, which is expected. It can also be noted in modes 3 – 5 that the motored section of the pressure trace is apparent before the peak pressure. This indicates that spark timing is not optimal at these modes and is, in fact, too retarded. The pressure trace given for mode 6, Figure 6.2, supports this observation by displaying essentially a motored pressure trace due to peak pressure occurring at top dead center. At this set

point, combustion is contributing a negligible amount to the in-cylinder pressure used for
work production.

Maximum Brake Torque (MBT) timing, the optimum spark timing to achieve
peak engine torque, is desired for the test engine at all modes of the test procedure.
MS&T uses an empirical and widely accepted observation that signifies MBT timing has
been reached. This observation states that MBT timing occurs when the location of the
peak cylinder pressure is 16˚ after top dead center (ATDC). This MBT timing will
advance slightly with increases in engine speed and load [10]. Peak pressure location
was determined for several spark timing baseline tests. The average peak pressure
location for each cylinder and mode can be seen below in Table 6.1.
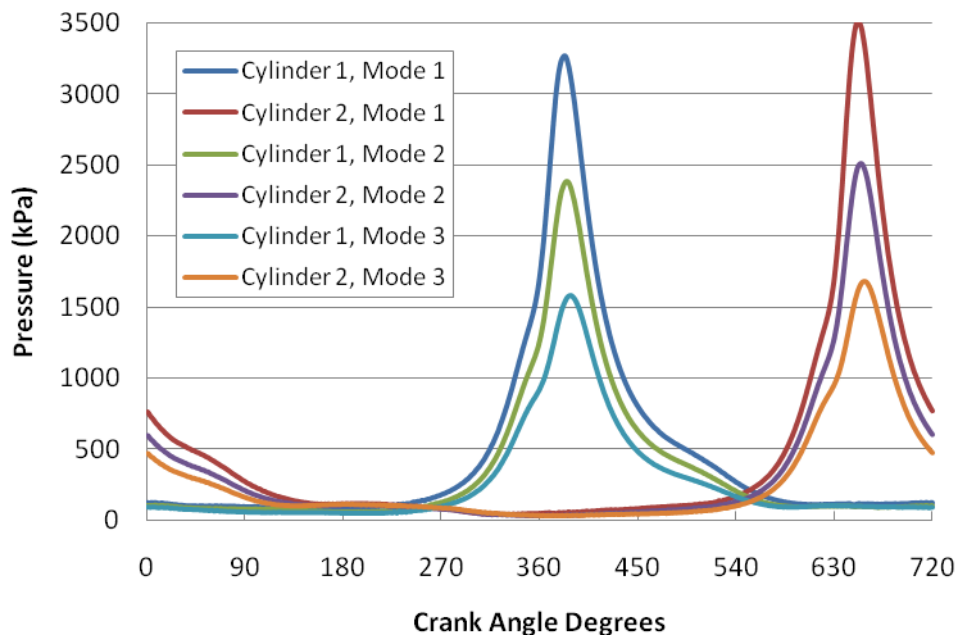
Figure 6.1: In-cylinder pressure for modes 1 – 3
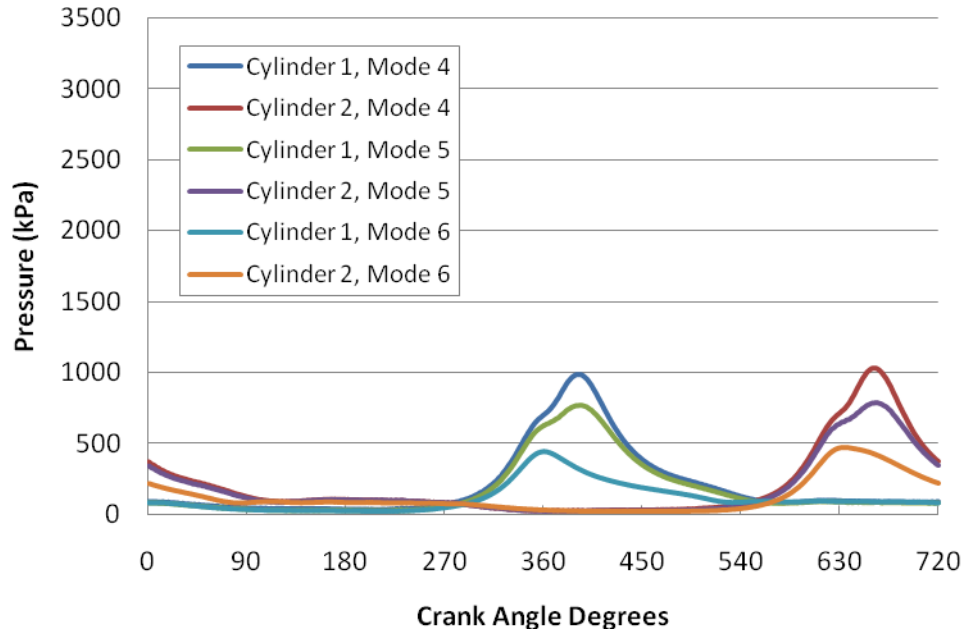
Figure 6.2: In-cylinder pressure for modes 4 – 6

Table 6.1: Average peak pressure locations using stock ignition system

Mode	1	2	3	4	5	6
Cylinder 1 (°ATDC)	23.0	24.5	27.5	31.0	33.0	1.0
Cylinder 2 (°ATDC)	22.0	24.0	27.0	31.0	33.0	4.0

One can see that the peak pressure location for every mode is several degrees on the retarded side of MBT timing with mode 1 being the only one in which the engine is operating relatively close to MBT. The engine gets further from MBT as speed and load decrease which verifies the observation made previously regarding the motored pressure being an indication of retarded spark timing for modes 2 – 6. The spark timing should be advanced for improvements in engine performance and efficiency to be attained.

7. HEAT RELEASE RATE ANALYSIS

7.1. MODEL DESCRIPTION

The occurrence of cylinder peak pressure location late in the engine cycle establishes the observation that combustion phasing is inappropriately retarded for all engine speeds tested. Modifying this as well as the speed of the combustion process would have a very advantageous impact on energy and availability distributions. Therefore, combustion speed and duration are of significant importance in this investigation. Avinash Singh, a graduate student at Missouri S&T, has developed a method to quantify and help visualize combustion speed using heat release rates. The approach is based on the first law of thermodynamics and incorporates the same energy output avenues as the energy balance analysis. Matlab was used to generate this single-zone model which uses cylinder pressure measurements to determine the amount of chemical energy released by combustion of fuel. A single-zone combustion model assumes that the contents of the cylinder can be described very accurately by property values taken from an average of the state of the cylinder [1]. The key components to the rate of energy released in the cylinder include sensible energy of the gases, work, heat transfer, and lost mass to cylinder crevices.

Using measured cylinder pressure as the input, work output and sensible energy (related to the temperature of the gas in the combustion chamber) are determined using a model by Gatowski [16]. The heat transfer component was determined with the commonly used Woschni model [17]. This model requires the computation of average gas velocity using mean piston speed, displacement volume, motored pressure, and a set

of scaling parameters. The final component, the crevice effect, is defined as the fuel energy lost to the crevice volumes and contributes a minor proportion to heat release rate.

7.2. TEST ENGINE RESULTS

Each of the components described in the previous paragraph are computed in Matlab then added to give gross heat release rate (kJ/deg) displayed in Figure 7.1 for a typical data set. The word "gross" designates the combination of sensible and heat transfer energy release rates as well as that contained in the crevice volume. The data supplied in this section comes from the analysis completed on cylinder 1 of the test engine. Results from cylinder 2 are very similar and thus omitted.
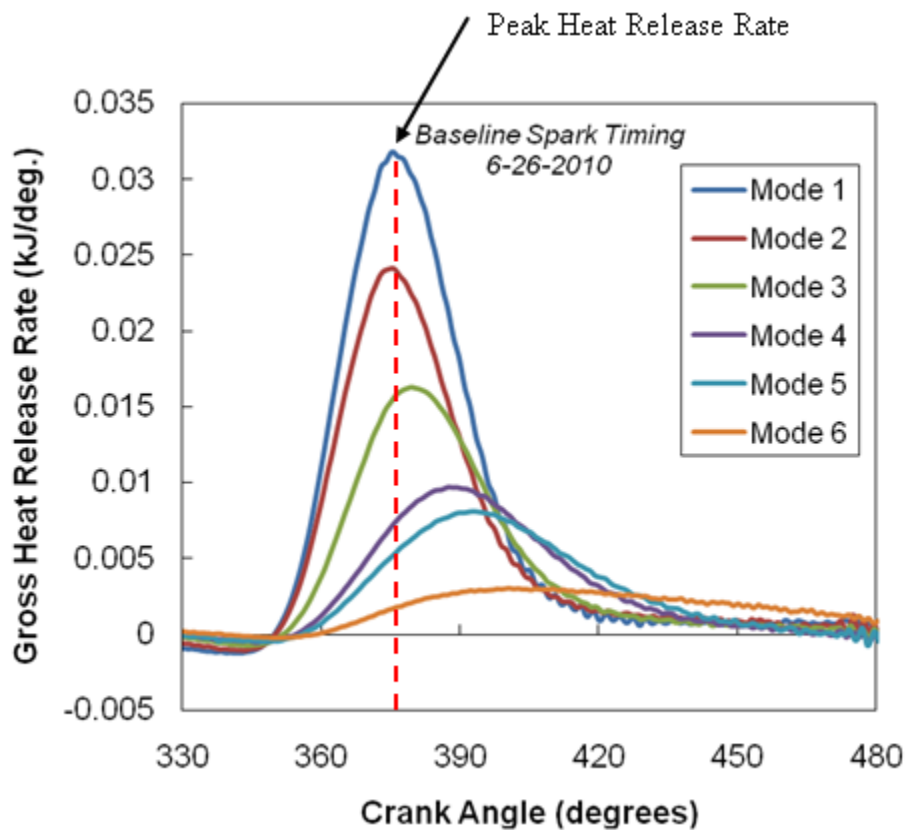
Figure 7.1: Gross heat release rate for each mode of the test procedure

One will notice that only portions of the compression and expansion strokes are included due to this being the only phase of the engine cycle in which energy is being released from the combustion zone. Also, the peak heat release rates occur shortly after top dead center (360 CAD) for each mode which signifies the fastest rate of combustion and highest rate of energy release. This is due to the dependence of combustion rate on two factors. The first is the density of the unburned mixture. It can be seen in Figure 7.2 that peak cylinder pressure also occurs shortly after top dead center which signifies greatest unburned mixture density and fastest rate of combustion.
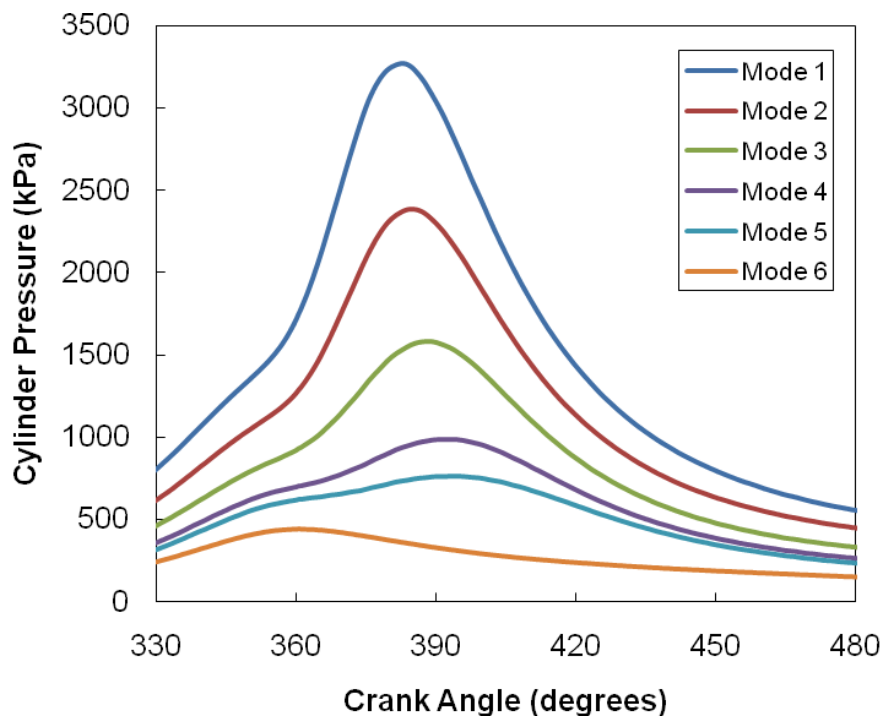
Figure 7.2: Cylinder pressure as a function of crank angle degrees

The second factor that affects combustion rate near top dead center is the high bulk gas temperature. This causes the laminar flame speed, hence rate of combustion, to

be significantly higher than it would be for lower bulk gas temperatures. A plot of bulk gas temperature as a function of crank angle degree is included in Figure 7.3. This is obtained by using the intake temperature and pressure along with the ideal gas law to compute the gas temperature inside the cylinder between intake valve closed (IVC) and exhaust valve open (EVO).
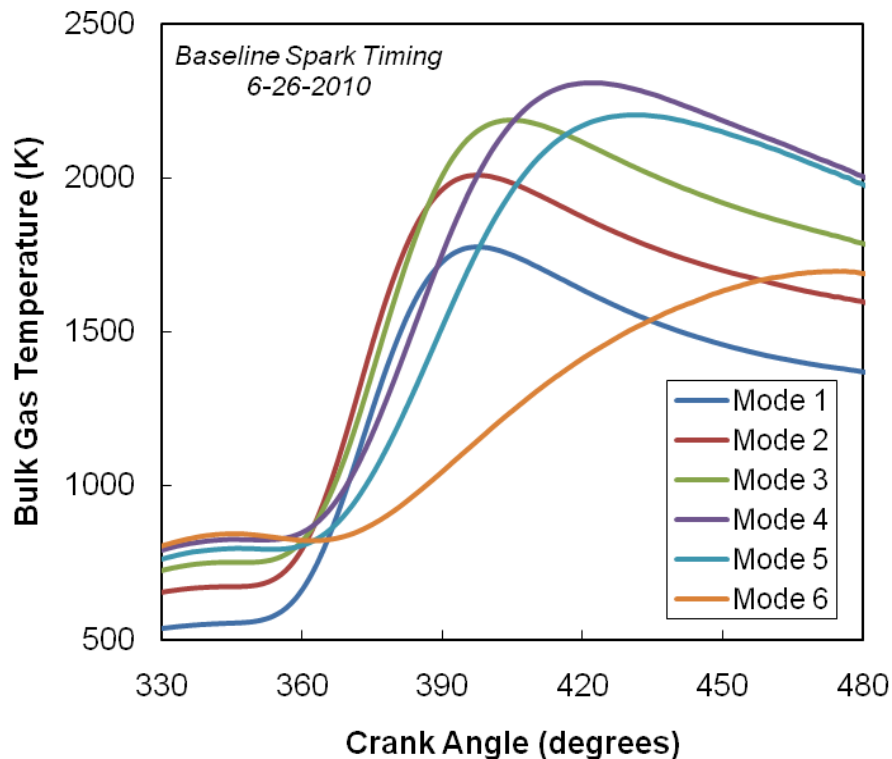
Figure 7.3: Bulk gas temperature plotted as a function of crank angle degree

Heat release rate, synonymous with burn rate, decreases with decreasing engine speed and load due to turbulence and mixture density. Turbulence within the cylinder is directly linked to burn rate and increases with increasing engine speed. As engine speed increases, turbulence increases and, therefore burn rate increases. At lower load conditions, the mixture density in the cylinder is reduced, due to lower peak pressures,

while the combustion residuals increase, both of which result in a slower burn rate. This slower burn rate results in a longer combustion duration which is signified by wider bell curves at low loads.

Once the heat release rate, in kJ/deg, is attained, it can be integrated over the phase of the engine cycle to determine cumulative heat release rate. These results can be seen in the Figures 7.4 and 7.5 for each of the six modes. When the heat release rate results are displayed in this manner, it is easy to see similarities to the energy balance results. Each of the energy forms is shown in the plot. The dashed black line represents the fuel energy supplied to the system. Similar to the energy balance, this supplied energy decreases as mode number is increased due to the decreasing amount of fuel being inducted into the engine. The crevice effect is incorporated here and can be seen as a slight dip in the line. The work and sensible bulk gas energy are contained in the sensible energy component of heat release rate, shown in black. When heat transfer losses are added to the sensible component, heat release takes the form of the plot shown in red. Combustion inefficiency, or chemical energy still contained in the exhaust, is the difference of the red line and the input energy line as shown. One will notice that, based on percentage of input energy, the combustion inefficiency values obtained are very close to the energy balance results discussed in Section 3.2. This fact validates the heat release rate method as an accurate first law analysis and provides another method of obtaining energy balance results using cylinder pressure data instead of engine output parameters and emissions measurements. These cumulative heat release rate results are displayed only for cylinder 1 of the test engine, as noted on each figure. The results obtained for

cylinder 2 are extremely similar to the cylinder 1 results so they are not included in this discussion.
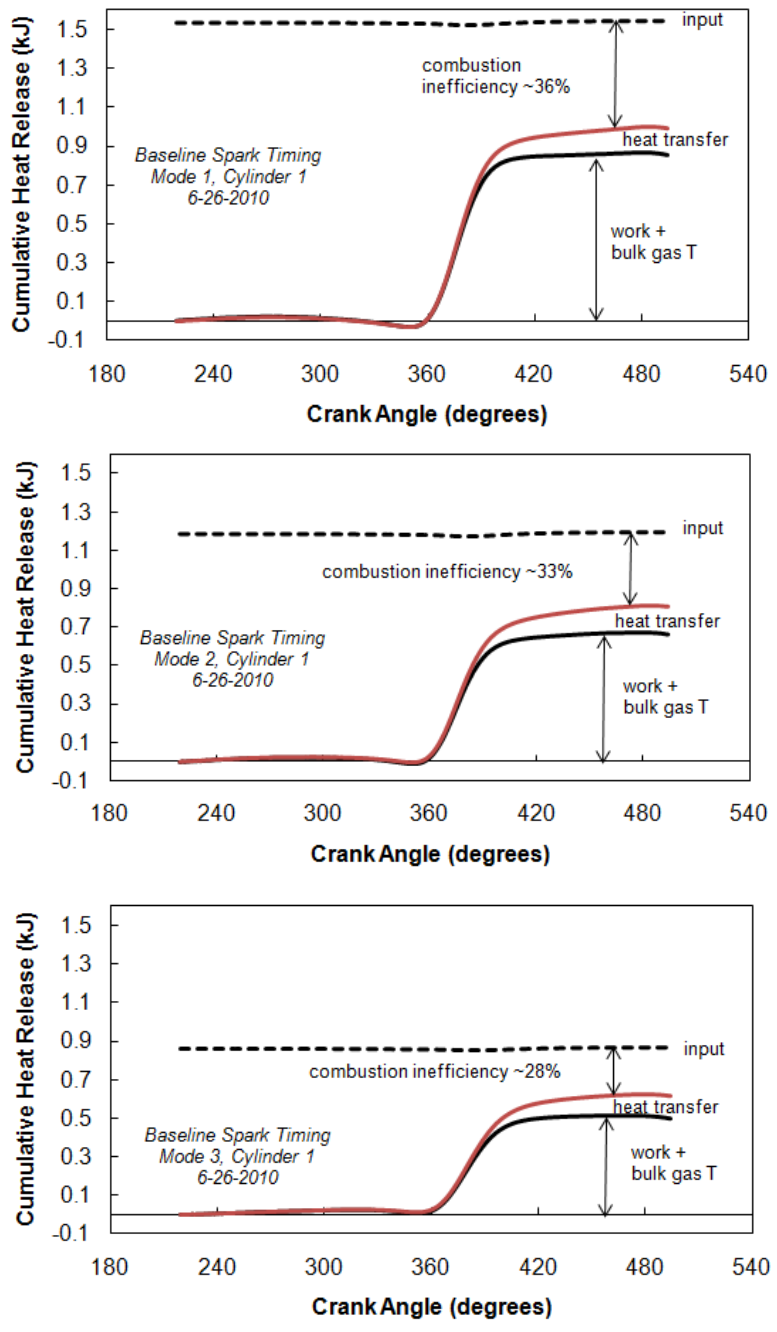
Figure 7.4: Cumulative heat release results for modes 1 through 3
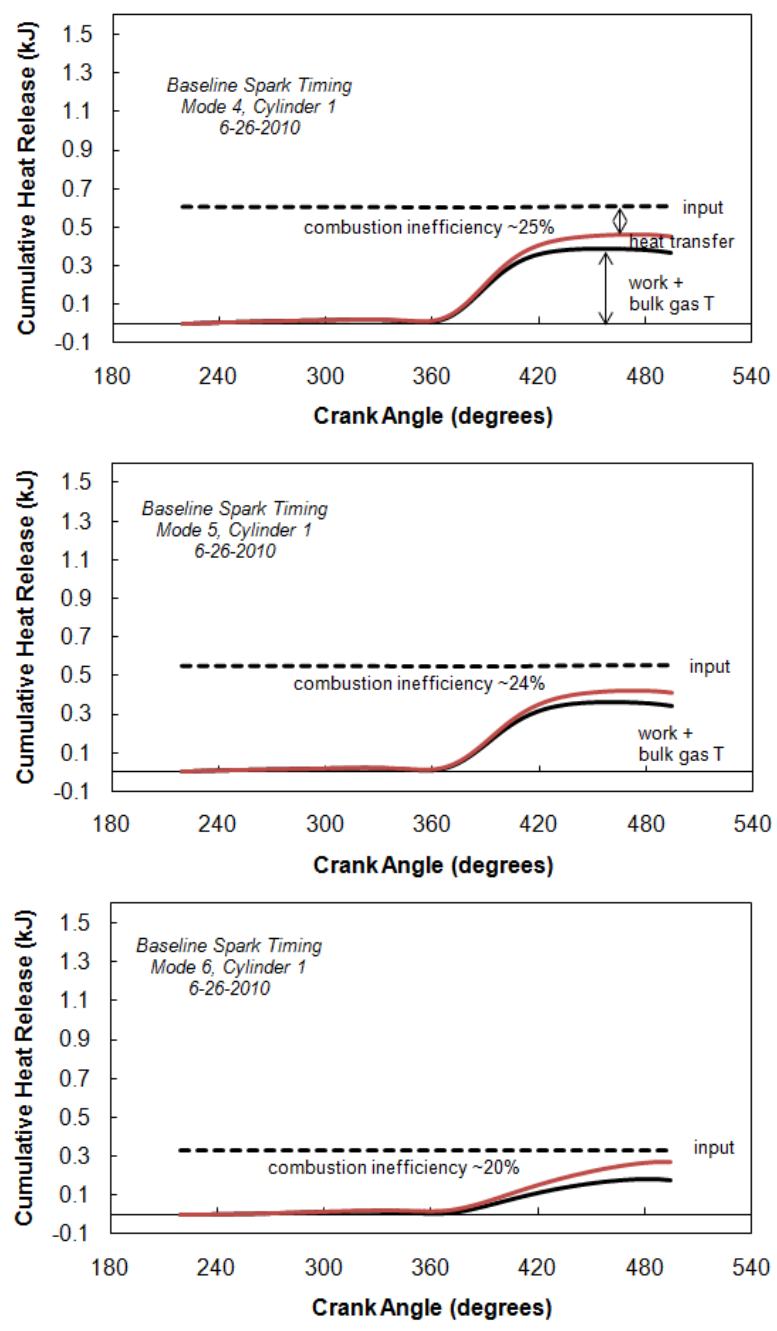
Figure 7.5: Cumulative heat release results for modes 4 through 6

From the heat release analysis, burn rates can be quantified with a calculation of

mass fraction burned which is designated x_b. This is completed by dividing the gross heat

release rate at each crank angle by the input fuel energy. This is shown in equation 51 below.

$$x_b = \frac{\left(\dfrac{dQ_{released}}{d\theta}\right)}{Fuel\ Energy\ In} \tag{51}$$

where:

$$\frac{dQ_{released}}{d\theta} = heat\ release\ rate$$

Typical plots of mass fraction burned for the test engine can be seen in Figure 7.6.
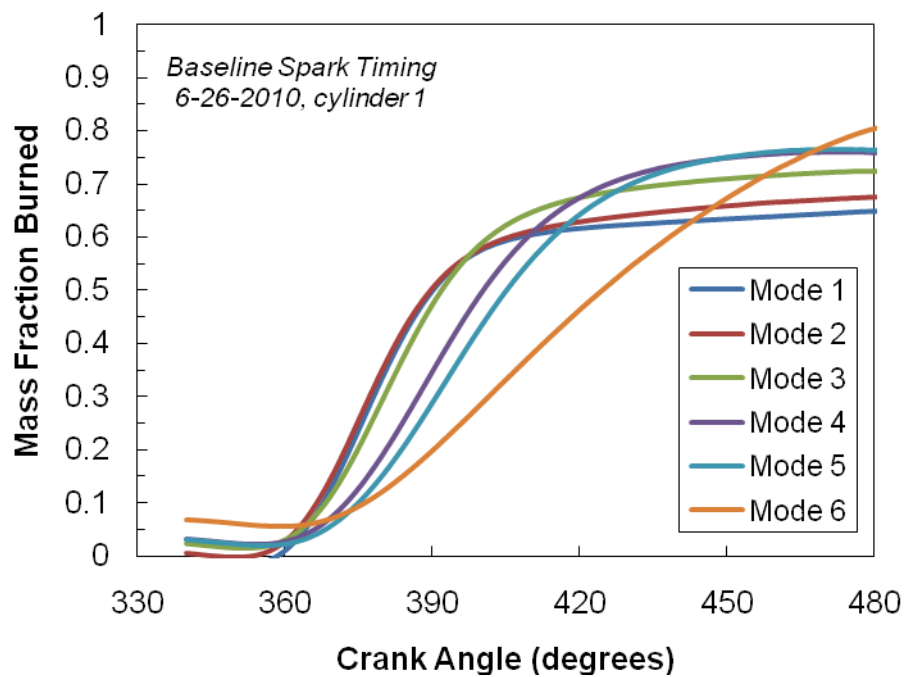
Figure 7.6: Mass fraction burned as a function of crank angle

It can be seen in Figure 7.6 that none of the modes ever reach a mass fraction burned of 1.0, meaning that no mode burns 100% of the supplied fuel energy. This is due

to the extremely rich mixtures being inducted into the test engine. The above results can be normalized so that they all end with MFB equal to 1.0. From these normalized results, the crank location at which 50% of the mixture is consumed (CA50) can be estimated. Numerical results of CA50 as well as the location of peak heat release rate (pHRR) can be seen for the stock engine configuration in Figure 7.7 that follows.
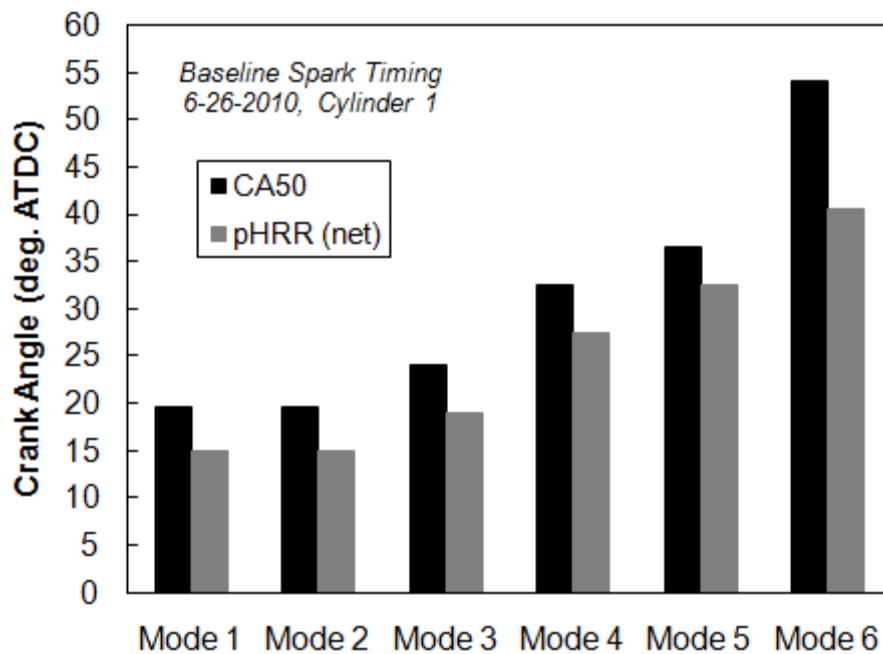
Figure 7.7: CA50 and peak heat release rate for each mode

There is a definitive trend that pHRR (net) location and CA50 retard with decreased engine speed and load. This is due to these burn rate parameters' dependence on peak cylinder pressure which retards in the same manner. Both of these measures provide a means to establish the speed of the combustion process. Typically, having CA50 near 10° after TDC results in the peak torque from the engine (MBT) [18]. Clearly, modes 3 through 5 have delayed combustion processes. The cumulative heat

release for modes 3 through 5 show this is a result of a slower combustion process as evidenced by the reduced slope of the red line during the combustion phase.

7.3. OBSERVATIONS

If the above heat release rate analysis is taken with the energy balance results, two clear observations can be made for the baseline configuration of the test engine. First, combustion inefficiency goes down, less fuel chemical energy leaves the engine unused, as the engine transitions from mode 1 to mode 5. This is primarily due to the engine operating closer to a stoichiometric fuel-to-air ratio. However, not all of this chemical energy is converted into work. This can be seen by the increase in percentage of the input fuel energy which goes to convective heat transfer from the engine (and to some degree exhaust energy) as the engine transitions from mode 1 to mode 5. A primary cause of this shift to convective heat transfer is the later combustion timing for higher modes, as shown in the figure above. This energy, as well as the availability, must be properly redistributed in order to achieve improved performance and efficiency.

8. REPEATABILITY ANALYSIS

Several engine performance data sets were collected in order to verify the repeatability of the experimental setup and test procedure. Typical emission gas concentrations can be seen in Figures 8.1 – 8.4 for several baseline tests run at Missouri S&T as well as a test run by the engine manufacturer, labeled "EM". The charts display the emission values collected at each mode of the six-mode test procedure for several baseline engine data sets, designated by the date of the test. The proximity of each tests' values to one another is evident which proves repeatability of the exhaust gas concentration measurements. This is important due to the fact that the exhaust gas concentrations are used extensively in the energy and availability balances.
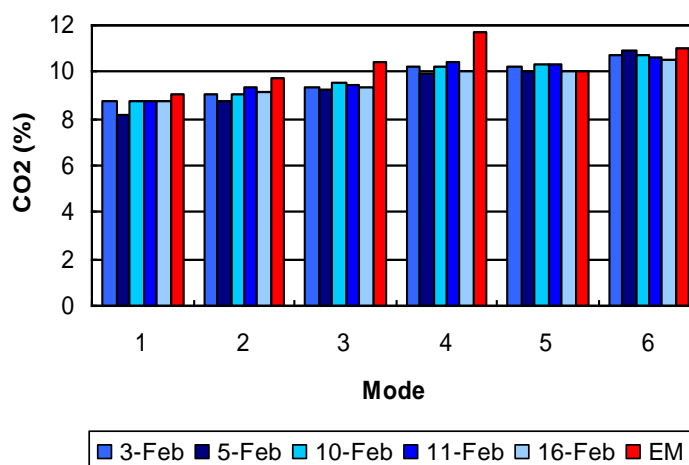
Figure 8.1: CO_2 gas concentrations at each mode for several baseline engine tests
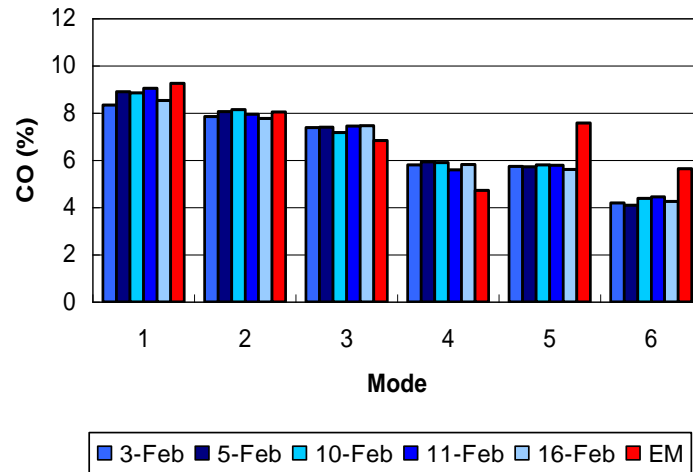
Figure 8.2: CO gas concentrations at each mode for several baseline engine tests
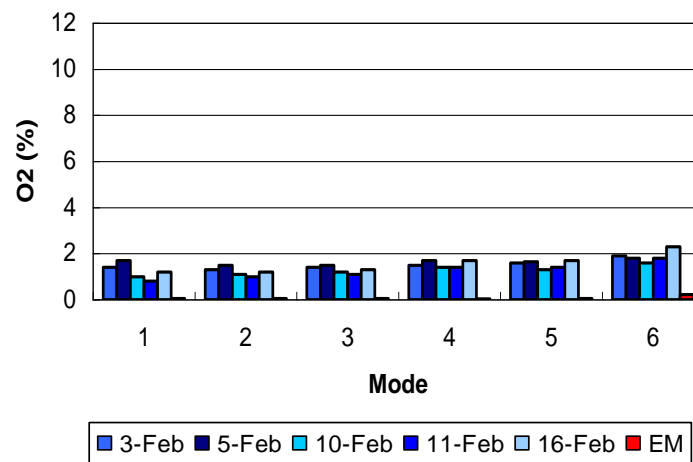
Figure 8.3: O_2 gas concentrations at each mode for several baseline engine tests
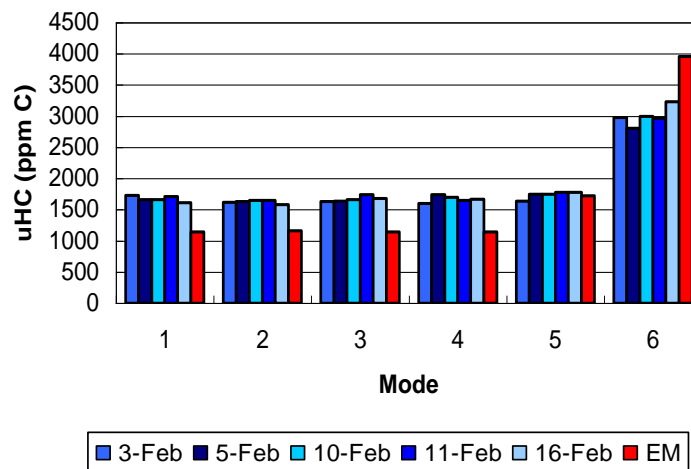
Figure 8.4: uHC gas concentrations at each mode for several baseline engine tests

The repeatability of cylinder pressure measurements is also verified since it is used for combustion phasing and energy release rate analysis. This is done in two ways. First, the magnitude of the peak pressure, in kPa, is shown for several data sets collected on the test engine setup. These are shown in Figures 8.5 and 8.6. The dates of these tests are later than those of the emissions results but the test procedure remains the same.
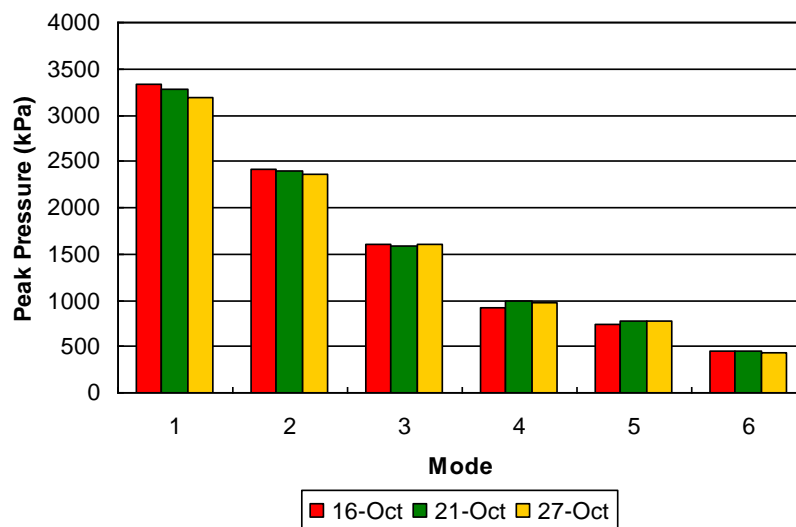
Figure 8.5: Cylinder 1 peak pressure for each mode for several engine data sets
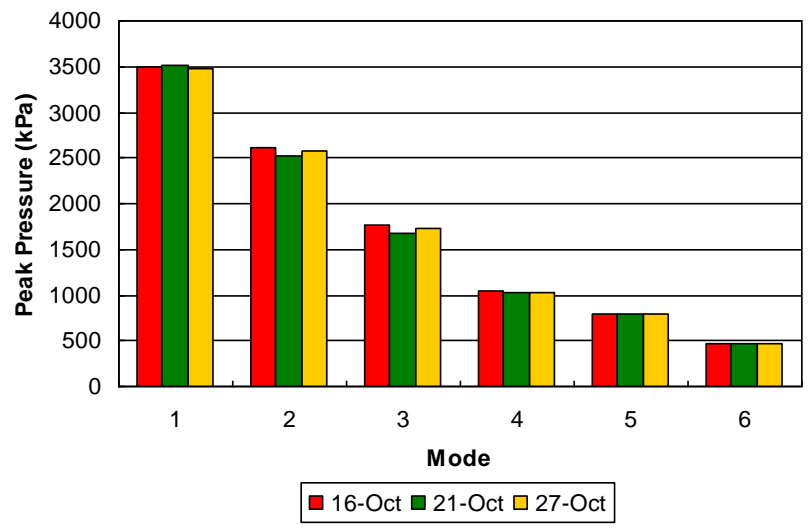
Figure 8.6: Cylinder 2 peak pressure for each mode for several engine data sets

Cylinder pressure repeatability is also demonstrated with peak pressure location. This is shown in Figures 8.7 and 8.8 for several data sets in degrees after top dead center (ATDC).
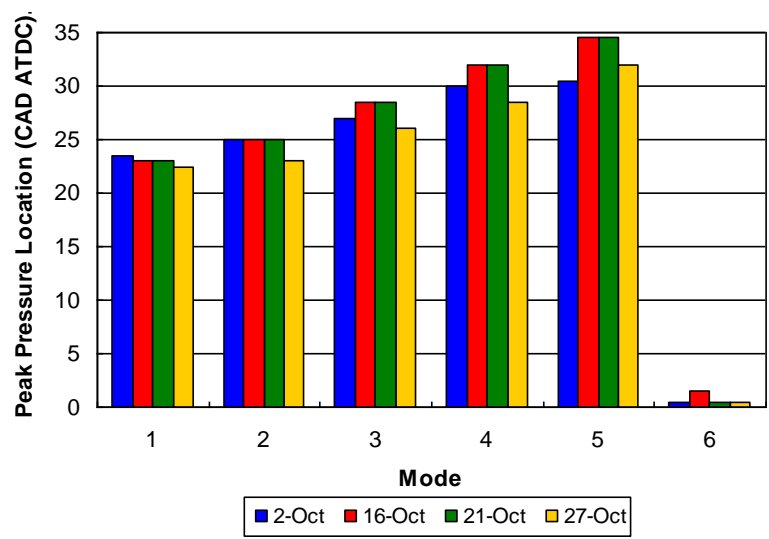
Figure 8.7: Cylinder 1 peak pressure location for each mode for several data sets
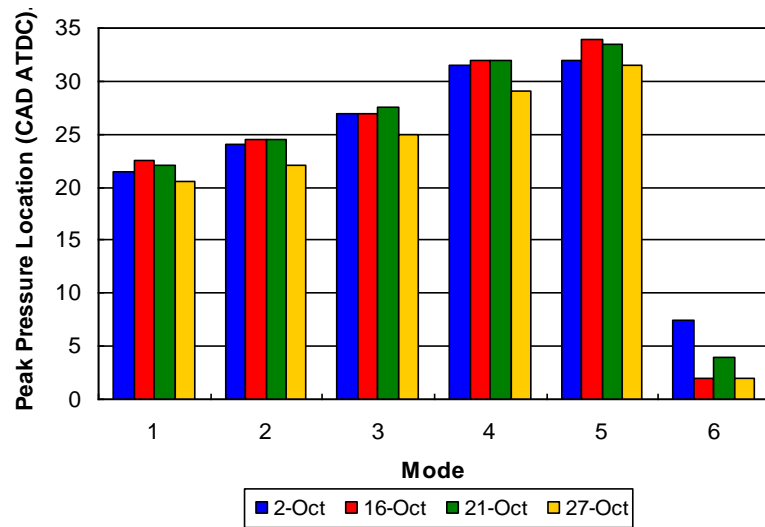
Figure 8.8: Cylinder 2 peak pressure location for each mode for several data sets

Acceptable repeatability of cylinder pressure measurements is verified by the small difference between pressure magnitude and location values in separate data sets. Greater variation is seen in later modes, especially mode 6, due to the large cyclic variability causing these average pressure numbers to differ more for these modes.

9. VARIABLE SPARK TIMING SYSTEM

Many useful observations have been made from the investigations of cylinder pressure, heat release rate, and balances of energy and availability. These include the fact that peak cylinder pressure and the location at which 50% of the fuel mass is consumed both occur too late in the engine cycle, as defined by literature, for maximum power and efficiency to be attained. Also based on literature, a portion of the output energy and availability forms can be redistributed to brake power if the combustion duration is shortened through advancement of combustion phasing [1, 8]. All of these observations point to the notion that spark timing should be varied over several engine set points until an optimal timing is discovered. This is done electronically with a system developed specifically for spark control of small internal combustion engines.

9.1. SYSTEM DESCRIPTION

The variable spark timing system used on the test engine is composed of many hardware components. The half crank angle signal and gate signal (once per revolution) from the shaft encoder are used to communicate the exact engine revolution location, in crank angle degrees, to the spark timing system. The controlling hardware for the system is a National Instruments cRIO-9022 Real-Time controller mounted on a National Instruments cRIO-9114 reconfigurable chassis. The shaft encoder signals are routed into the controller using a NI 9411 differential digital input module. The information is then transferred over the building Ethernet network to a computer running the controlling program coded in LabVIEW 2009. The computing processes are completed in LabVIEW as well as on the 9022 controller itself to increase computation speed. Once the timing of

the spark signal for each cylinder is generated, they are output from the 9022 controller

through an Engine Synchronous ESTTL module purchased from Drivven Inc. Each

signal travels to a GM Smart Coil-Near-Plug ignition coil connected to the spark plug of

each cylinder to initiate combustion. A National Instruments PS-15 power supply is used

to power the 9022 controller while a Tripp Lite PR20 power supply is used for the

ignition coils. A diagram of these hardware components of the system is included in

Figure 9.1.
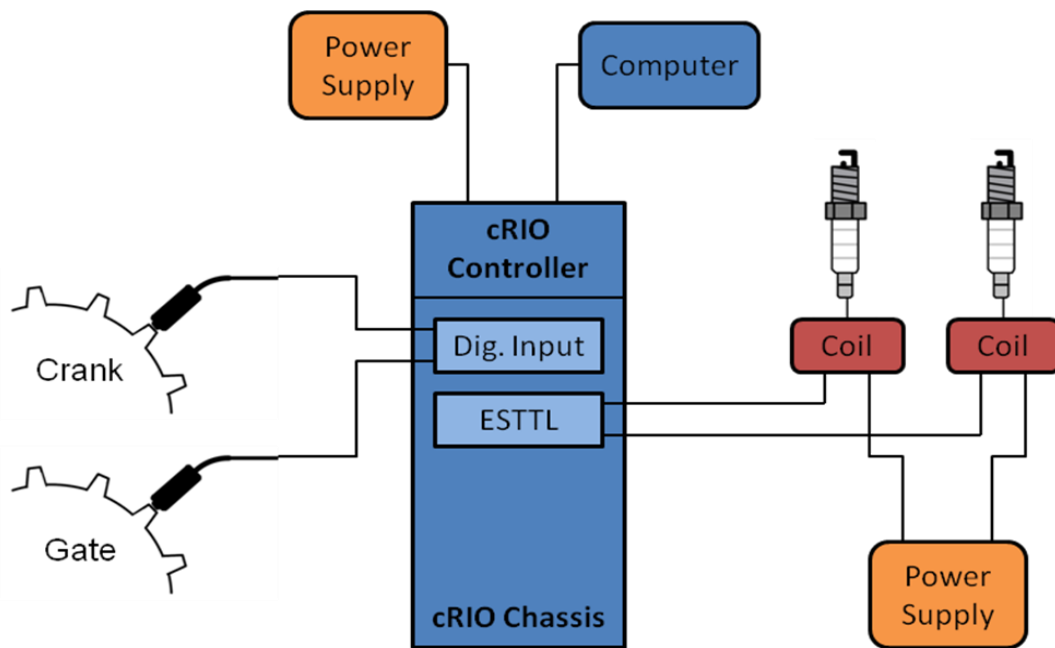
Figure 9.1: Variable spark timing system hardware

The software components used to drive the system are somewhat complicated in

nature. They are comprised of a FPGA computer code written in LabVIEW that

communicates with the input and output modules to ensure that all the signals are read

and output on the appropriate channels. It has several subroutines developed by Drivven

Inc. which carry out the spark commands utilizing user-defined timings and spark dwells. These user-defined values are found on a Real-Time code, also written in LabVIEW, which interfaces with the FPGA code and acts as the control panel for the variable spark timing system.

9.2. SYSTEM TESTING

The system has been tested extensively before being utilized as the primary ignition source on the test engine. These tests are completed by running the engine on the stock ignition system but also operating the variable spark timing system. The spark plugs for the variable system are grounded to the engine stand table so the spark can be discharged and spark signal acquired with a timing light and optical sensor that is routed into the engine stand data acquisition system. These tests are completed in two different ways. The first set of tests is conducted while operating the engine on the Six-Mode Cycle B test procedure which is used for all the engine data collection tests. The variable spark timing system is set to fire both cylinders at 18.5° BTDC. The purpose of this test is to verify that a specific user-defined spark timing value is actually seen by the engine for all set points of the test procedure. Spark timings for both cylinders prove to uphold very tight dispersions at every mode. The wide cylinder 2 dispersions seen with the stock system are eliminated by switching to the variable spark timing system. The highest frequency of spark timing values occurs at 18.5° BTDC which verifies the accuracy of the variable spark timing system. The results of this test for cylinder 1 can be seen in Figures 9.2 and 9.3 that follow this discussion. Since the cylinder 2 results are extremely similar to those of cylinder 1, they are not included here but can be found in Appendix A.
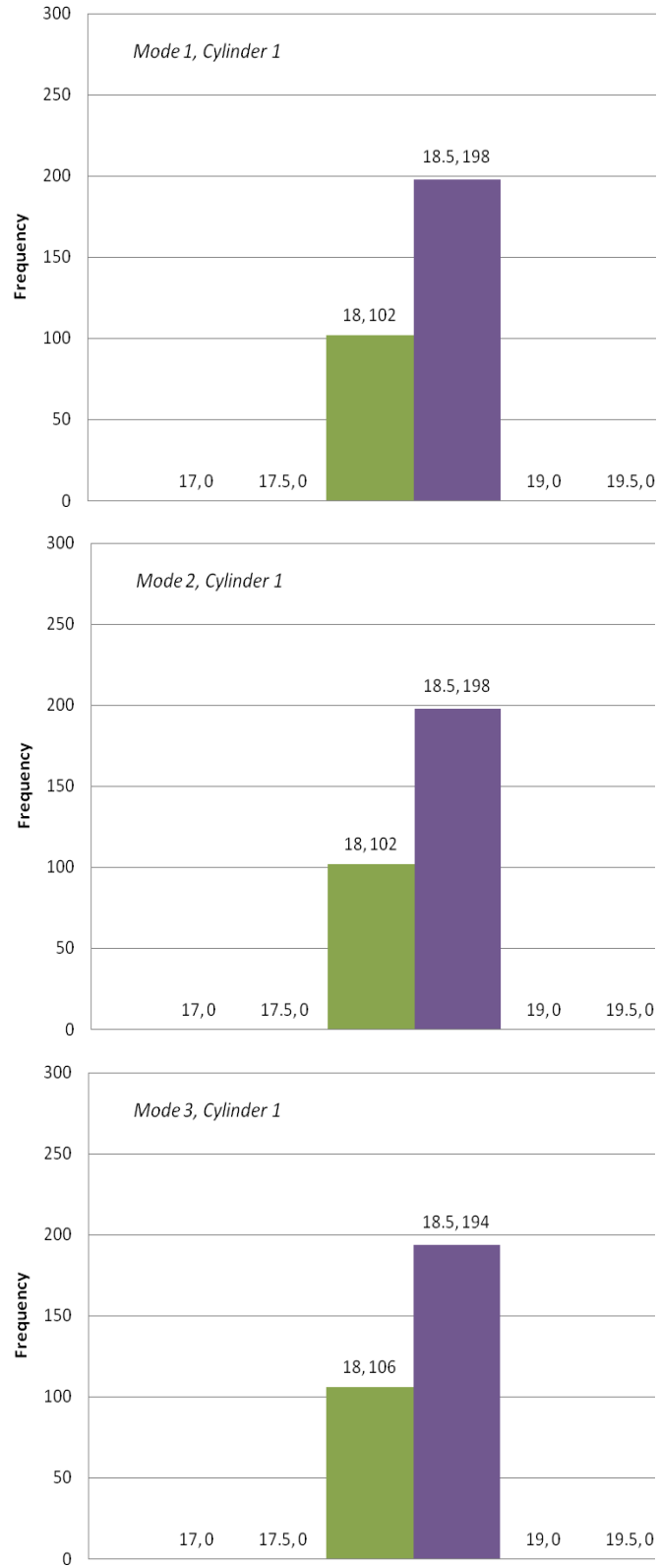
Figure 9.2: Cylinder 1 spark timing dispersions for modes 1 through 3
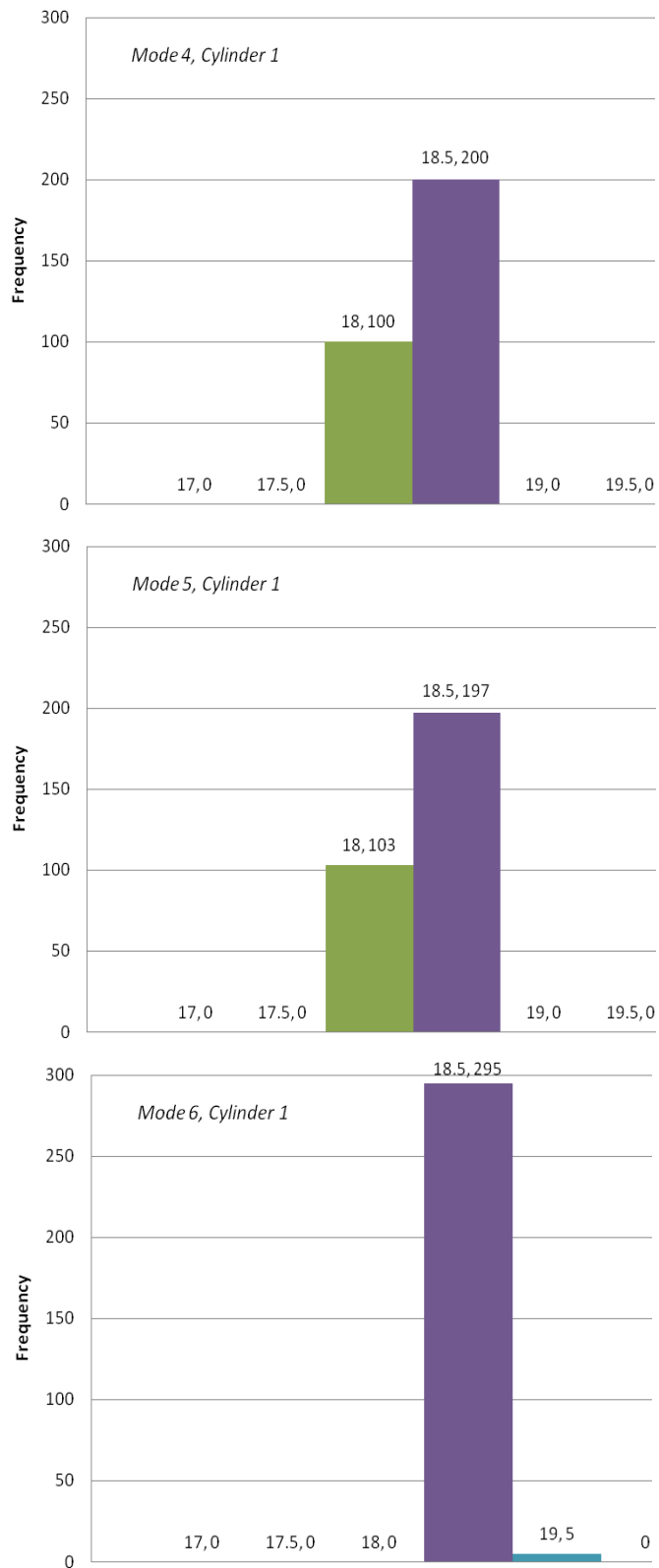
Figure 9.3: Cylinder 1 spark timing dispersions for modes 4 through 6

The second set of tests keep the engine set point fixed and vary spark timing so that the accuracy and precision of variable spark timing can be verified. These tests incorporate mode 1 of the test procedure and spark timing values of 15, 17, 19, 21, 23, 25, 27, 29, and 31° BTDC. The results of this set of tests can be seen in Figures 9.4 – 9.6. From examination of these figures, it can be seen that the specified spark timing values are achieved with very tight dispersions. The dispersions for cylinder 2 have a slightly larger spread than cylinder 1 but remain within one half of a crank angle degree of the user-defined value. Due to the proximity of dispersions between cylinders, the results for cylinder 2 are included in Appendix A. This verifies the precision of the variable spark timing system for a large range of spark timings.
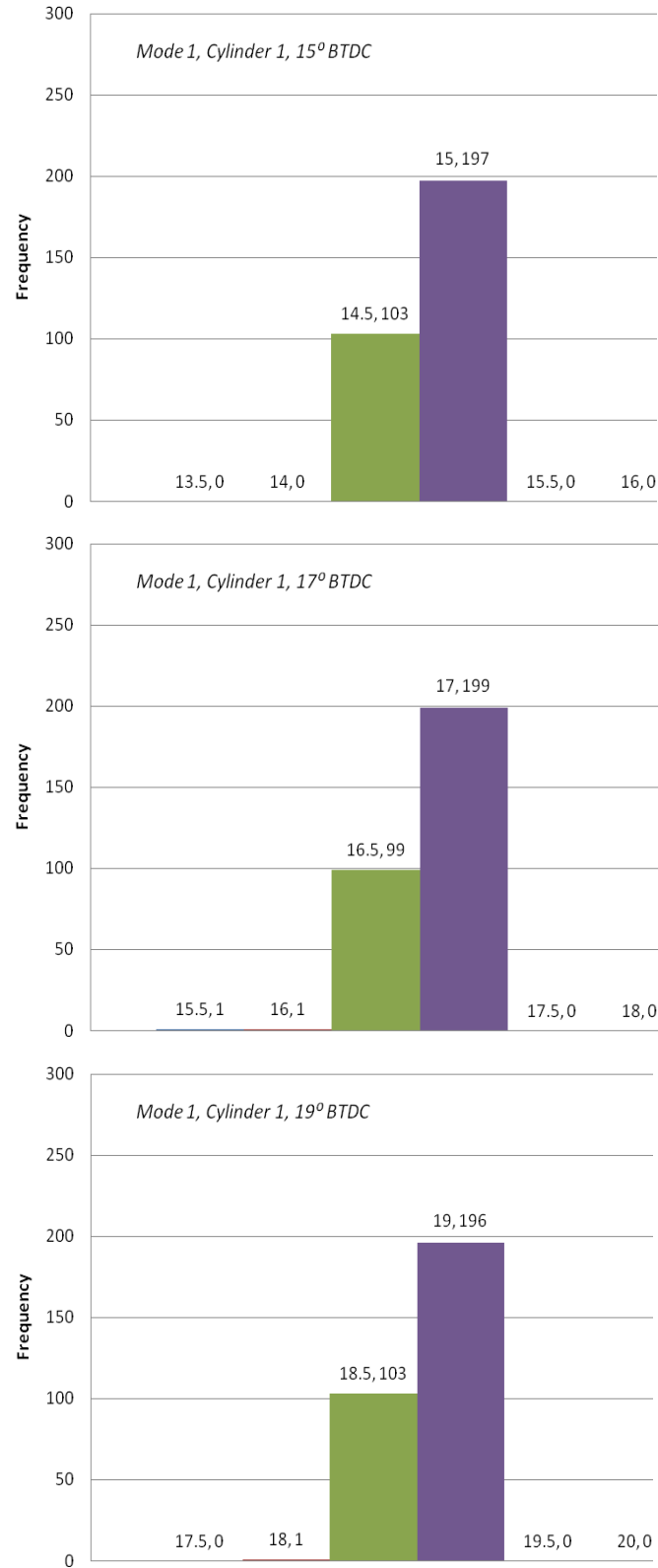
Figure 9.4: Cylinder 1, mode 1 spark dispersions for timings 15, 17, and 19° BTDC
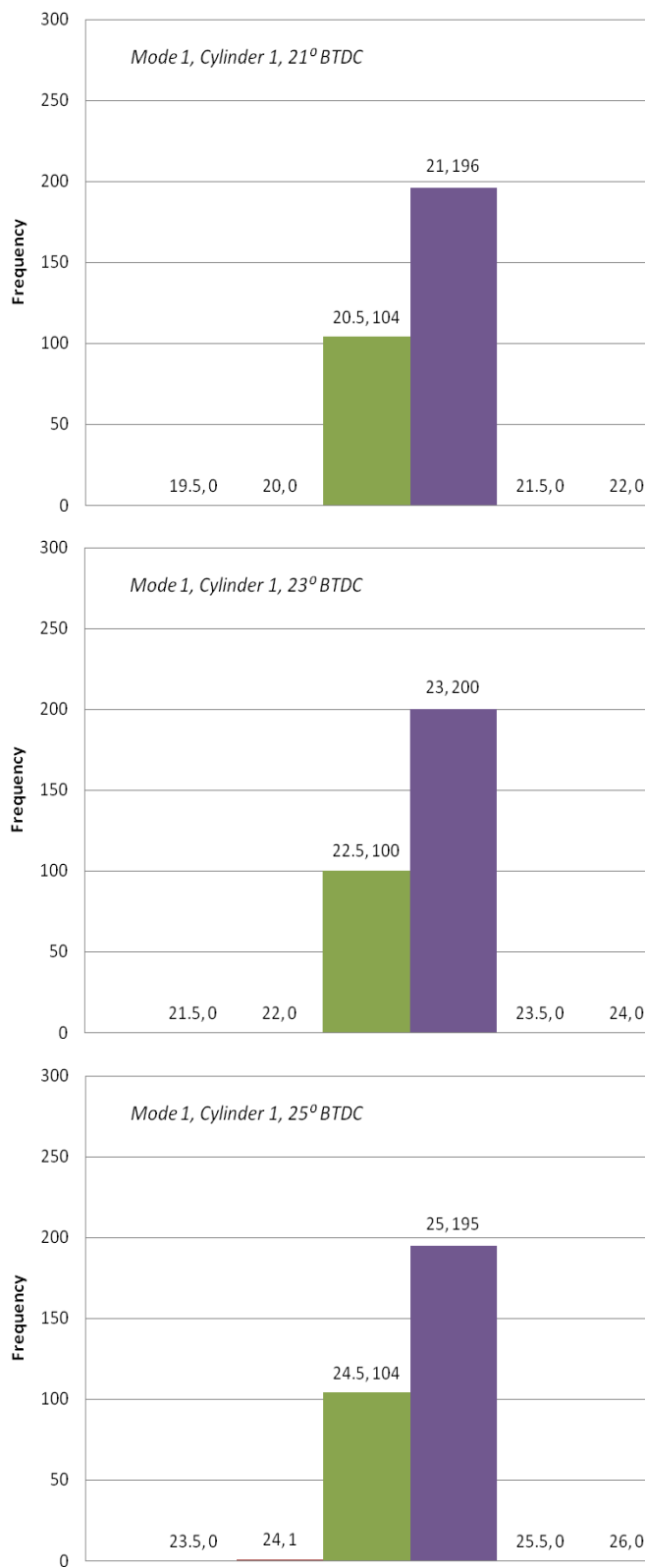
Figure 9.5: Cylinder 1, mode 1 spark dispersions for timings 21, 23, and 25° BTDC
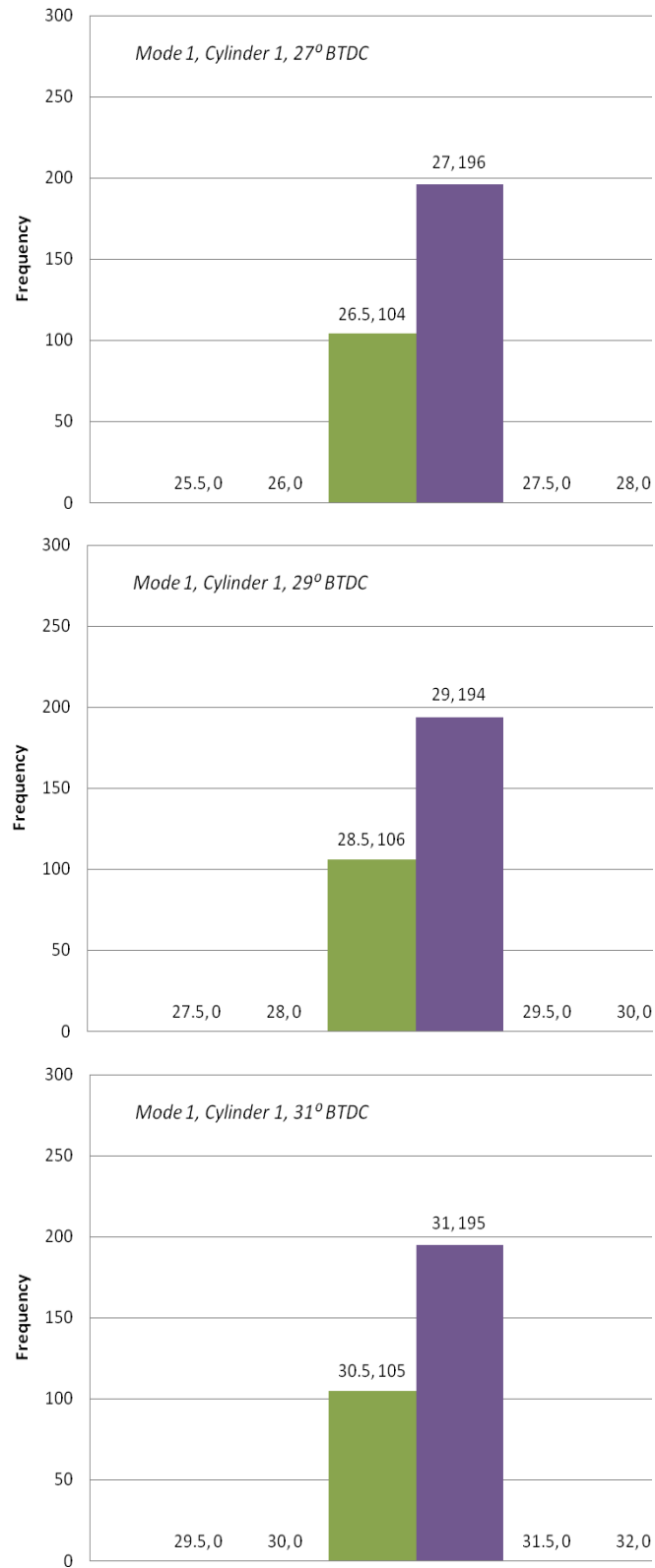
Figure 9.6: Cylinder 1, mode 1 spark dispersions for timings 27, 29, and 31° BTDC

10. COMBUSTION PHASING

10.1. VARIABLE SPARK TIMING SYSTEM VALIDATION

Due to the fact that the entire ignition system has been replaced, validation tests are required to prove that, when running at the stock spark timing, the engine still behaves as it does on the stock ignition system. This validation is completed by running a test with the engine operating on the variable spark timing system. The system is set to the stock spark timing setting of 19° BTDC. The results can be seen in the charts that follow where results are plotted for each mode of the test procedure.

One can see in Figure 10.1 that the CA50 values collected from both ignition systems are very similar with differences within the experimental error range displayed by the repeatability analysis. Both of these data sets are taken from cylinder 1. Cylinder 2 returned very similar results so they are not included. Cylinder pressure is also investigated in order to validate the variable spark timing system. Peak cylinder pressure locations for both cylinders can be seen in Figures 10.2 and 10.3.
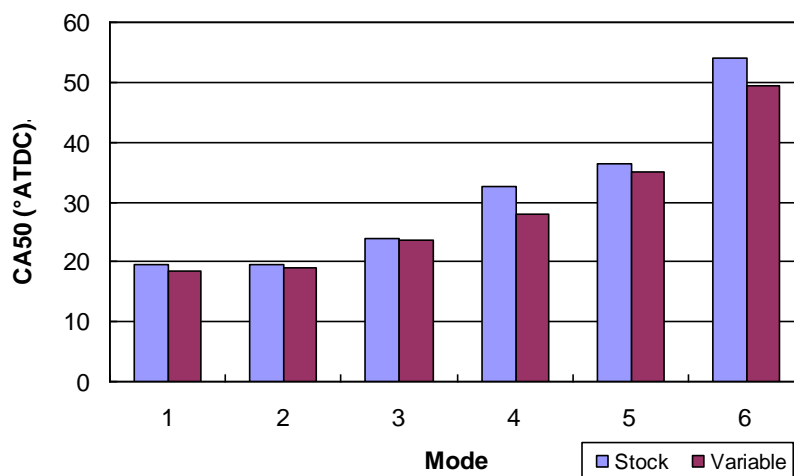
Figure 10.1: Typical CA50 values for both ignition systems taken from cylinder 1
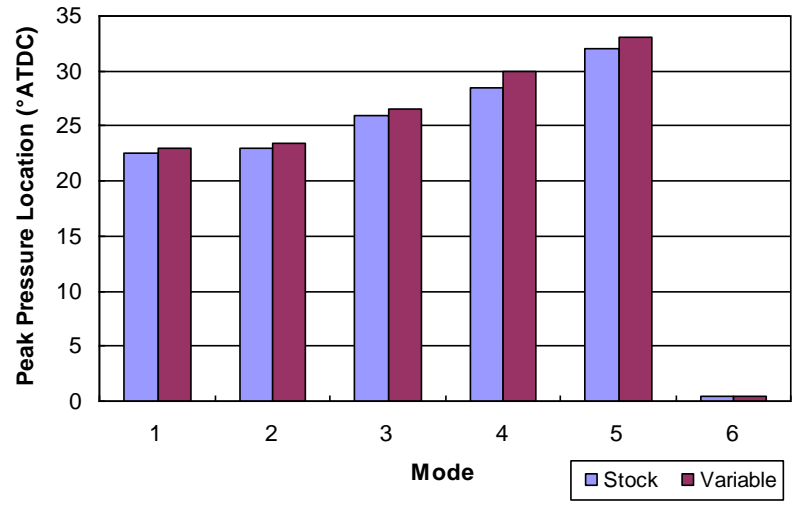
Figure 10.2: Typical cylinder 1 peak pressure locations
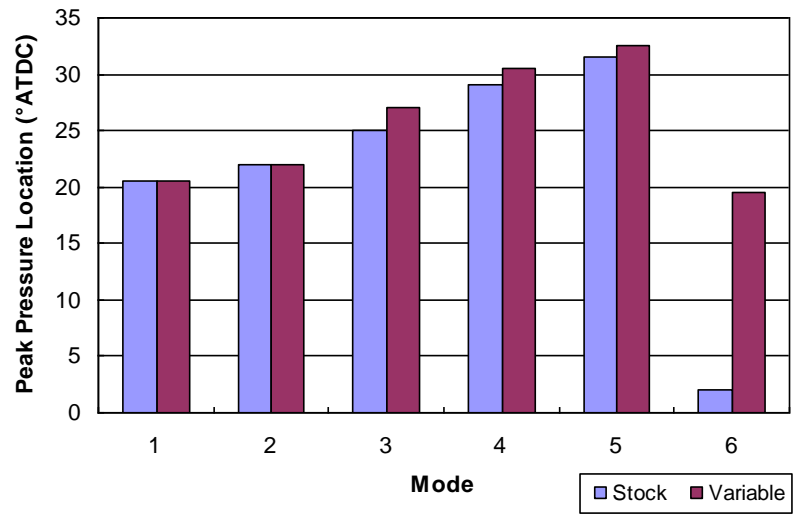
Figure 10.3: Typical cylinder 2 peak pressure locations

Just like CA50, peak cylinder pressure locations collected for both ignition systems are nearly the same with the exception of cylinder 2 at mode 6. The stock spark timing is extremely late for mode 6 and results in essentially a motored pressure trace. Little useful expansion work is attained. When the variable spark timing system is used,

expansion work is attained from a large number of cycles for cylinder 2, resulting in peak

pressure locations at 19.5° ATDC. The remaining cycles have peak pressures near top

dead center. This is a result of the reduced variation in spark timing of the variable spark

timing system. Even with this exception, this data proves that changing the ignition

hardware on the engine has negligible effect on cylinder pressure or mass fraction burned

parameters. Energy and availability analyses are completed next and shown in Figures

10.4 – 10.7.
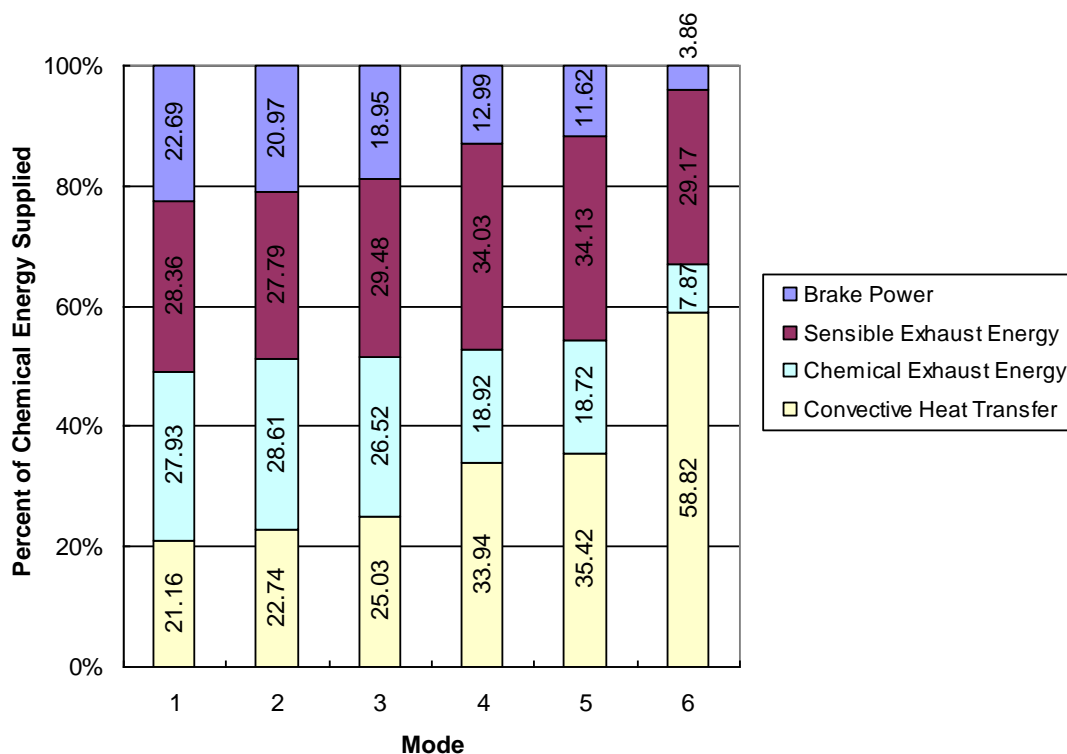
Figure 10.4: Energy balance results for variable spark timing system
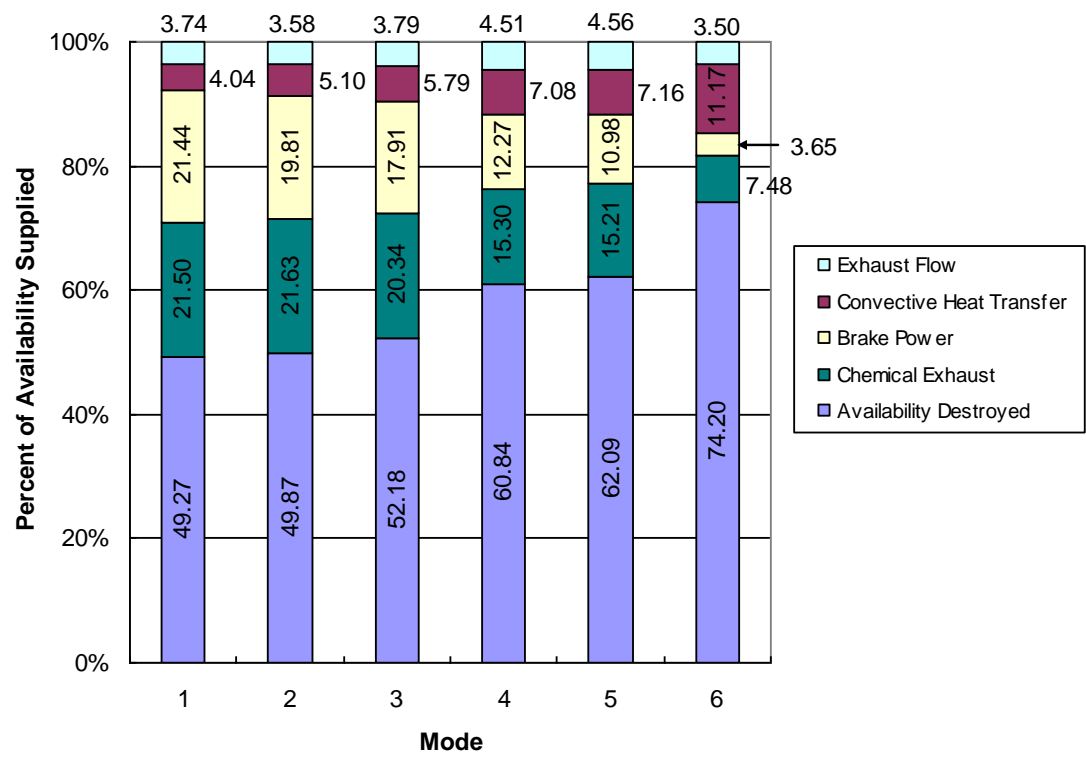
Figure 10.5: Availability balance results for variable spark timing system
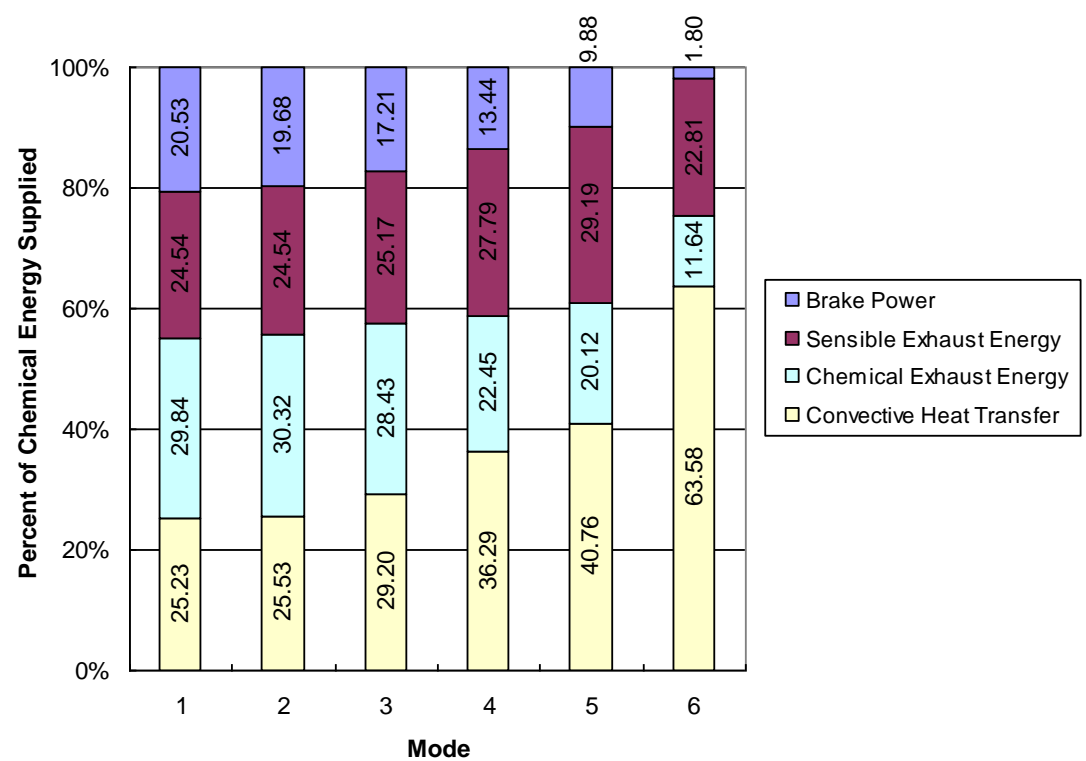
Figure 10.6: Energy balance results for stock ignition system
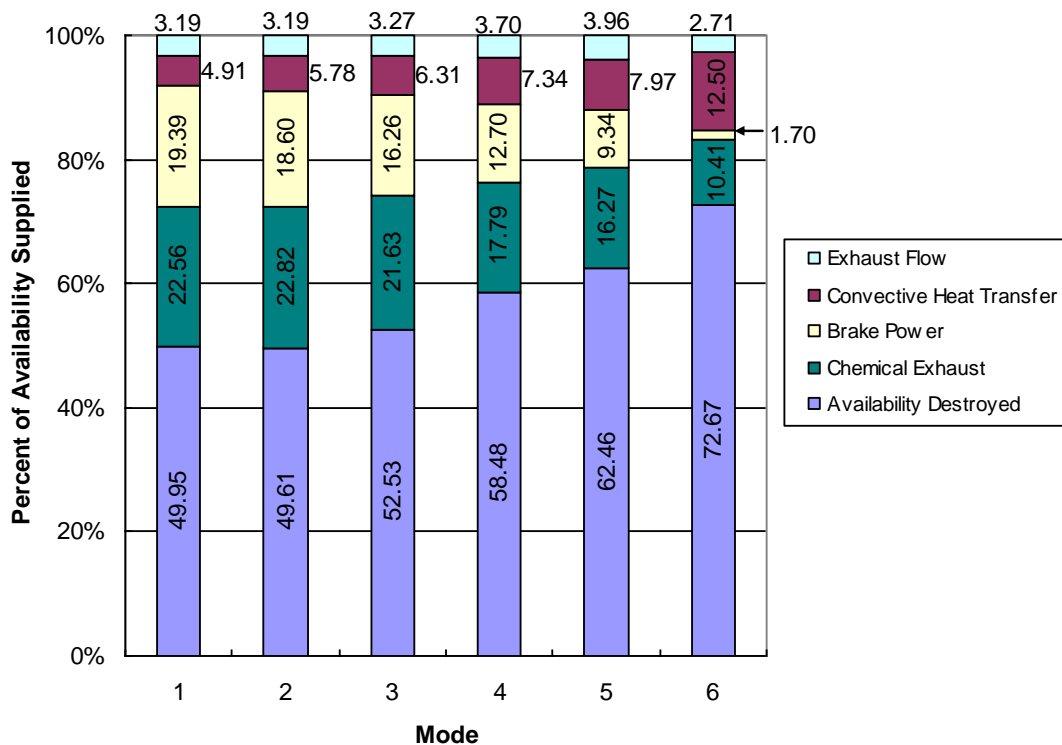
Figure 10.7: Availability balance results for stock ignition system

When comparing the energy and availability distributions supplied in Figures 10.4
and 10.5 to the typical distributions of the stock ignition system, provided again in
Figures 10.6 and 10.7, one will notice very similar results with a slight improvement in
energy and availability distributions achieved when operating the variable spark timing
system. Specifically, this improvement involves higher brake power and reduced
chemical exhaust and convective heat transfer forms of energy or availability due to a
considerably higher concentration of O_2 in the exhaust stream. This small improvement
in engine performance is caused by a reduction in cyclic variability due to the variable
spark timing system achieving much tighter spark dispersions, shown in Section 9.

10.2. VARIABLE SPARK TIMING SYSTEM RESULTS

Once the variable spark timing system is properly validated, engine performance data can be collected. This data is collected by operating the test engine at a certain mode of the test procedure and varying spark timing from 17 to 31° BTDC in increments of 2°. Engine performance data is acquired at each of these spark timings. All six modes of the test procedure are analyzed in this manner. The results from these tests are included in the paragraphs that follow.

10.2.1. Mode 1. As spark timing is advanced for mode 1, the cylinder pressure increases noticeably. This is evidenced in the plot supplied in Figure 10.8 where each curve represents a distinct spark timing.
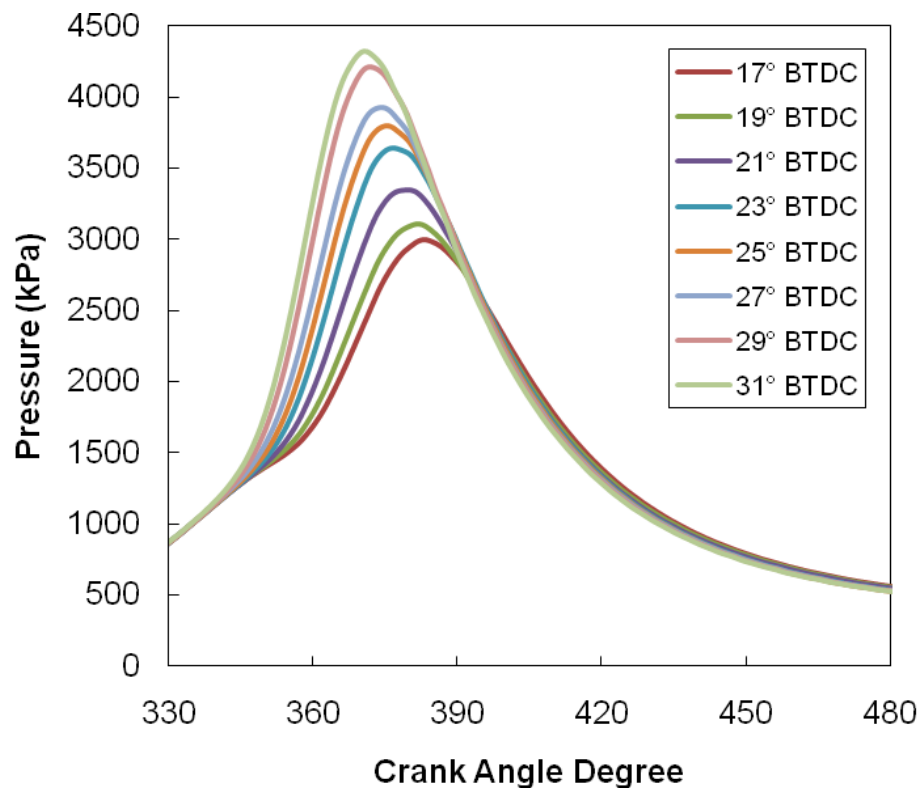
Figure 10.8: Cylinder pressure at mode 1 for various spark timings

The increasing cylinder pressure drives the unburned gas density higher. This effect results in higher laminar flame speeds and, thus, burn rates. This can be seen in Figure 10.9 which shows a gradual increase in peak heat release rate with advancing spark timing. The faster burn rates are also displayed in mass fraction burned results by the increasing slope of the curves, Figure 10.10.
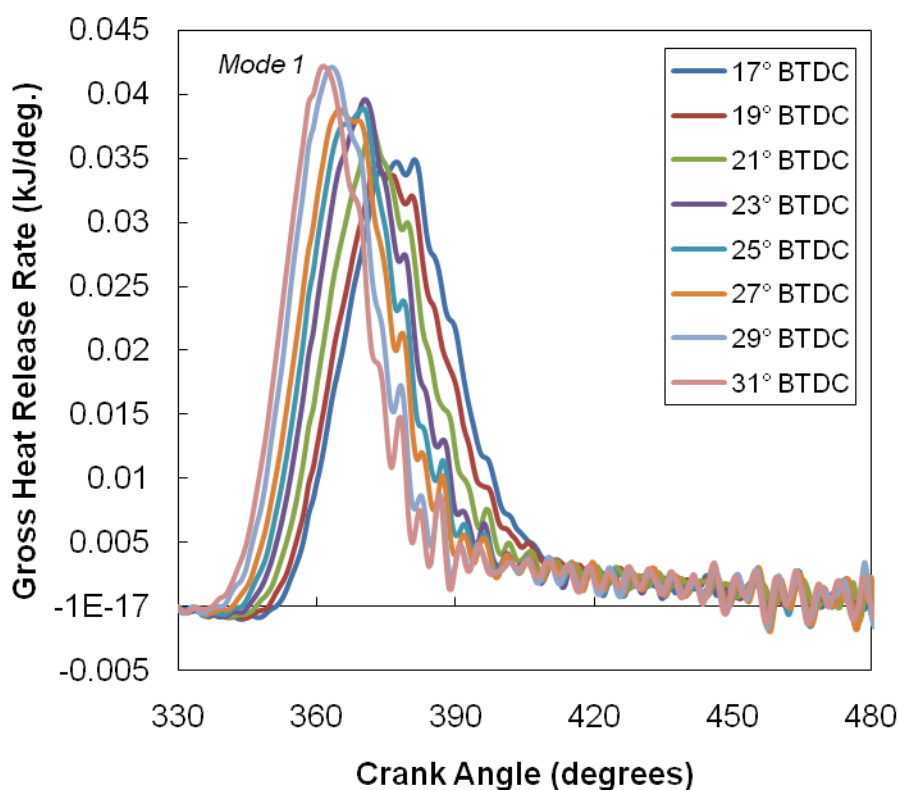
Figure 10.9: Heat release rate at mode 1 for various spark timings

One notable observation is that the mass fraction burned at the end of combustion is roughly 0.75 for all the spark timings. This is a result of the extremely rich mixtures being inducted into the test engine that cannot be completely consumed and is evidenced by the chemical exhaust energy in the energy distribution supplied in Figure 10.11.
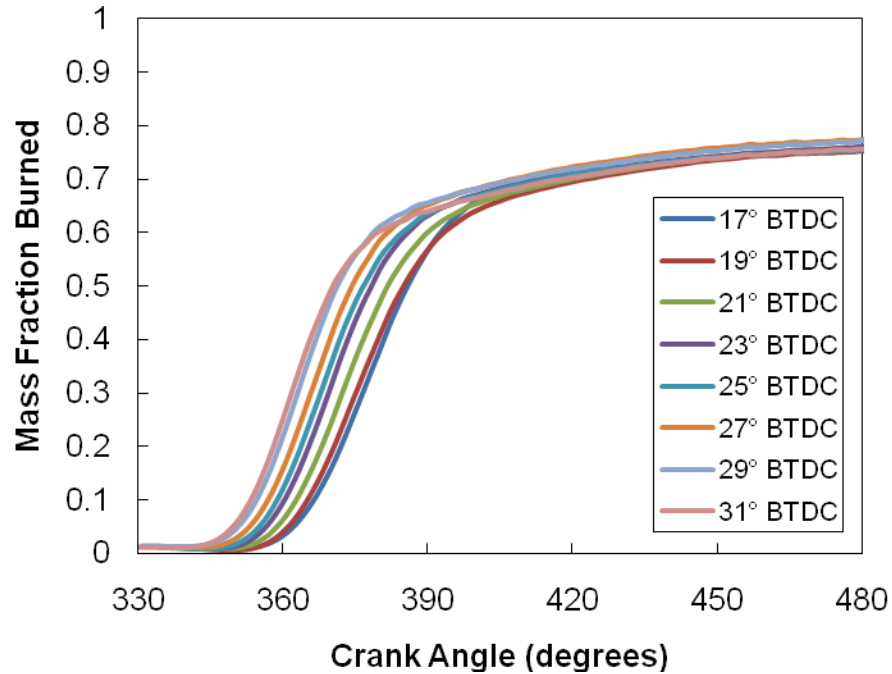
Figure 10.10: Mass fraction burned at mode 1 for various spark timings

In Figure 10.11, a separate energy distribution is displayed for each spark timing. Only slight differences in energy distributions are observed as spark timing is advanced at this mode. There are, however, some notable trends. As combustion duration decreases with advanced timing, the energy contained in the exhaust (sensible and chemical) decreases to a certain point then begins to increase due to the timing being advanced too far. The minimum point in exhaust energy corresponds to the largest brake power output. This maximum brake power is also caused by the expansion stroke work transfer being largest at that spark timing. These observations also apply to results obtained from the availability balance, supplied below in Figure 10.12.
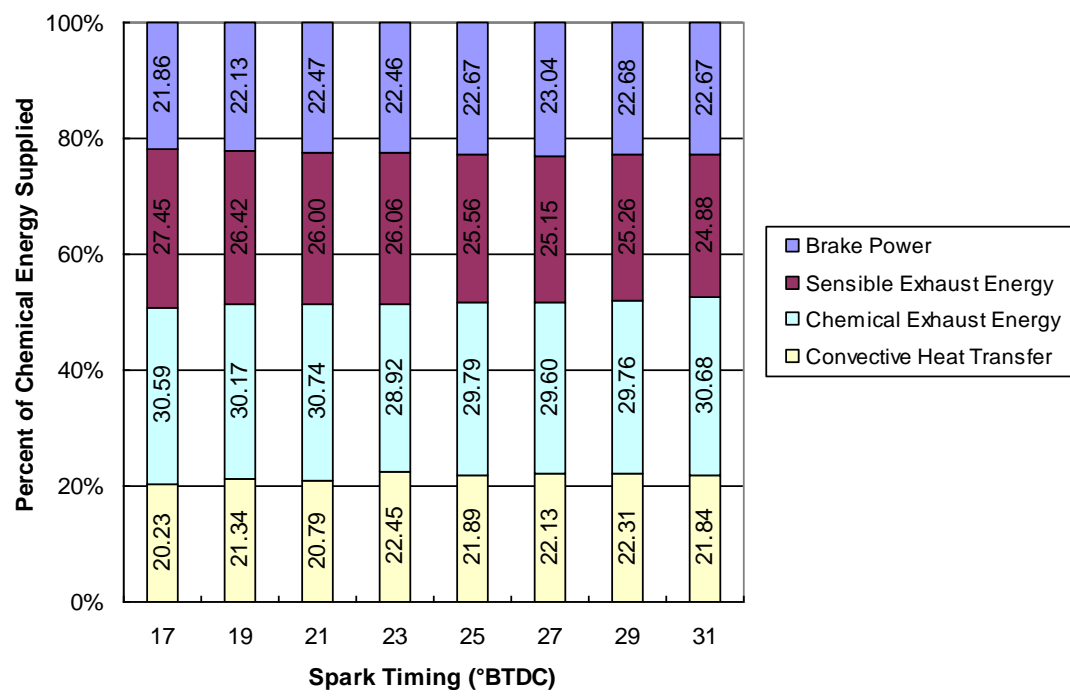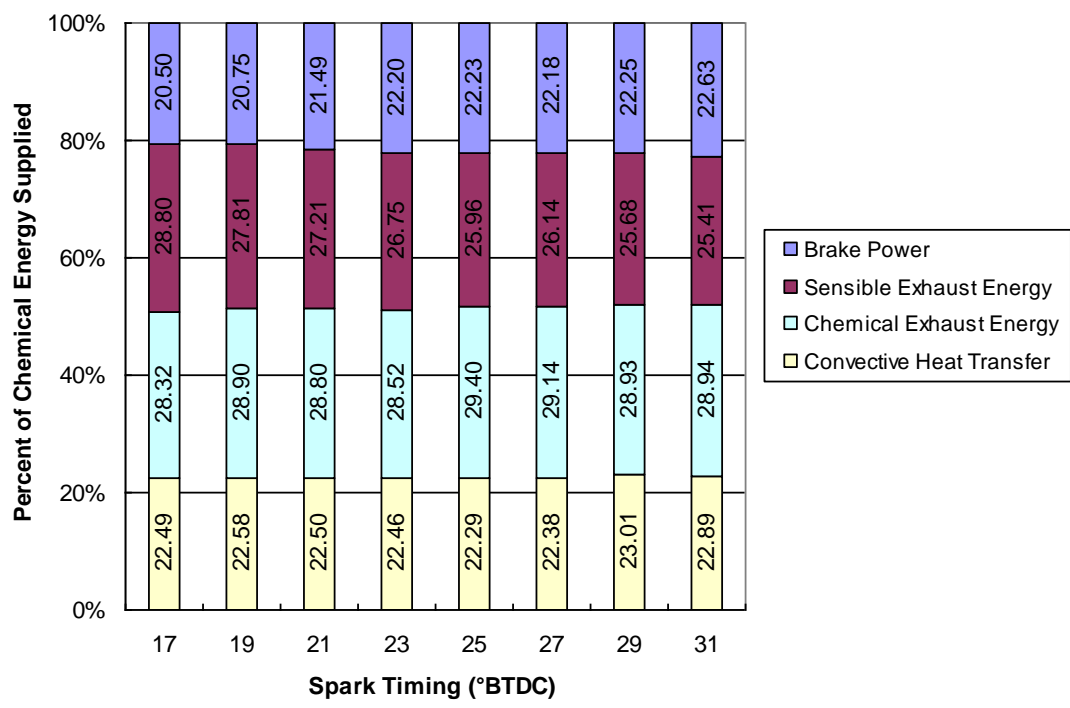
Figure 10.11: Energy distributions at mode 1 for various spark timings
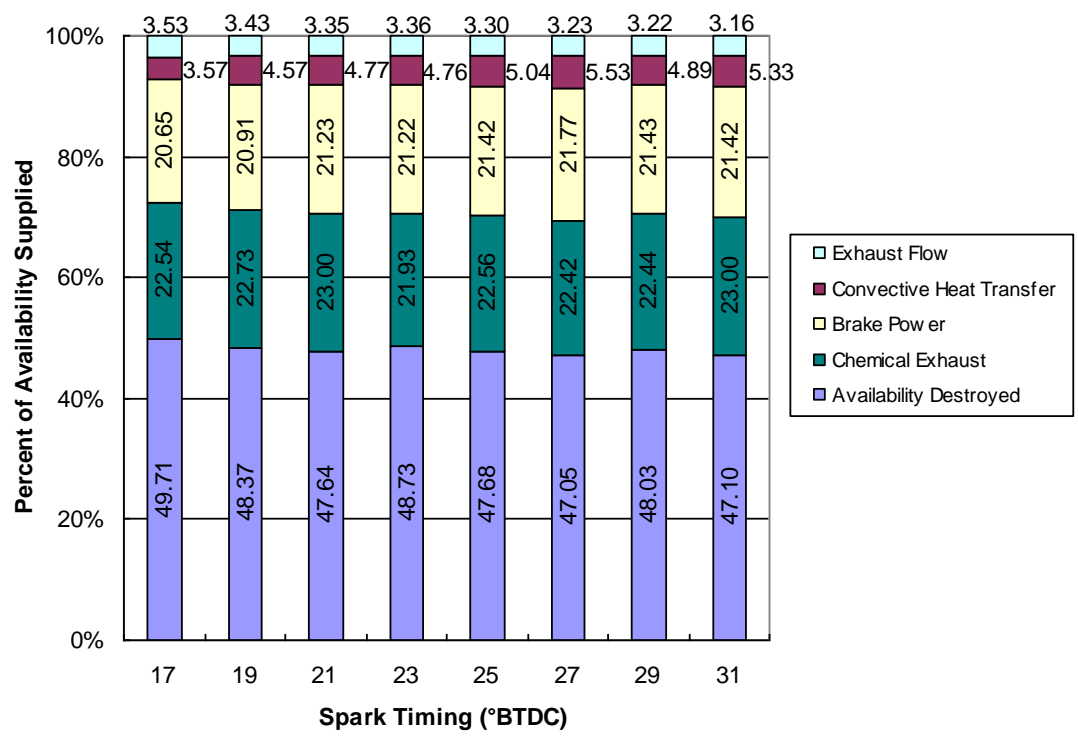
Figure 10.12: Availability distributions at mode 1 for various spark timings

The most important observation to be gathered from this figure is that availability destroyed only decreases by a small amount as ignition timing is advanced. This suggests that negligible improvement in the availability distribution is seen at this mode.

10.2.2. Mode 2. The results obtained from the analysis of mode 2 are similar in nature to those of mode 1. The magnitude of peak heat release rate and the slope of the mass fraction burned curves, Figures 10.13 and 10.14, both increase gradually as spark timing is advanced. This shows that there is a definitive increase in burn rate with spark timing advancement.
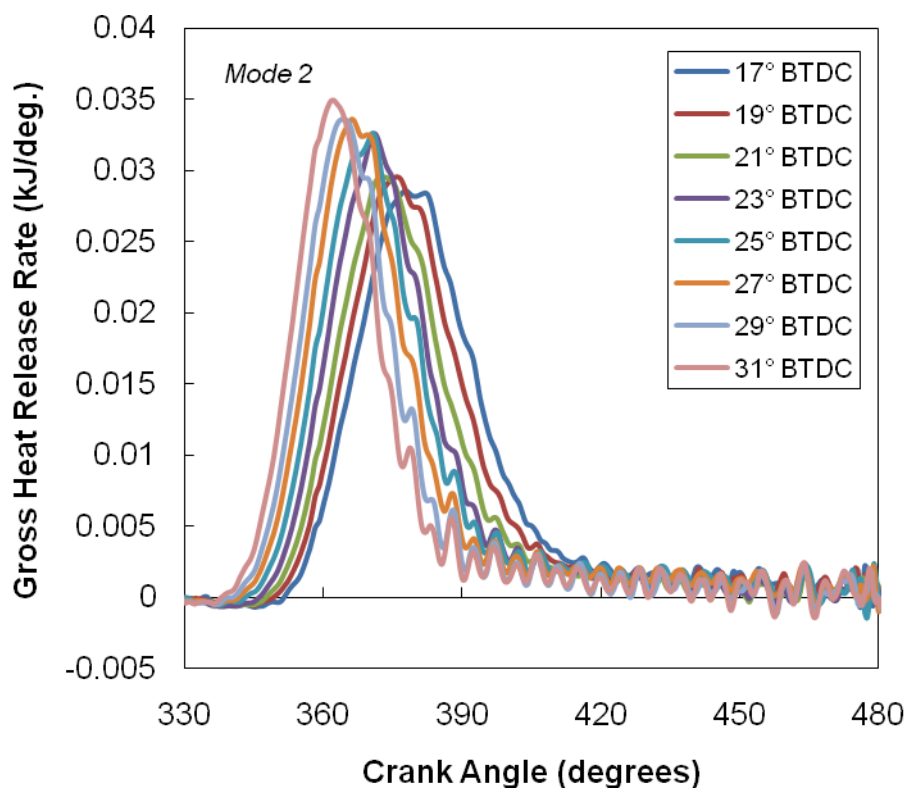
Figure 10.13: Heat release rate at mode 2 for various spark timings
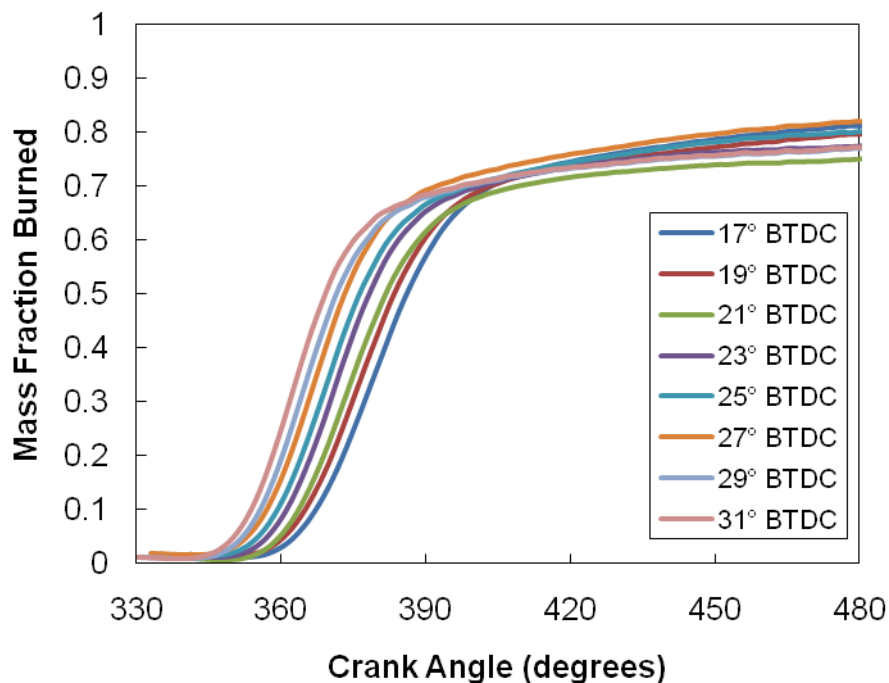
Figure 10.14: Mass fraction burned at mode 2 for various spark timings

This mode results in a greater difference in mass fraction burned at the end of combustion with the peak occurring at a timing of 27° ATDC. This indicates that the heat release rate model predicts better fuel utilization and higher engine efficiency as spark timing is advanced to a certain point.

The increase in burn rate causes the notable shifts in energy and availability distributions, Figures 10.15 and 10.16. From the energy balance results, Figure 10.15, it is evident that only the sensible exhaust energy decreases with advancements in spark timing. The minimum sensible exhaust energy corresponds to the maximum brake power. This effect is mirrored in the availability balance results shown in Figure 10.16.

Figure 10.15: Energy distributions at mode 2 for various spark timings
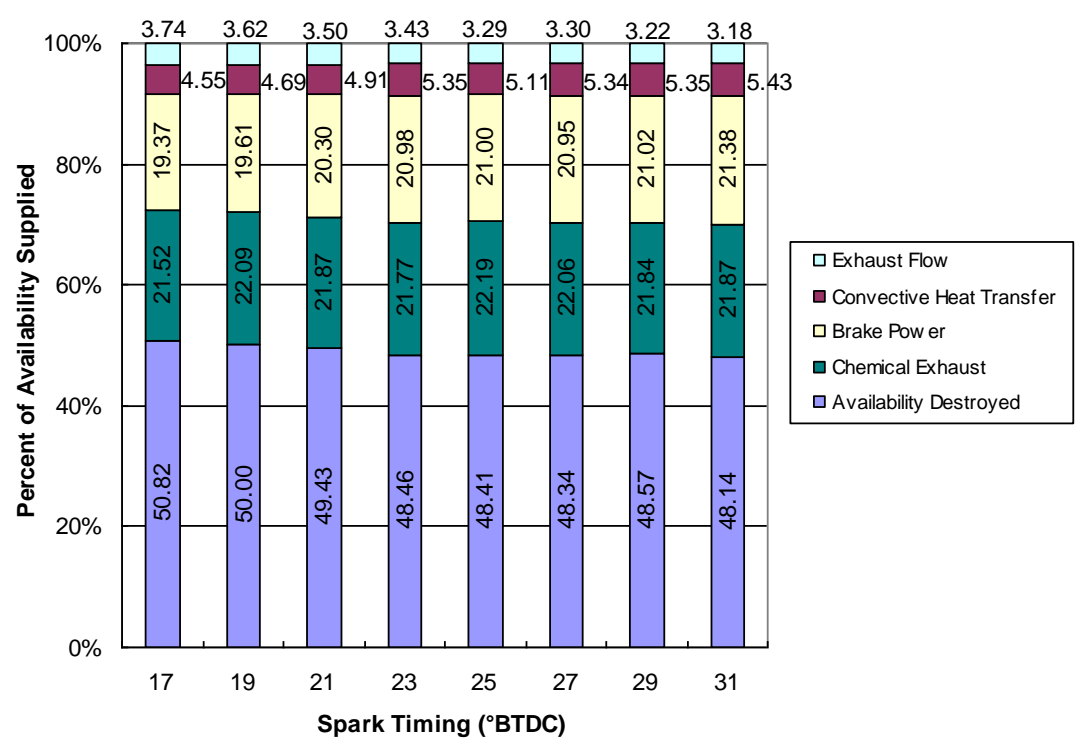
Figure 10.16: Availability distributions at mode 2 for various spark timings

A greater decrease in availability destroyed can also be seen for this mode than for mode 1. In internal combustion engines, the vast majority of availability destroyed is a result of the combustion process rather than heat transfer or other irreversibilities [14, 19]. Studies completed by Teh, Miller, and Edwards [14] show that availability destroyed is extremely dependent on the internal energy of the reactant mixture at the point of combustion. Furthermore, availability destroyed can be minimized by completing combustion at the highest possible internal energy state [15]. This high internal energy state is achieved as a result of the increased cylinder pressures and temperatures seen by advancing the spark timing. This explains the reduction in availability destroyed that occurs as spark timing is advanced.

From engine dynamics it is known that the maximum combustion temperature occurs when the reaction is near stoichiometric, i.e. complete combustion of the fuel occurs with no excess oxidizer. Combustion temperature decreases as the mixture becomes lean (larger air-to-fuel ratio) and also as it is richened (smaller air-to-fuel ratio). The maximum combustion temperature results in an increased internal energy state and, hence, a reduction in availability destroyed compared to the lower combustion temperatures seen with mixtures that are not stoichiometric. This illustrates how leaning the mixture of the rich-running test engine to a setting closer to stoichiometric will result in a reduction in availability destroyed. This concept is depicted in Figure 10.17 below. This generalized figure shows the behavior of availability destroyed with different reactant mixtures, displayed as equivalence ratios. Equivalence ratio is calculated as the ratio of the fuel-to-air ratio of the current mixture to the fuel-to-air ratio of the stoichiometric mixture. Therefore, an equivalence ratio of 1.0 is stoichiometric. Lean

mixtures are designated as ratios less than 1.0 and rich by ratios greater than 1.0. In [15],

Teh, Miller, and Edwards discuss this concept and show results for lean engine operation.
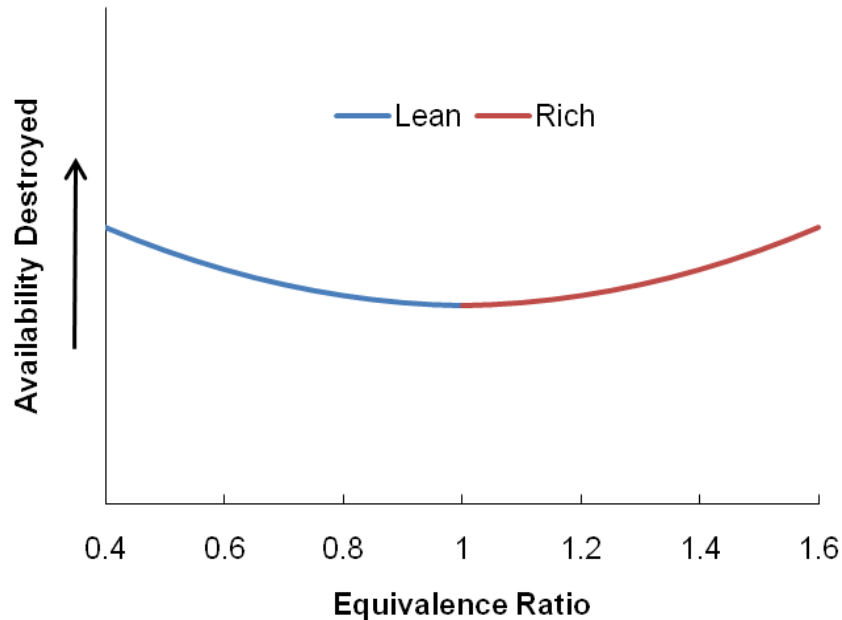

Figure 10.17: Behavior of availability destroyed with varying mixtures

10.2.3. Remaining Modes. For the remaining modes (3 – 6), the heat release rate

and mass fraction burned results are similar to those obtained for modes 1 and 2 so they

are not included in this discussion. The energy and availability distributions for each of

modes 3 through 6 are displayed below in Figures 10.18 – 10.25. These charts verify that

definitive improvements in energy and availability distributions are realized by advancing

the combustion phasing. These improvements come in the forms of increased brake

power, reduced exhaust energy and availability, decreased convective heat transfer

energy, and reduced irreversibilities in the destruction of availability.
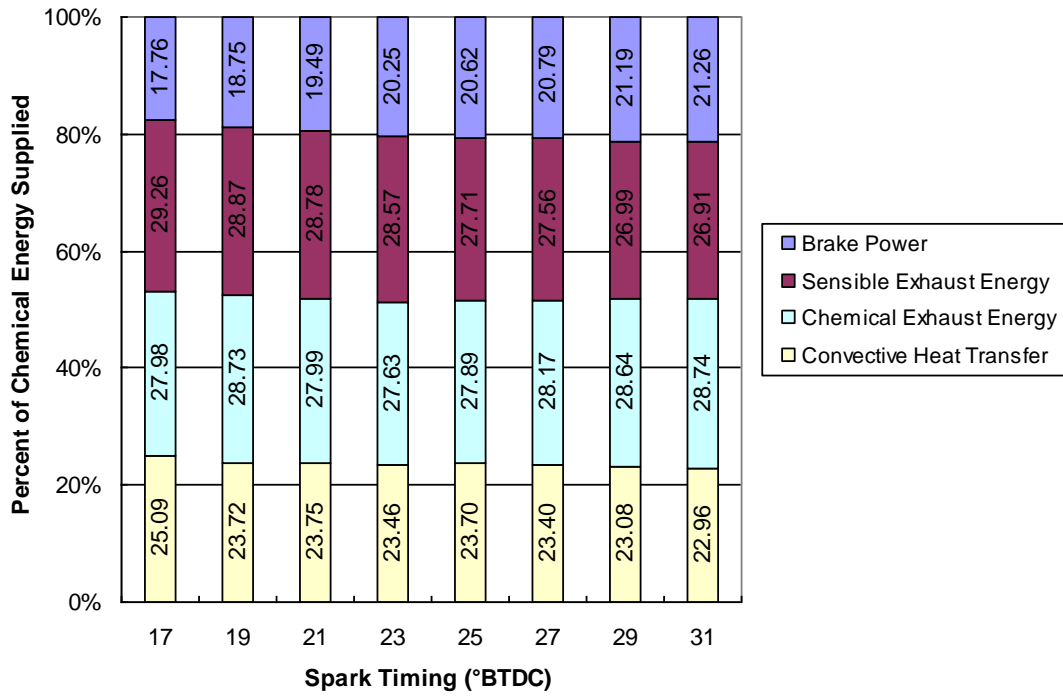
Figure 10.18: Energy distributions at mode 3 for various spark timings
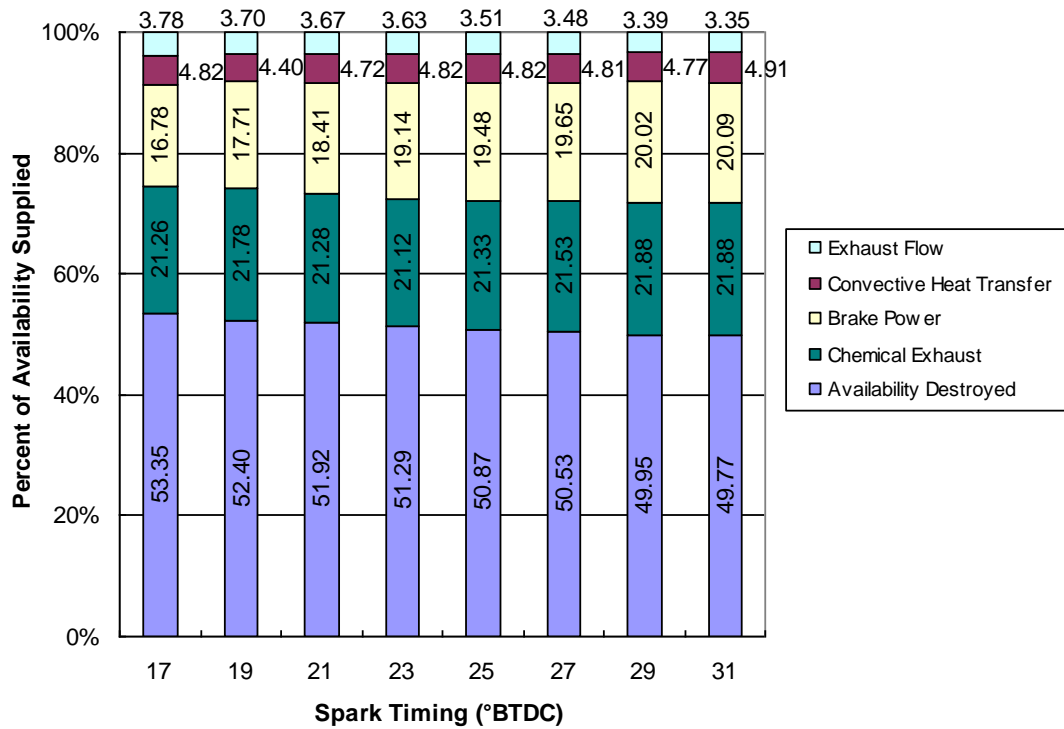
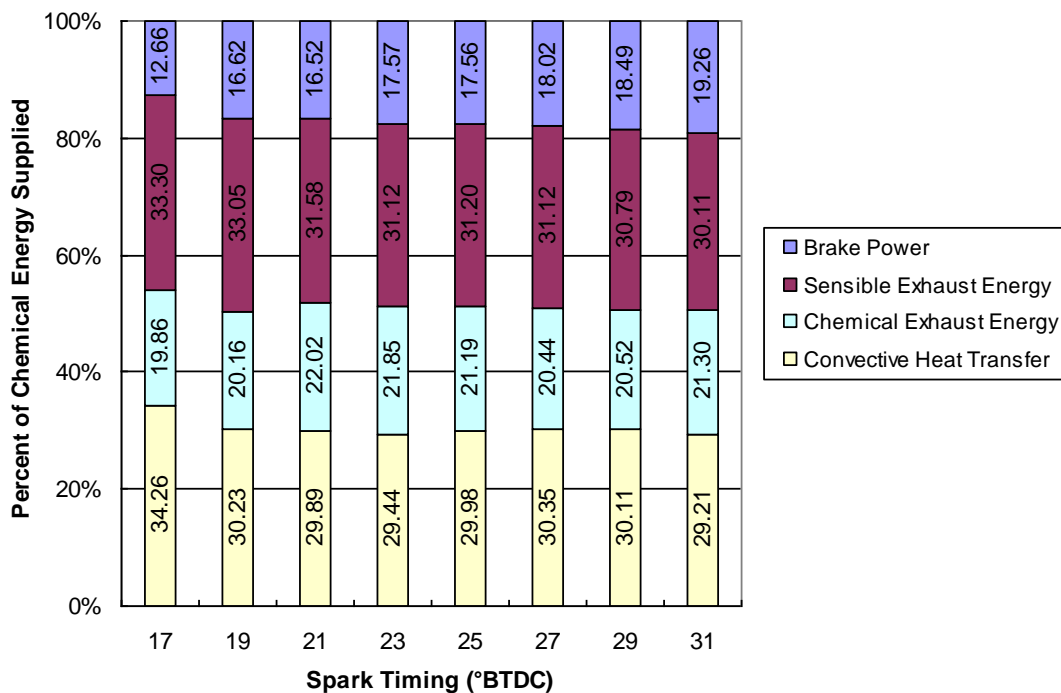**Figure 10.19:** Availability distributions at mode 3 for various spark timings

Figure 10.20: Energy distributions at mode 4 for various spark timings
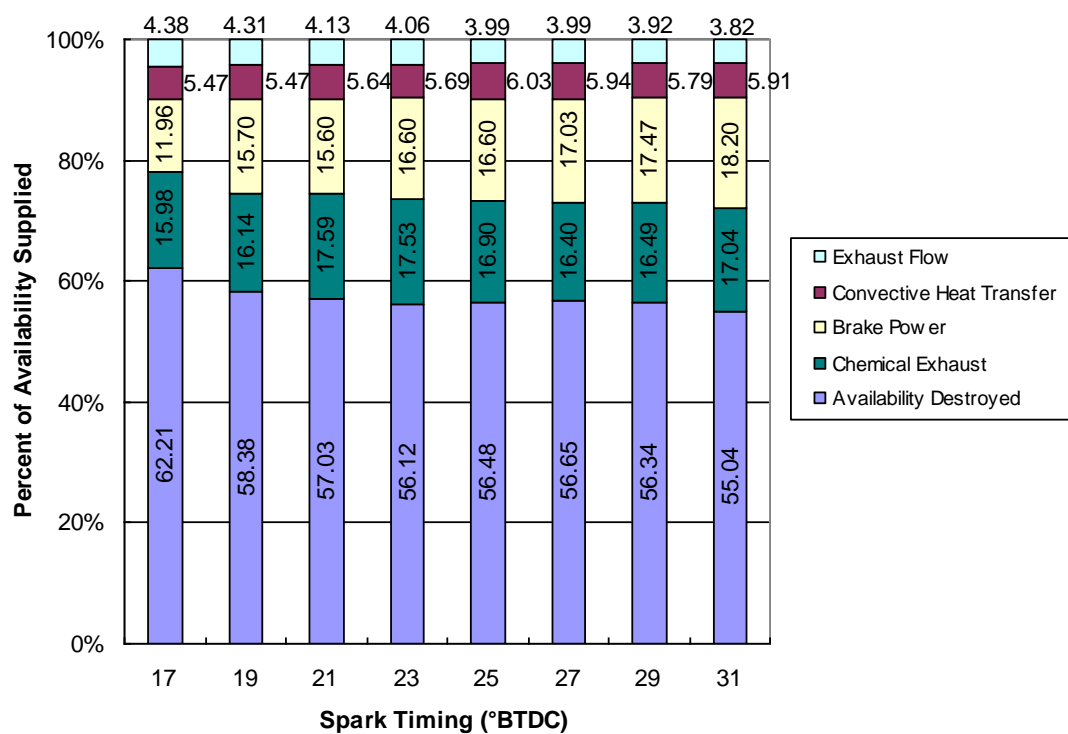

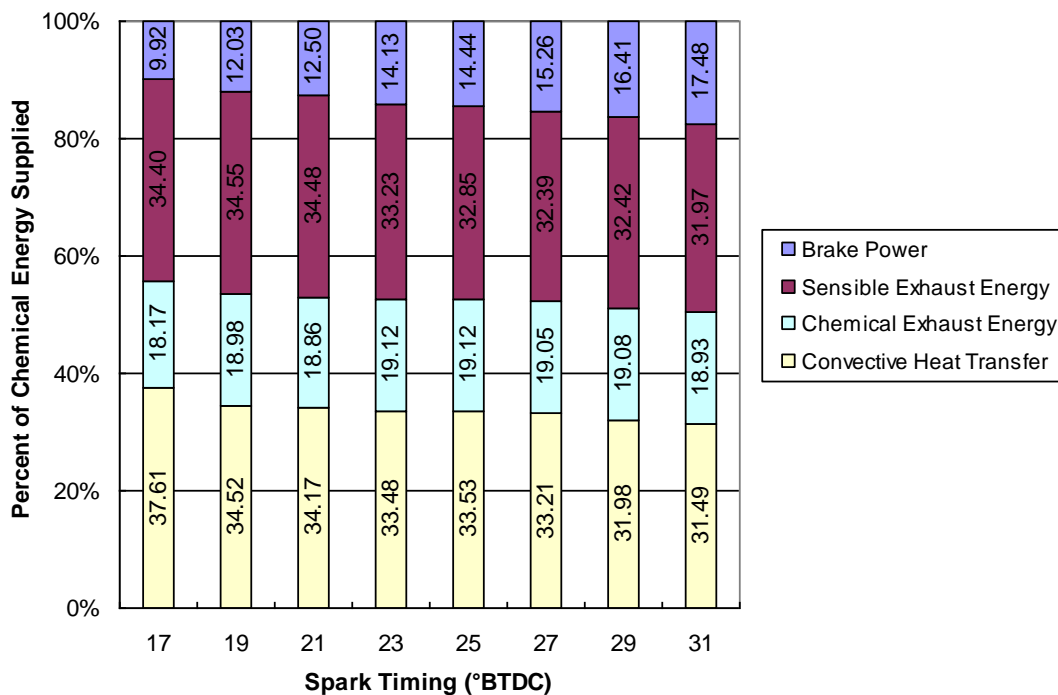**Figure 10.21:** Availability distributions at mode 4 for various spark timings

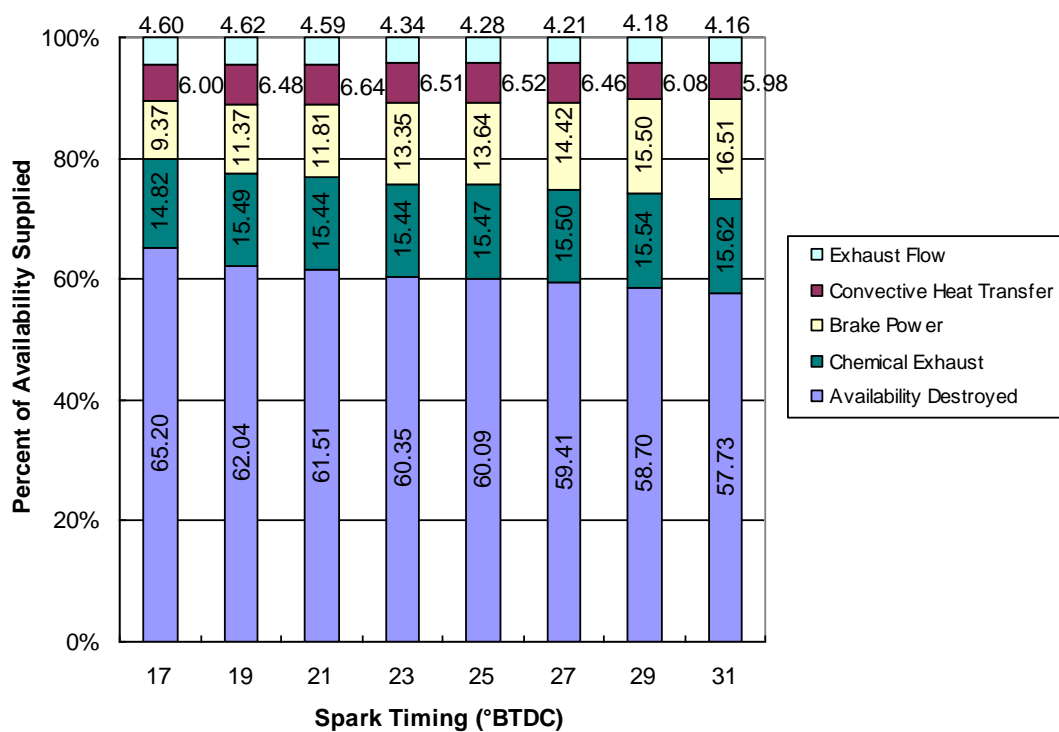**Figure 10.22:** Energy distributions at mode 5 for various spark timings

Figure 10.23: Availability distributions at mode 5 for various spark timings
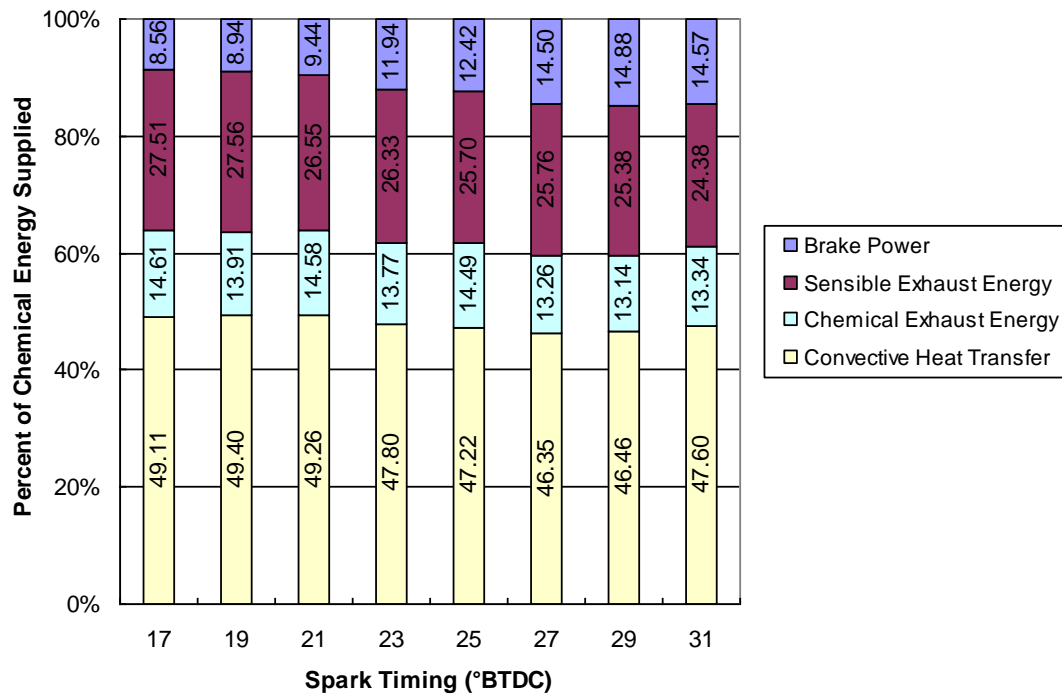
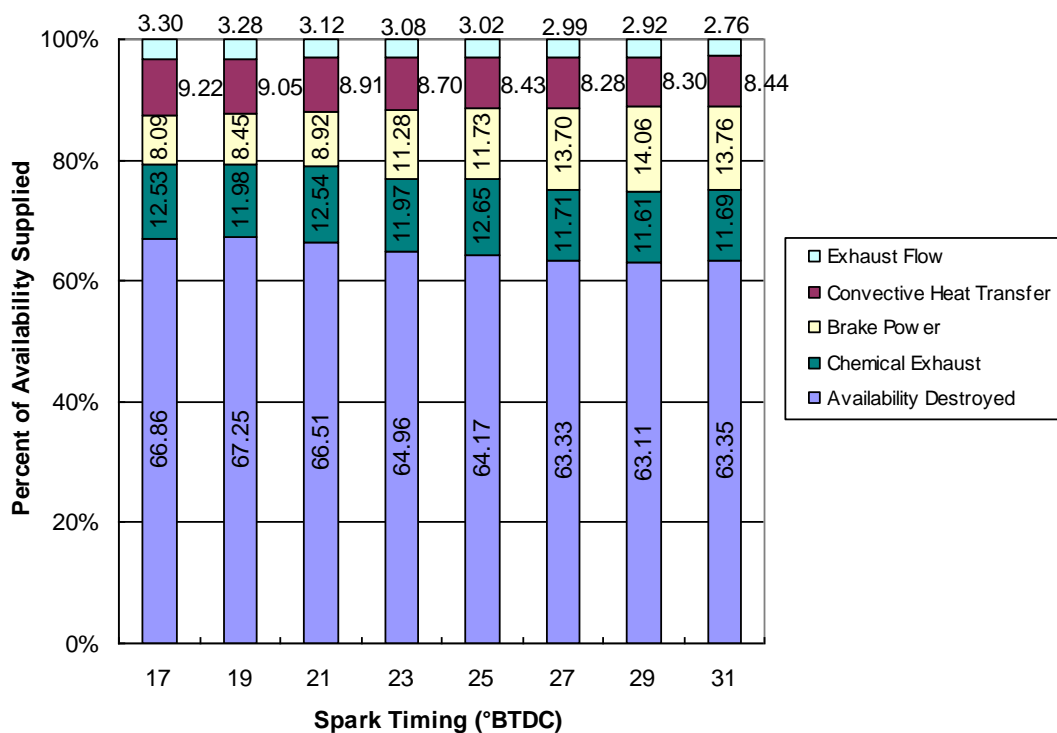**Figure 10.24:** Energy distributions at mode 6 for various spark timings

Figure 10.25: Availability distributions at mode 6 for various spark timings

10.2.4. Improvements in Efficiency. The numerous forms of improvements in the energy and availability distributions manifest themselves in first and second law efficiency. These efficiencies are determined at each spark timing for every mode and are displayed in Figures 10.26 and 10.27. The improvement in engine efficiency with advancements in spark timing can very easily be seen in these figures. This is especially true for the lower load and engine speed set points (higher modes) due to the fact that the engine is operating further from its optimal ignition timing in the stock configuration.
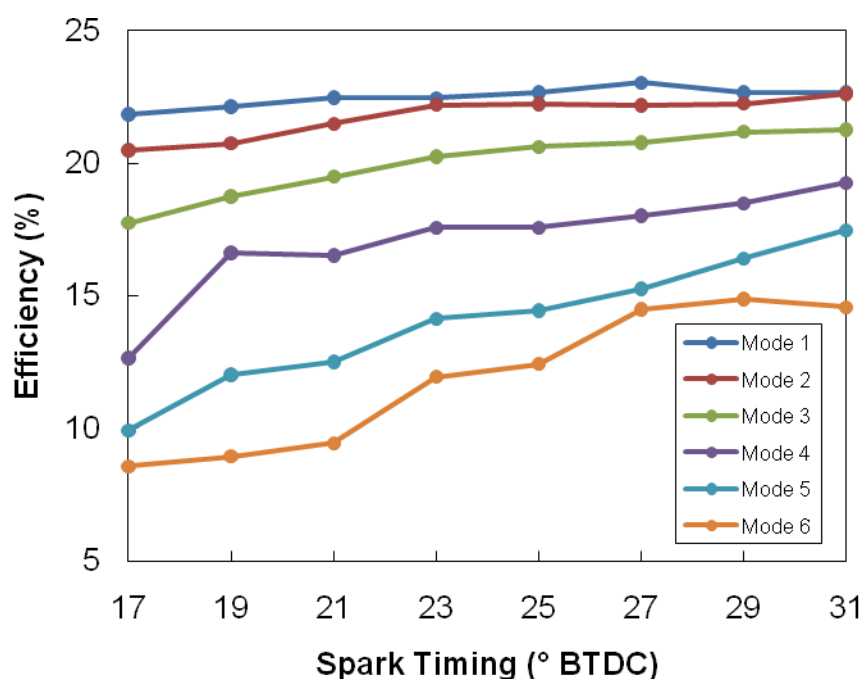

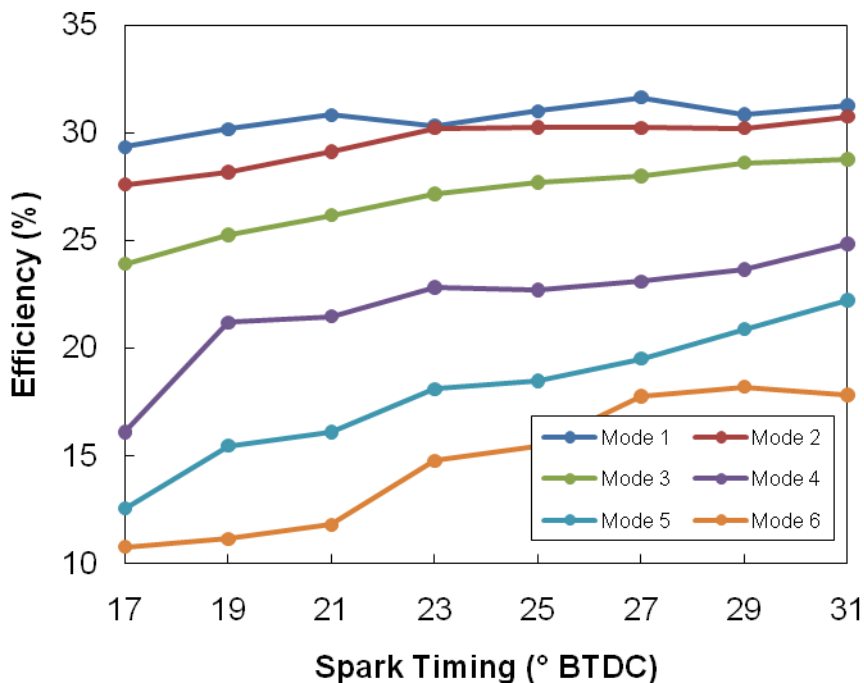**Figure 10.26:** First law efficiencies for various spark timings

Figure 10.27: Second law efficiencies for various spark timings

10.2.5. Emissions. An analysis is also conducted on the emissions measurements collected during variable spark timing performance tests. The exhaust gas concentrations for CO_2, CO, O_2, unburned hydrocarbons (uHC), and NO_x are plotted against spark timing values in Figures 10.28 – 10.32 below. In all of these figures, the measurements for the different modes are each specified by a different color plot. CO_2, CO, and O_2 concentrations are given in percent (%) while NO_x and unburned hydrocarbons are shown in parts per million (ppm) and parts per million Carbon.
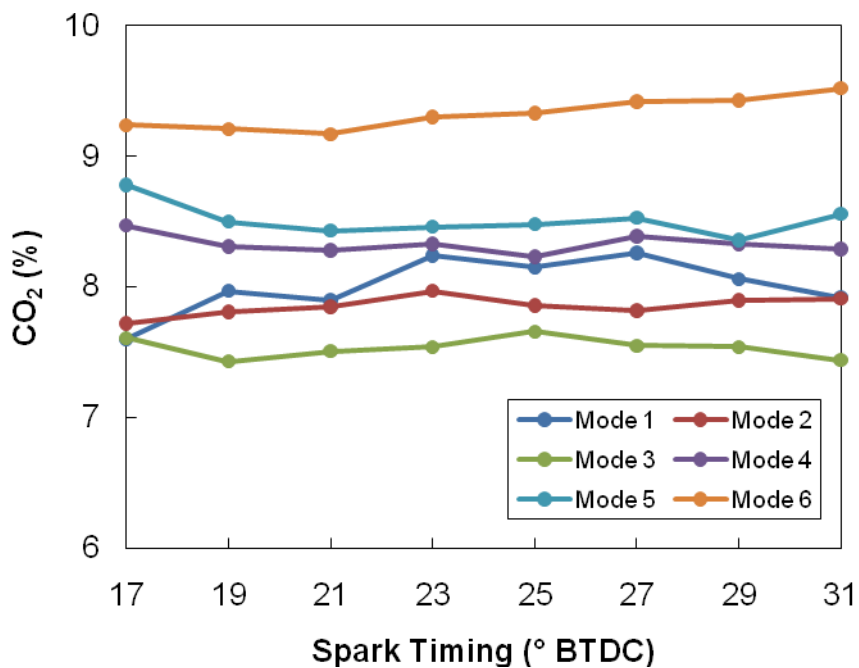
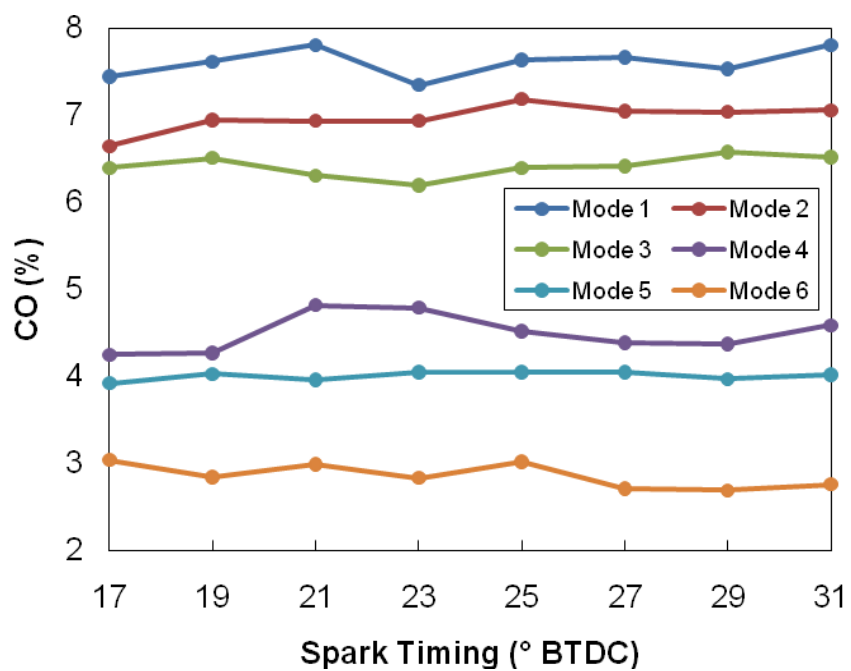**Figure 10.28:** CO_2 concentrations for varying spark timing

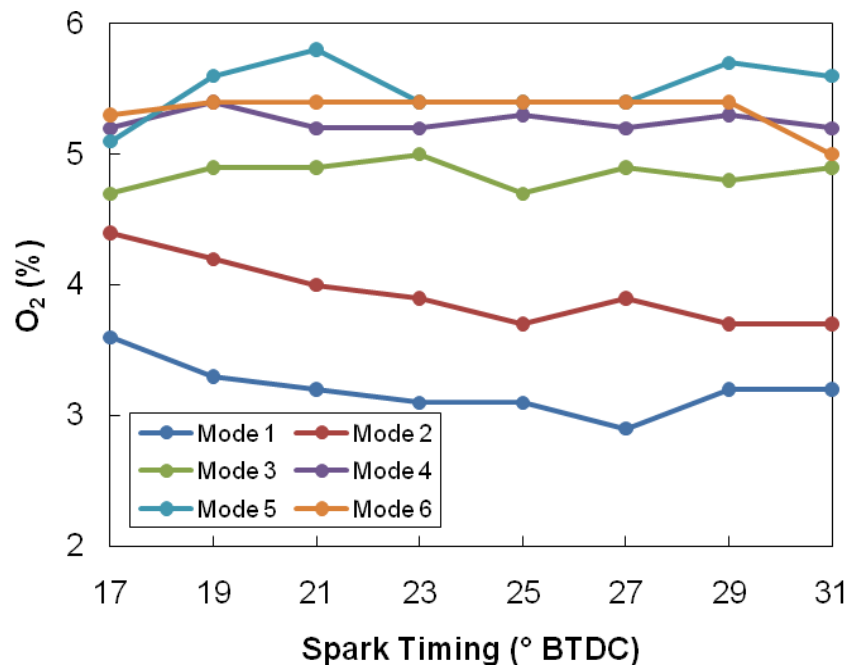**Figure 10.29:** CO concentrations for varying spark timing

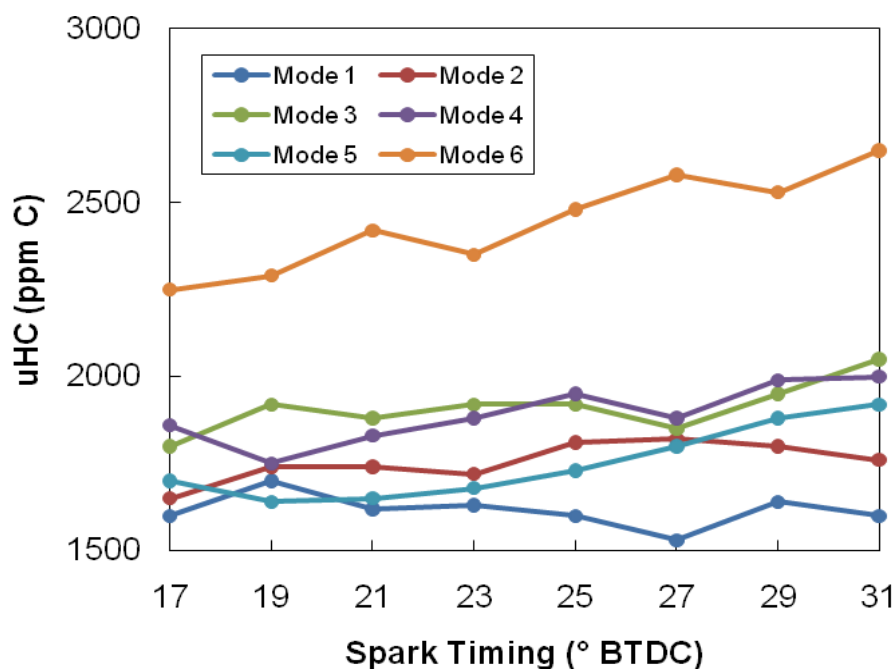**Figure 10.30:** O$_2$ concentrations for varying spark timing

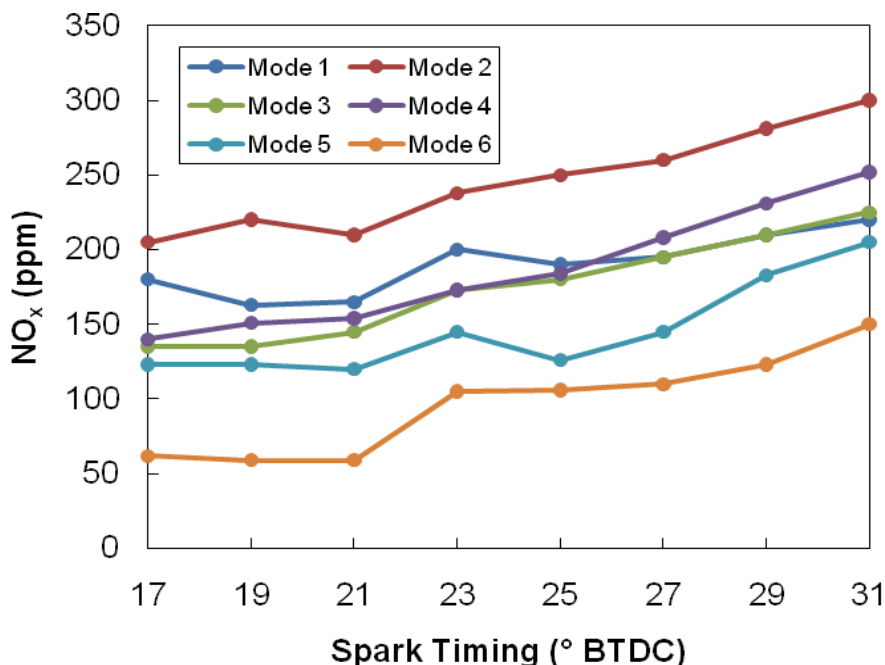**Figure 10.31:** uHC concentrations for varying spark timing

Figure 10.32: NO_x concentrations for varying spark timing

Figures 10.28 through 10.30 show that the CO_2, CO, and O_2 concentrations remain fairly constant as ignition timing is advanced. There are, however, large differences among modes. CO_2, CO, and O_2 concentrations are highly dependent on the air-to-fuel ratio being inducted into the engine. Lean mixtures result in a small amount of CO and high concentrations of CO_2 and O_2. The opposite effect is seen when a rich mixture is used. It is shown in Figure 10.33 below that the reactant mixture is leaned significantly (increasing air-to-fuel ratio) as the mode number increases. This fully explains why CO_2 and O_2 concentrations increase with mode while the CO concentration decreases. In searching for an optimal ignition timing, the CO concentration is of primary concern due to its environmental impact and federal regulations restricting the production of this exhaust component.
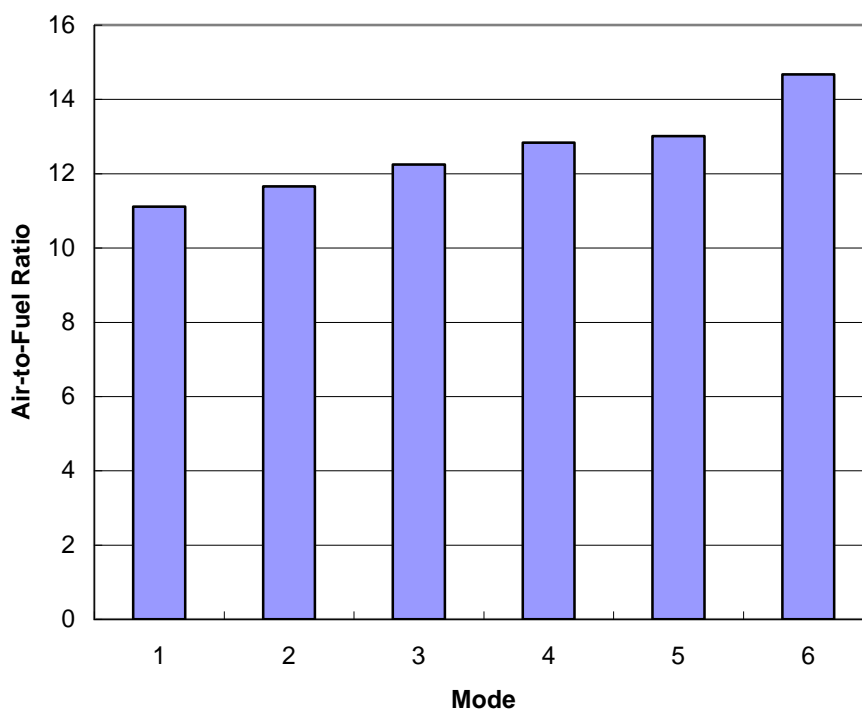
Figure 10.33: Air-to-fuel ratios per mode

A small increase in uHC concentration is seen with advanced spark timing with the exception of a slight reduction at mode 1. Larger variations are seen when different modes are compared. The inducted mixture is the leanest at mode 6 (shown in Figure 10.33) due to carburetor properties but the ignition timing is so retarded for this mode that minimal combustion occurs. This means that only a small portion of this inducted fuel is consumed in the reaction. More uHC is expelled in the exhaust at this mode than the others (shown in Figure 10.31) where more complete combustion occurs.

An increase in NO_x concentration is also evident as spark timing is advanced. This is due to the direct correlation of combustion temperature to NO_x formation. As combustion temperature is increased, with advanced spark timing, NO_x concentration also increases. NO_x concentration also decreases with increasing mode number, with a

slight exception for mode 2. The decreasing cylinder pressure with increasing mode number causes a reduction in combustion temperature which, in turn, shrinks NO_x concentration.

10.2.6. Maximum Brake Torque. The first and second law analyses as well as the emissions investigation provide great visualizations of the impact of combustion phasing. They also provide good estimates of the optimal spark timing for the test engine but, in order to determine this with certainty, an examination of maximum brake torque (MBT) is conducted. A generally accepted rule of thumb states that MBT will be achieved when the peak cylinder pressure and CA50 occur at 16° and 10° ATDC, respectively [18]. This rule can be validated by the data collected in this variable spark timing study. It is shown below in charts that display CA50 and peak pressure location for each cylinder on the left axis and brake torque values on the right plotted with respect to spark timing.

In these three figures, 10.34 through 10.36, maximum brake torque is identified by the black, bold outline. It can be seen in the modes 1 and 2 figures that, as spark timing is advanced, a peak torque is reached then a decrease in torque results. For mode 3, the peak torque is seen at the most advanced timing. At these maximum brake torque timings, the CA50 and peak cylinder pressure locations are well within 2° of the rule of thumb specifications. This observation validates the general MBT rule for use on small internal combustion engines such as the test engine. The spark timing is not advanced far enough at modes 4 – 6 to identify the maximum brake torque timing. These modes require further advancement of ignition timing which is unfeasible due to the onset of abnormal combustion that will occur with further advancements.
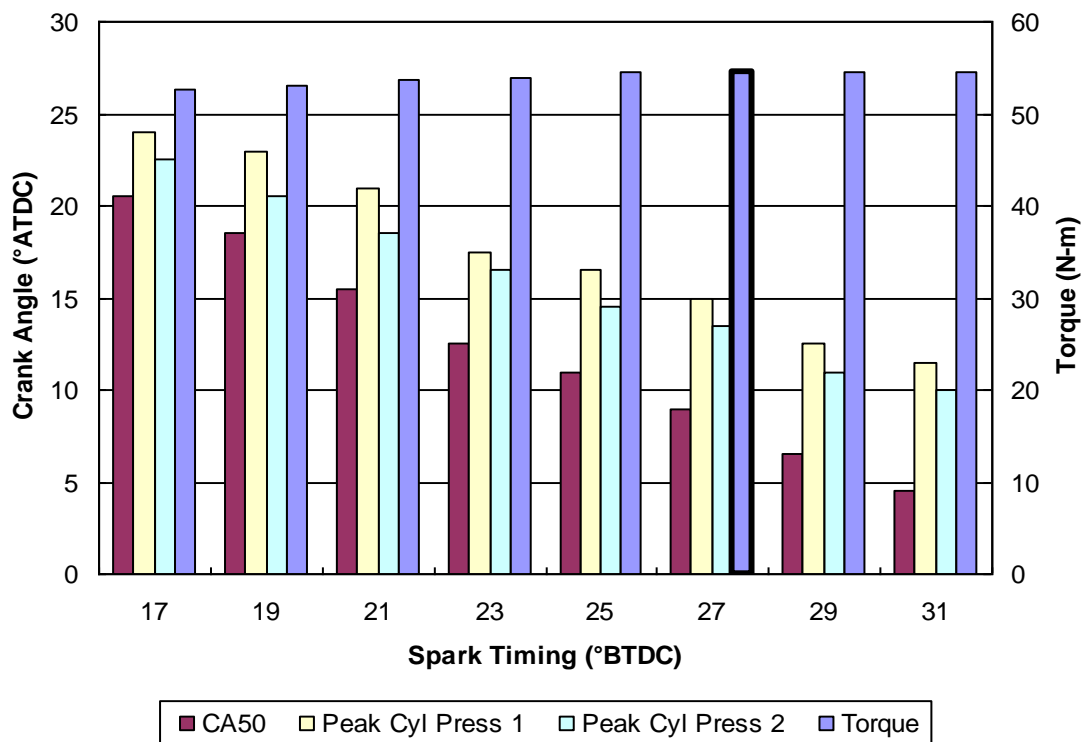
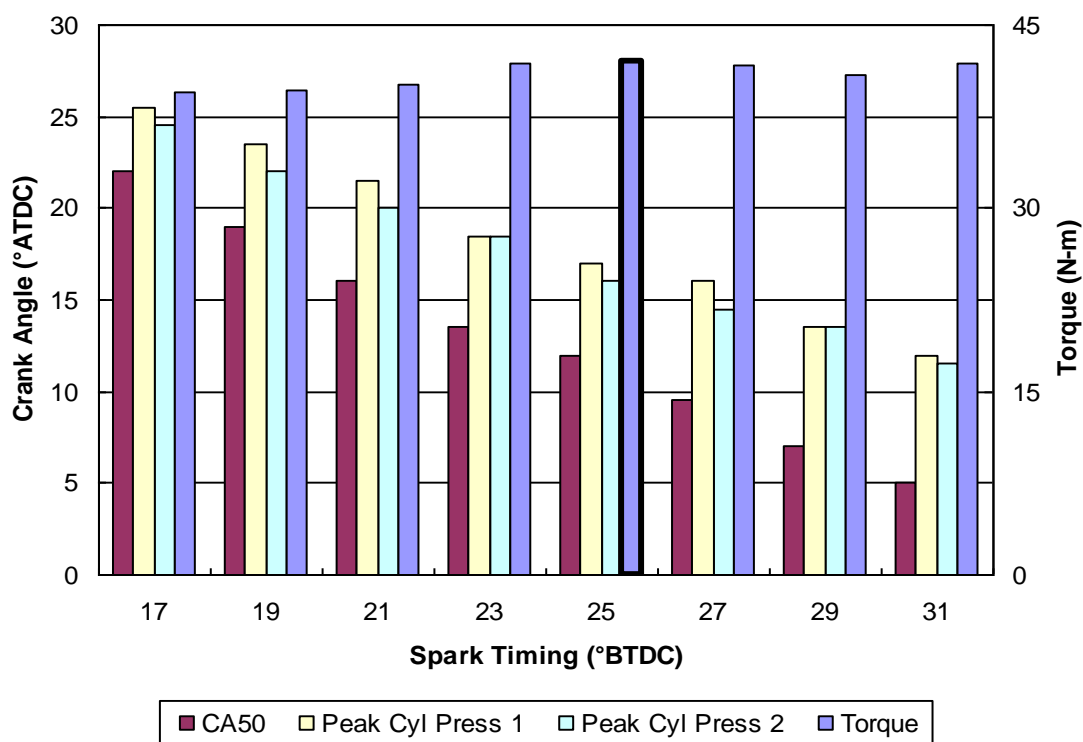**Figure 10.34:** MBT validation for mode 1
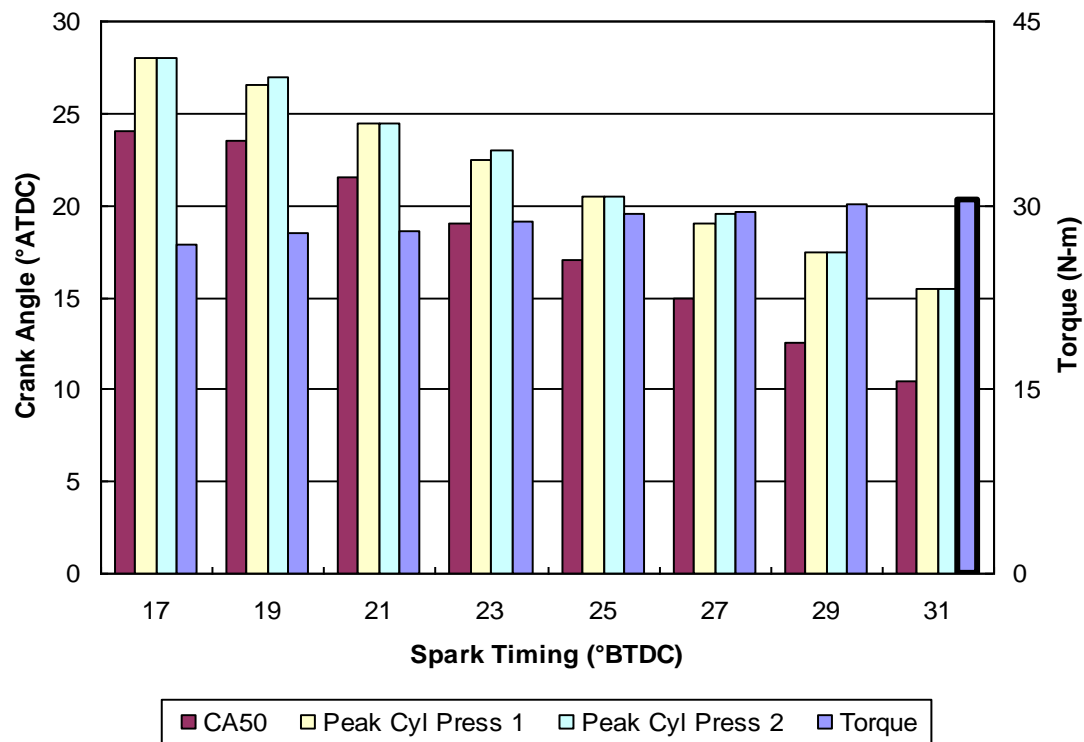

Figure 10.35: MBT validation for mode 2

Figure 10.36: MBT validation for mode 3

11. CONCLUSIONS

11.1. ANALYSIS TECHNIQUES

Many techniques are presented in this thesis that are used to analyze the combustion process in an internal combustion engine. Combustion duration and burn rate can be explored with the use of the heat release rate model developed for this investigation. This model returns several important combustion-related metrics that, when used in unison, provide a complete picture of the burning process in the combustion chamber. The energy and availability balances display engine performance as well as the impact of changes in the phasing and duration of combustion. Maximum brake torque is also extracted from this information to aid in the identification of optimal engine configurations.

The combination of these analysis techniques prove to be extremely valuable in experimenting with variations in the combustion process. The specific approach and equations described in this thesis are well adapted for small spark ignition engines.

11.2. OPTIMAL IGNITION TIMING

Using the previously described heat release rate model, energy and availability distributions, exhaust gas concentrations, maximum brake torque analysis, and efficiency calculations, optimal ignition timing for the test engine can be identified. For mode 1, this optimal timing is determined to be 27° BTDC. Although mode 2 achieved slightly higher efficiencies at a spark timing of 31° BTDC, 25° BTDC is chosen as the optimal ignition timing due to the maximum brake torque analysis along with the knowledge that abnormal combustion phenomena may take effect at the more advanced setting. This

setting also results in lower NO_x production than more advanced spark timings. Figure 10.34 illustrates that the MBT timing for mode 3 is 31° BTDC but this maximum torque value is only slightly larger than the values at 27 and 29° BTDC. There is also a negligible difference in the energy and availability distributions and efficiencies between timings of 27 and 29° BTDC. There are, however, much lower uHC and NO_x concentrations at 27° BTDC. Therefore, 27° BTDC is chosen as the optimal spark timing for mode 3. 31° BTDC is selected as the optimal ignition timing for modes 4 and 5 even though maximum brake torque and peak efficiencies are not found in the range of spark timings investigated. It is believed that further advancement will result in abnormal combustion, "knock", especially with the lower octane fuels that the majority of operators use. Less advanced spark timing at these modes would cause lower uHC and NO_x emissions but a large reduction in efficiency will also result. From the results presented in this thesis, 29° BTDC is the best spark timing for mode 6. Like modes 4 and 5, this is limited by the onset of abnormal combustion with advancement past 31° BTDC.

A comparison of emission measurements is completed between the stock ignition system and the engine operating on its optimal ignition timing for each mode. The CO_2, CO, and O_2 comparison can be seen for the stock and optimal timing in Figures 11.1 and 11.2, respectively. Then uHC and NO_x concentrations are compared where Figure 11.3 shows the stock measurements and Figure 11.4 displays measurements taken with the optimal spark timing.
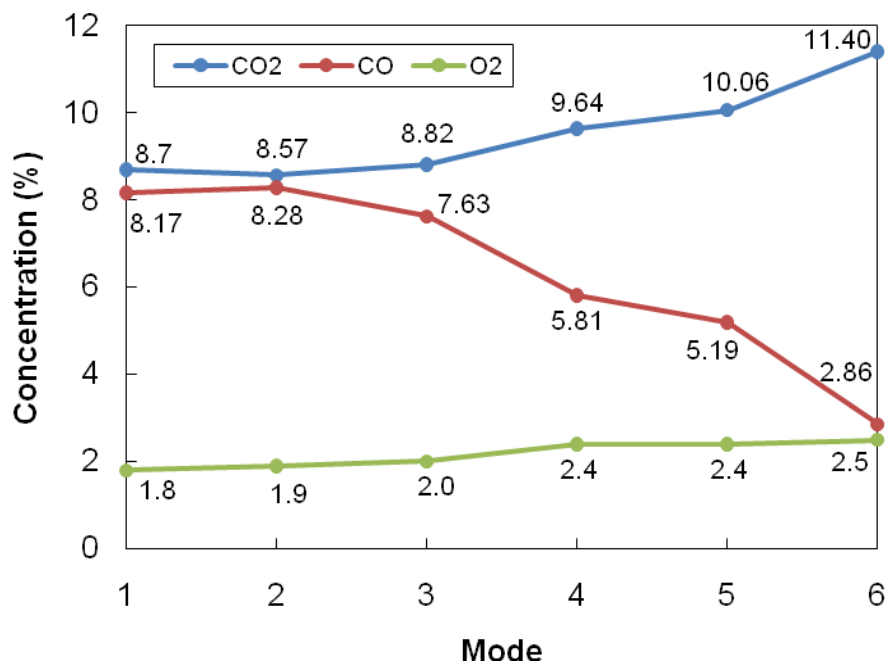
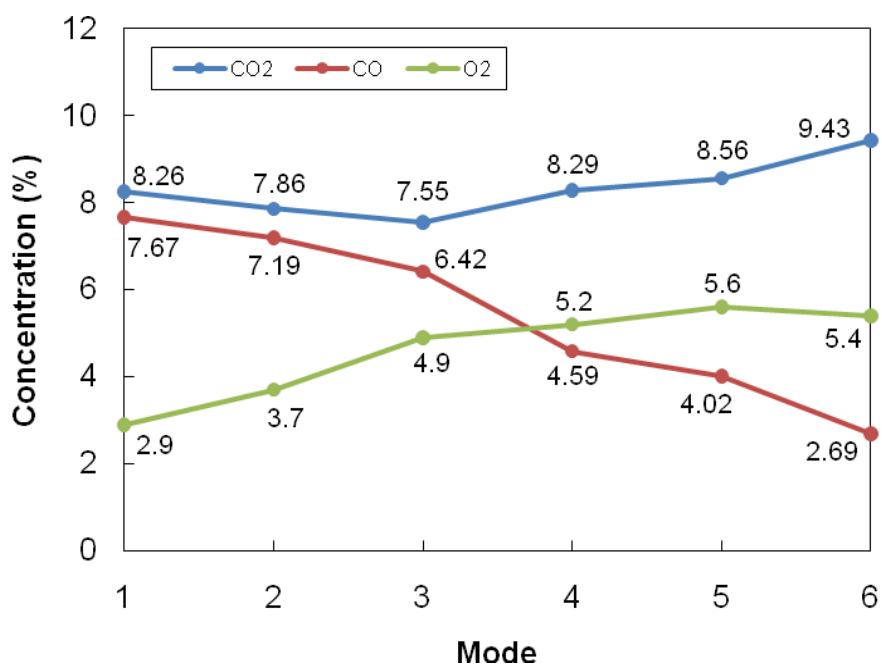**Figure 11.1:** CO_2, CO, and O_2 emissions for stock spark timing

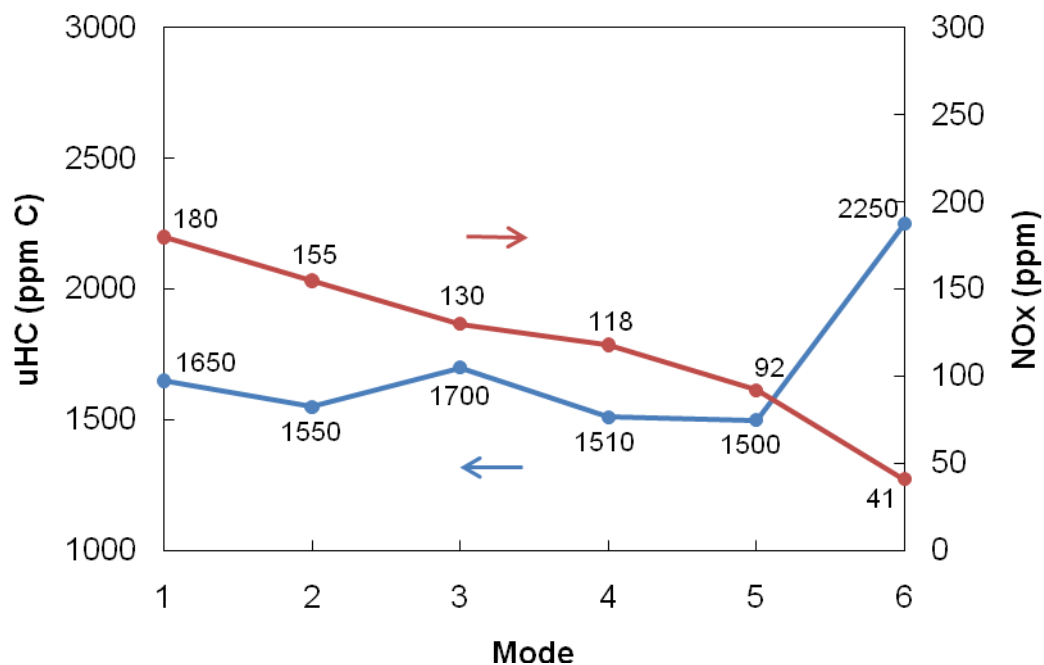**Figure 11.2:** CO_2, CO, and O_2 emissions for optimal spark timing

Figure 11.3: uHC and NO$_x$ emissions for stock spark timing
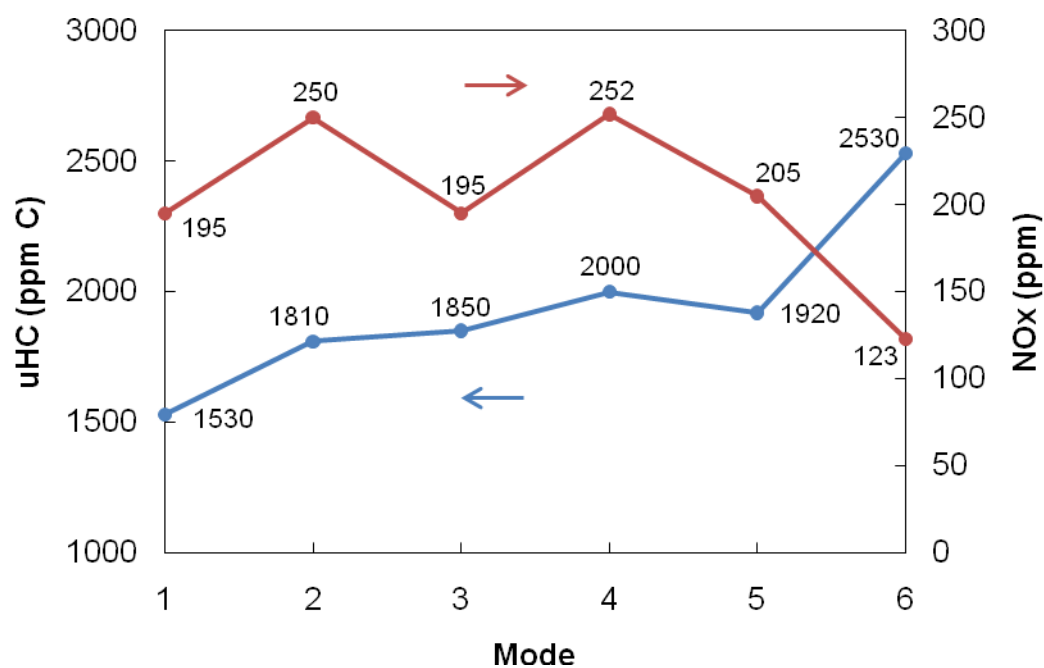

Figure 11.4: uHC and NO$_x$ emissions for optimal spark timing

From these results, it can be seen that the CO levels are lower at all modes when the optimal spark timing is used as opposed to the stock setting. NO_x and uHC react in a different manner. NO_x concentrations are higher at all modes for the optimal timing while uHC is only larger for modes 2 – 6 when the optimal spark timing is used. Brake weighted emissions for this optimal engine configuration are also calculated. The CO concentration is 349.97 g/kW-hr while 7.94 g/kW-hr is seen as uHC + NO_x. Neither of these emissions exceeds the Phase 3 limits specified in 40 CFR 1054.105. These limits are 610 g/kW-hr for CO and 8.0 g/kW-hr for uHC + NO_x.

The total efficiency, weighted for each mode then summed, is determined for the engine operating on the optimal ignition timing. These weighted efficiency values, along with the first and second law efficiencies at each mode, are provided in Table 11.1 below with the corresponding values obtained from the stock ignition system. A 30% improvement in first law efficiency and a 27% improvement in second law efficiency can be seen. Some of this improvement is due solely to the change to a more consistent ignition system, however, the majority results from operating at the engine's optimal spark timing. These calculations provide further proof that engine and, therefore, fuel efficiency is increased by advancing the ignition timing to its optimal setting.

Table 11.1: Weighted efficiency for stock and optimal ignition timing

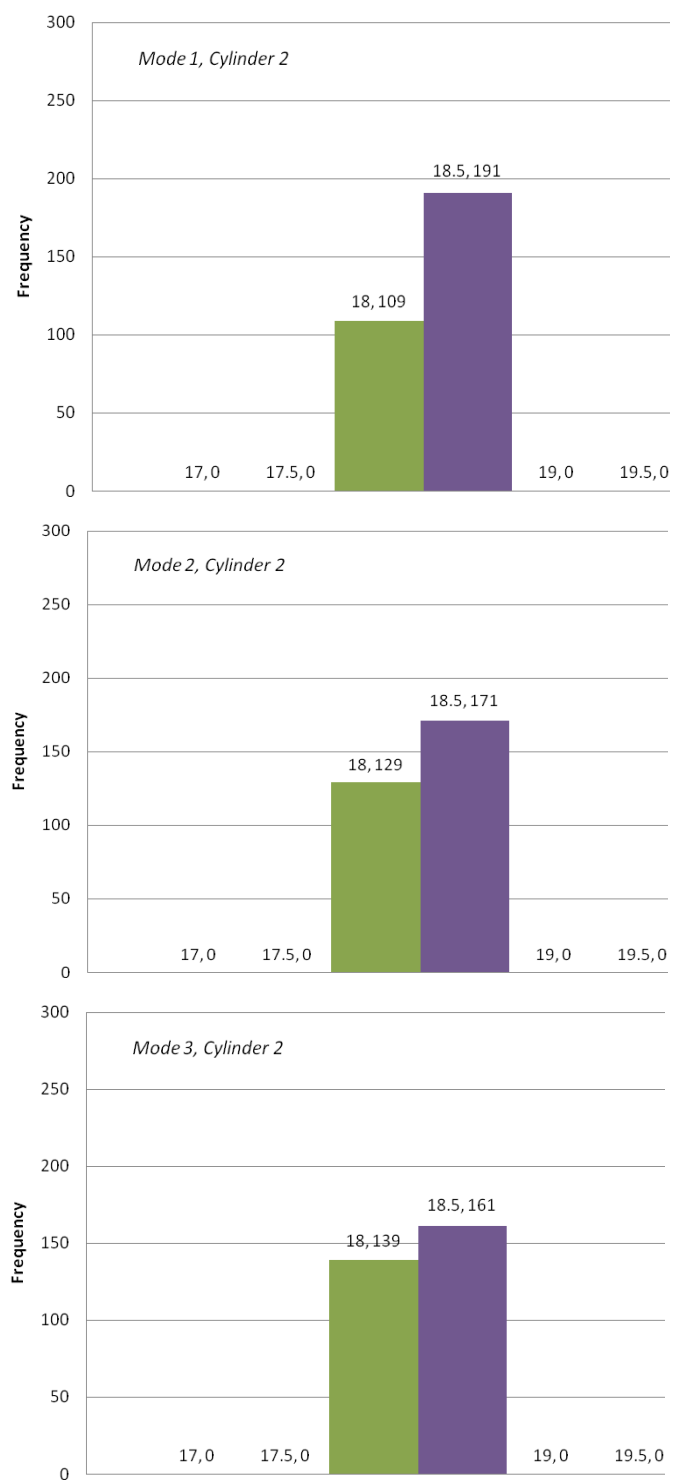|	1st Law Efficiency (%)		2nd Law Efficiency (%)	
	Stock	Optimal	Stock	Optimal
Mode 1 (9%)	20.53	23.04	27.97	31.63
Mode 2 (20%)	19.68	22.23	27.27	30.26
Mode 3 (29%)	17.21	20.79	23.64	27.99
Mode 4 (30%)	13.44	19.26	17.84	24.85
Mode 5 (7%)	9.88	17.48	13.00	22.24
Mode 6 (5%)	1.80	14.88	2.29	18.22
Weighted	**15.59**	**20.29**	**21.20**	**26.94**

APPENDIX

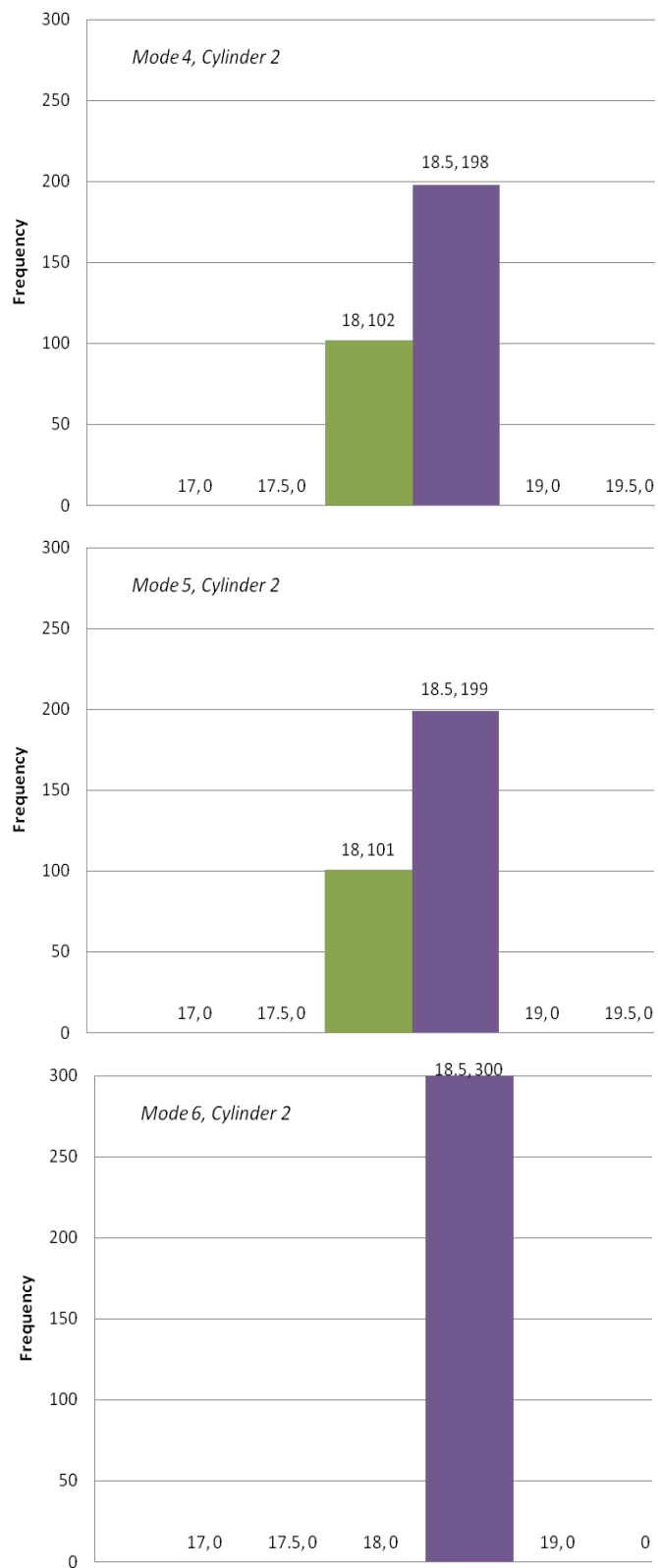**Figure A.1:** Cylinder 2 spark timing dispersions for modes 1 through 3

Figure A.2: Cylinder 2 spark timing dispersions for modes 4 through 6
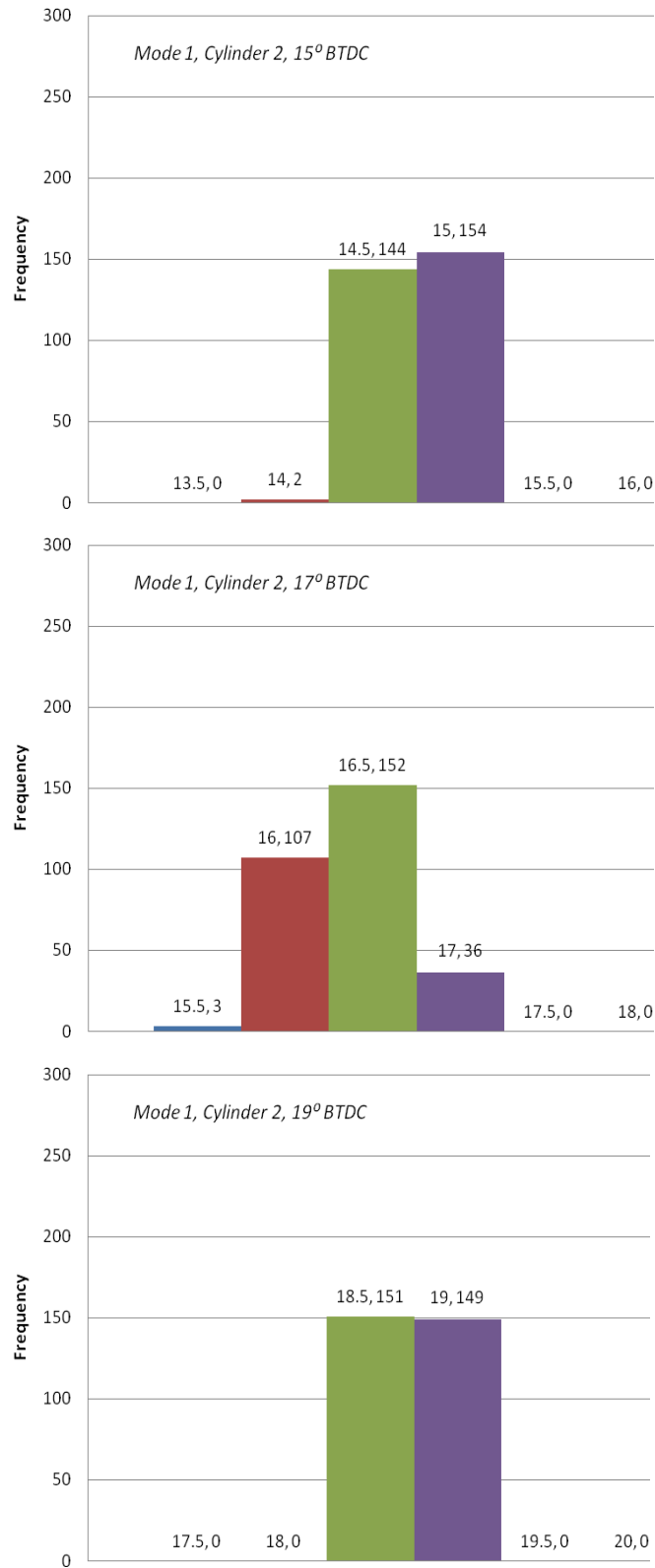
Figure A.3: Cylinder 2, mode 1 dispersions for timings 15, 17, and 19° BTDC
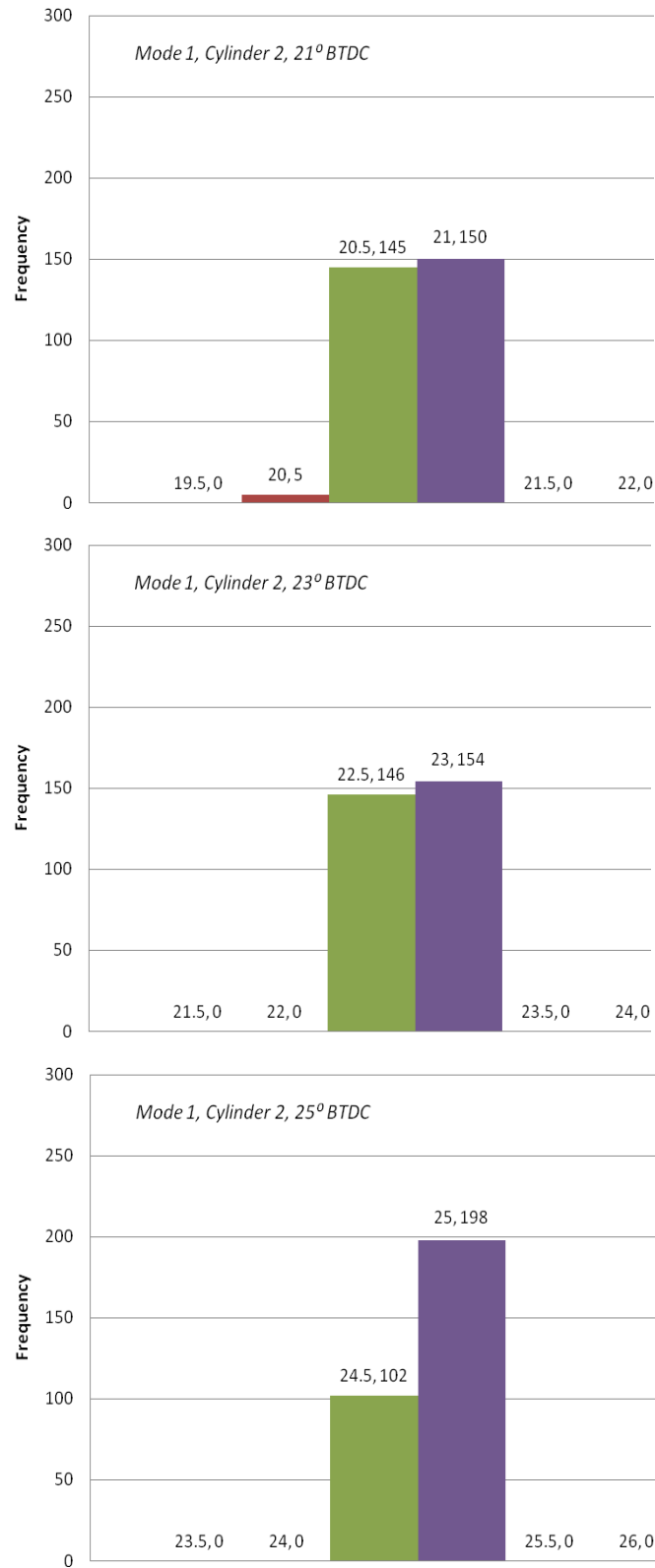
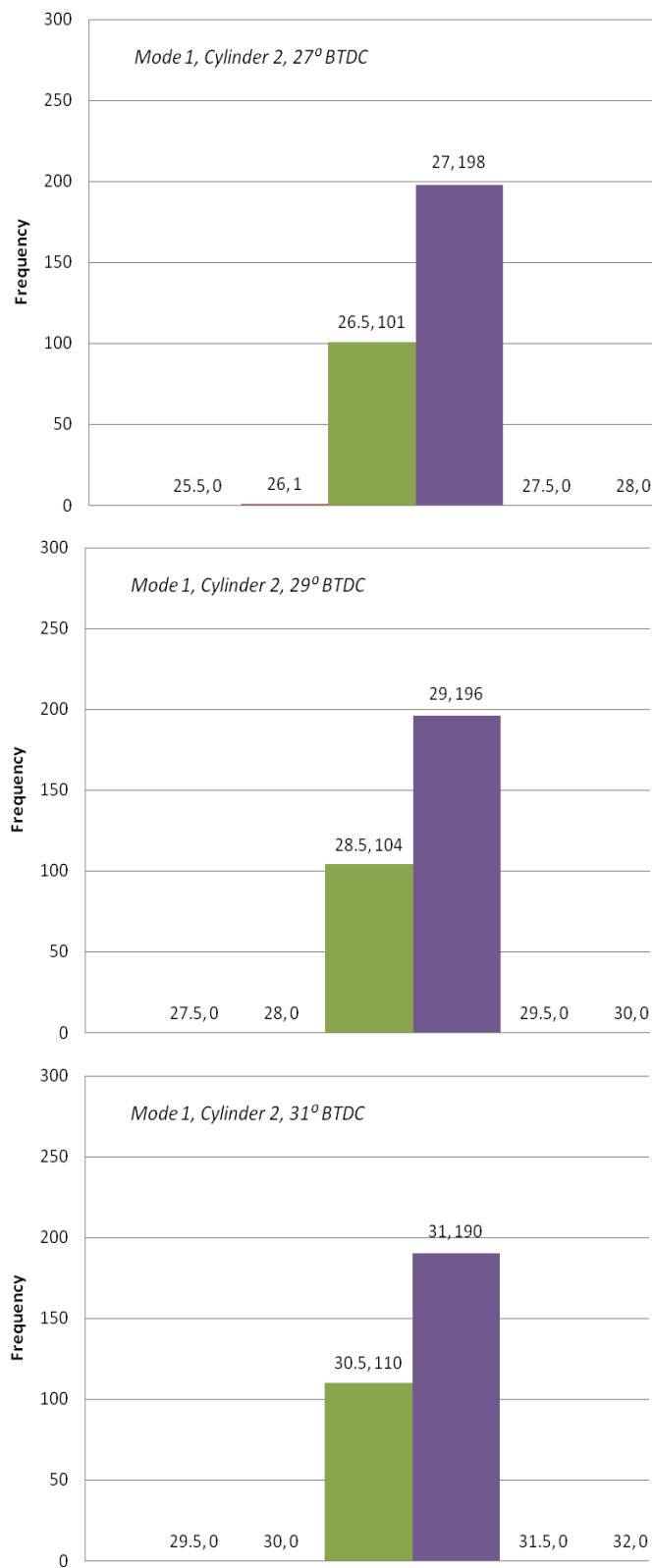**Figure A.4:** Cylinder 2, mode 1 dispersions for timings 21, 23, and 25° BTDC

Figure A.5: Cylinder 2, mode 1 dispersions for timings 27, 29, and 31° BTDC

BIBLIOGRAPHY

[1]   Heywood, John B. *Internal Combustion Engine Fundamentals.* New York: McGraw-Hill, Inc. 1988.

[2]   Spindt, R. S. "Air-Fuel Ratios from Exhaust Gas Analysis." Society of Automotive Engineers. SAE Paper No. 650507. (1965)

[3]   Chan. S. H., and J. Zhu. "Exhaust Emission Based Air-Fuel Ratio Model (I): Literature Reviews and Modeling." SAE Paper No. 961020. (1996)

[4]   Lynch, Dermot, and William J. Smith. "Comparison of AFR Calculation Methods Using Gas Analysis and Mass Flow Measurement." SAE Paper No. 971013. (1997)

[5]   Alkidas, A. C. "The Use of Availability and Energy Balances in Diesel Engines." SAE Paper No. 890822. (1989)

[6]   Rakopoulos, C. D., and E. G. Giakoumis. "Second-law Analyses Applied to Internal Combustion Engines Operation." *Progress in Energy and Combustion Science* 32 (2006): 2-47.

[7]   Rakopoulos, C. D. "Evaluation of a Spark Ignition Engine Cycle Using First and Second Law Analysis Techniques" *Energy Conversion and Management* 34.12 (1993): 1299-314.

[8]   Hongqing, Feng, and Li Huijie. "Second-law Analyses Applied to a Spark Ignition Engine under Surrogate Fuels for Gasoline." *Energy* 35 (2010): 3551-556.

[9]   Caton, Jerald A. "Use of a Cycle Simulation Incorporating the Second Law of Thermodynamics: Results for Spark-Ignition Engines Using Oxygen Enriched Combustion Air." SAE Paper No. 2005-01-1130. (2005)

[10]   Caton, Jerald A. "Operating Characteristics of a Spark-Ignition Engine Using the Second Law of Thermodynamics: Effects of Speed and Load." SAE Paper No. 2000-01-0952. (2000)

[11]   Flynn, P. F., K. L. Hoag, M. M. Kamel, and R. J. Primus. "A New Perspective on Diesel Engine Evaluation Based on Second Law Analysis." SAE Paper No. 840032. (1984)

[12]   Caton, Jerald A. "A Review of Investigations Using the Second Law of Thermodynamics to Study Internal-Combustion Engines." SAE Paper No. 2000-01-1081. (2000)

[13]   Caton, J. A. "First and Second Law Implications of Fuel Selection for an SI Engine." Proceedings of the 2010 Technical Meeting of the Central States Section of the Combustion Institute.

[14]   Teh, K-Y., S L Miller, C T Edwards. "Thermodynamic requirements for maximum internal combustion engine cycle efficiency. Part 1: optimal combustion strategy." International Journal of Engine Research Vol. 9 (2008): 449-465.

[15]   Teh, K-Y., S L Miller, C T Edwards. "Thermodynamic requirements for maximum internal combustion engine cycle efficiency. Part 2: work extraction and reactant preparation strategies." International Journal of Engine Research Vol. 9 (2008): 467-481.

[16]   Gatowski, J. A. "Heat Release Analysis of Engine Pressure Data." SAE Paper No. 841359. (1984)

[17]   Woschni, G. "A Universally Applicable Equation for the Instantaneous Heat Transfer Coefficient in the Internal Combustion Engine." SAE Paper No. 670931. (1967)

[18]   Zhu, Guoming G., Chao F. Daniels, James Winkelman. "MBT Timing Detection and its Closed-Loop Control Using In-Cylinder Pressure Signal." SAE Paper No. 2003-01-3266. (2003)

[19]   Miller, S.L., M.N. Svrcek, K.-Y. Teh, C.F. Edwards. "Requirements for designing chemical engines with reversible reactions." *Energy* 36 (2011): 99-110.

VITA

Shawn Nicholas Wildhaber was born in Jefferson City, MO to Jim and Lisa Wildhaber. He graduated from Helias Catholic High School in May of 2005. He worked as a Process Engineering Intern for ABB Inc. in Jefferson City, MO during the summer of 2006. During the summers of 2007 and 2008, he worked as a Product Engineering Intern for Cessna Aircraft Company in Wichita, KS. In May 2009, he received his B.S. with Honors in Mechanical Engineering from Missouri University of Science and Technology (formerly known as University of Missouri – Rolla). In May 2011, he received his M.S. degree in Mechanical Engineering from Missouri University of Science and Technology. He is also a Commercial Pilot and Certified Flight Instructor.